

A Survey of Visualization and Analysis in High-Resolution Connectomics

Johanna Beyer^{*1}, Jakob Troidl^{*1}, Saeed Boorboor², Markus Hadwiger³, Arie Kaufman², and Hanspeter Pfister¹

¹Visual Computing Group, Harvard University

²Department of Computer Science, Stony Brook University

³ Visual Computing Center, King Abdullah University of Science and Technology

(*) indicates equal contribution

Abstract

The field of connectomics aims to reconstruct the wiring diagram of neurons and synapses to enable new insights into the workings of the brain. Reconstructing and analyzing the neuronal connectivity, however, relies on many individual steps, starting from high-resolution data acquisition to automated segmentation, proofreading, interactive data exploration, and circuit analysis. All of these steps have to handle large and complex datasets and rely on or benefit from integrated visualization methods. In this state-of-the-art report, we describe visualization methods that can be applied throughout the connectomics pipeline, from data acquisition to circuit analysis. We first define the different steps of the pipeline and focus on how visualization is currently integrated into these steps. We also survey open science initiatives in connectomics, including usable open-source tools and publicly available datasets. Finally, we discuss open challenges and possible future directions of this exciting research field.

CCS Concepts

- **Human-centered computing** → **Visualization systems and tools; Scientific visualization;** • **Applied computing** → **Life and medical sciences; Systems biology;**

1. Introduction

In recent years, neuroscience has made significant advances in understanding the brain's structure and function based on novel high-resolution data acquisition techniques. Scientists aim to tackle questions of brain physiology, how diseases of the brain develop, and how the mind forms consciousness. The field of connectomics, in particular, approaches these questions by looking at the detailed connectivity between neurons at high-resolution to extract the brain's *wiring diagram*. The ultimate goal is to map and decipher a human's entire neuronal wiring, called the connectome [Seu12a].

Advances in tissue imaging such as high-resolution volume electron microscopy (EM) [BB12] enable this highly-detailed analysis by allowing scientists to collect unprecedented amounts of neuronal tissue data at nanometer resolution. This high-resolution data allows scientists to reconstruct individual neurons and all their connections (synapses) to other neurons. In addition, structural biologists and developmental neuroscientists are also interested in spatial and neighborhood analysis of neurons and analyzing the structural plasticity of how synapses and neurons change over time.

One of the main challenges in connectomics is the amount of data that scientists need to collect, process, and analyze. Even a single cortical cubic millimeter of mouse brain tissue consists of around 75,000 neurons and 523 million synapses [CBB^{*21}], mak-

ing brain connectivity exceptionally difficult to understand and analyze. Only the advent of automated high-throughput imaging techniques and automated computational segmentation tools have made analyzing the neuronal connectivity within brain volumes of a cubic millimeter or more now possible [YBB^{*20}, SCJB^{*21}, CBB^{*21}]. However, for neuroscientists to analyze these large and complex 3D datasets, they need scalable visualization methods throughout the entire connectomics data processing pipeline (see Fig. 1) that allow them to interact with their data intuitively and flexibly. For example, visualization can be used for interactive image quality assessment during the image acquisition stage [HHM^{*17}] or for interactive proofreading of the segmentation data. Visualization is also vital for data exploration, such as interactive spatial and connectivity analysis tools.

This survey discusses how visualization and visual computing can be integrated into the connectomics pipeline to help scientists in analyzing their high-resolution and large-scale data volumes.

1.1. Survey Scope and Previous Surveys

This state-of-the-art report summarizes previous research and recent developments in visualizing large, high-resolution biological data volumes. We describe and categorize visualization methods for each step of the connectomics pipeline, including novel ap-



Figure 1: The connectomics pipeline: In this survey, we discuss visualization approaches for each step of the connectomics data processing pipeline. Visualization is not just important for the final analysis step but vital for efficient image acquisition, registration, segmentation, and proofreading of segmentations.

proaches to visual proofreading, large-scale volume exploration, and connectivity-focused visualization methods.

In addition to the specific visualization methods, we refer to the most relevant work in image acquisition, registration, and segmentation. Furthermore, we discuss relevant topics in large-scale volume visualization and connectivity-focused visualization. We further outline methods for quantitative analysis of spatial and connectivity data and refer to relevant STARs in those areas.

We limit our discussion primarily to visualization-centered techniques for *high-resolution* 3D light- and electron-microscopy data that can depict individual neurons as well as individual synapses, respectively. In contrast to a previous survey on visualization in connectomics from 2012 [PKB^{*}12], the present work focuses on micro- and nanoscale datasets and the visualization of individual neurons and synapses. Developments in high-throughput data acquisition and automatic segmentation have paved the way for novel approaches to semi-automatic proofreading and connectivity-based visual analysis at the level of individual synapses. These novel and scalable visualization methods for micro- and nanoscale neuronal structures differ significantly from previous macro-scale connectivity visualization approaches, such as visualizing fiber tracts and brain regions. The latter we do not discuss in this survey.

The most relevant previous surveys in the area of visualization include a micro-, meso-, and macro-scale connectomics report [PKB^{*}12], a survey on large-scale GPU-based volume visualization [BHP15], surveys on modern (scientific) visualization on the web [MKRE16, FH20], and a survey on macroscopic brain circuit visualization [CSC18]. Other relevant surveys include biomedical image registration [VMK^{*}16], segmentation [MBK^{*}19, LRL^{*}21], motif discovery in graphs [YFZ^{*}20] and subgraph counting [RPS^{*}19].

1.2. Survey Structure

This survey gives an overview of the current state of the art in the visualization and analysis of high-resolution neuronal data for connectomics. We start with an introduction to fundamentals in neuroscience in Section 2, outlining the biological background and the connectomics data processing pipeline, from acquisition to analy-

sis. The remainder of our survey follows the different steps of the connectomics pipeline.

Section 3 talks about data acquisition for microscale and nanoscale datasets, as well as how visualization can support the data acquisition process. Next, we discuss image alignment and registration methods (Section 4) before outlining current methods for semi-automatic and automatic image segmentation (Section 5). To further improve segmentation results from automatic methods, many different semi-automatic proofreading methods have been proposed, which we discuss in Section 6.

While visualization approaches play a crucial role in all steps of the connectomics pipeline, the exploratory analysis of registered, segmented, and proofread volumes relies on many diverse visual techniques. To this end, we discuss visual exploration and analysis methods in Section 7. After outlining scalable data structures in Section 7.1, we discuss methods for spatial exploration, including approaches for large or segmented volumes, in Section 7.2. Next, we outline visual methods for exploring neuronal connectivity in these data volumes, going from node-link diagrams to more specialized neuron-centric views in Section 7.3. In Section 7.4, we discuss methods for a more quantitative analysis of neurons and spatial neighborhoods, including visual query systems that interactively drill into the data. Finally, we outline visualization methods used for the communication of connectomics insights in Section 7.5.

To complete this survey, we provide a list of popular and publicly available datasets, as well as open-source tools to help foster future research in connectomics and visualization in Section 8. We also list datasets, tools, and surveyed papers on our website (connectomics-vis-survey.github.io). Finally, we look at future trends and open problems in Connectomics visualization in Section 9 and conclude in Section 10.

2. Neuroscience Fundamentals

We first introduce the fundamentals in neuroscience to clarify the most important biological concepts for connectomics. Then, we outline the connectomics pipeline, which is the typical data acquisition and processing workflow in connectomics research.

Modern neuroscience began around the end of the 19th century

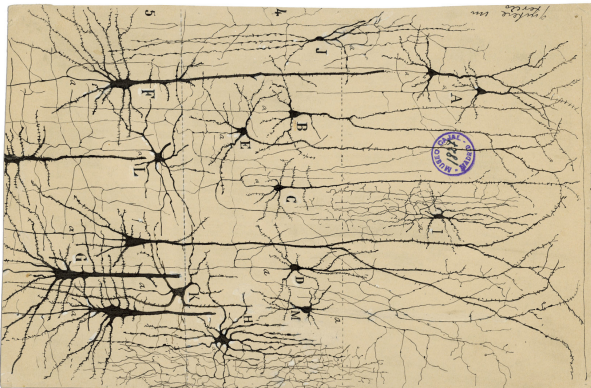


Figure 2: Cajal's original drawing of neurons as individual cells.

with the discovery of neurons. Santiago Ramón y Cajal was the first to report the delicate anatomy of the nervous system (see Fig. 2) and argued that neurons are information processing units that form connections and propagate electrical impulses to accomplish their various functions. Thus, laying the foundations of modern neuroscience and the conceptual framework for connectomics [SL16].

The term connectome originally meant “a comprehensive structural description of the network of elements and connections forming the human brain” [STK05], but has since been extended in its definition to include any systematic account of connections, from local circuits to networks constituting entire nervous systems [SL16]. The corresponding research field *connectomics* uses computer-assisted and high-throughput techniques for image acquisition and analysis for the structural mapping of neural circuits. Current research is also studying how the brain’s functional architecture rises from the underlying structural circuit architecture.

2.1. Biological Background

The adult human brain consists of approximately 100 billion neurons with each neuron having up to thousands of neural connections to other neurons. A recent dataset of one cubic millimeter of a human cerebral cortex contained 50,000 neurons with 130 million interconnections [SCJB*21]. Neurons process and transmit information as electrical impulses by forming synaptic connections with other neurons. The size and form of neurons can vary widely, but typically, neurons receive input on tree-like structures called *dendrites* and transmit signals via their *axon*, a long tubular structure that transmits signals away from the cell body (*soma*) towards other neurons (see Fig. 3). Axons and dendrites are collectively called neurites and make up the topological skeleton.

A *synapse* is the small gap between two neurons, where nerve impulses are relayed. A typical mammalian synapse consists of a presynaptic terminal (a *bouton*) on the side of the axon that releases neurotransmitters when activated, a *post-synaptic terminal* at the side of the dendrite, and the *synaptic cleft* between dendrite and axon. The signaling process is partly electrical and partly chemical, where a nerve impulse (i.e., action potential) travels along the axon and activates synaptic connections. A synapse can either be excitatory or inhibitory, depending on whether a spike on the axon

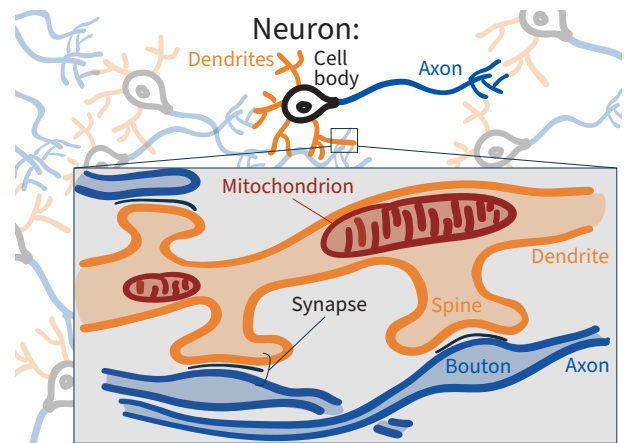


Figure 3: Structure of neurons and their connecting synapses. Neurons consist of a cell body, dendrites, and an axon. Most neurons receive signals via dendrites (orange) and send out signals via the axon (blue). Synapses transmit the signal between two neurons. Neurons contain different cell organelles, such as mitochondria that provide energy for cell metabolism.

increases or decreases the chance of provoking a spike in the receiving dendrite. Compared to the size of a neuron in the human body (i.e., a fraction of a centimeter to a meter), a synapse is extremely small (20-40 nm) [LD11]. Therefore, to capture synapses, tissue needs to be imaged at a very high resolution, resulting in large datasets. In addition to synapses, subcellular structures of neurons, so-called *cell organelles*, are also of high interest to neuroscientists. *Mitochondria*, for example, are responsible for providing energy to the cell and its synapses. Interestingly, only half of the cells in the mammalian brain are neurons. The rest are *glia cells*, which provide supporting features to neurons.

Neurons, their cell organelles, and synapses exhibit high structural variability. For example, synapses can vary by the position of the post-synaptic terminal (i.e., either on a dendrite’s shaft or a small extension called a dendritic spine) or by the number of vesicles (cell organelles containing neurotransmitters) in the bouton. However, it is an active area of research on what influences or causes the variability of these attributes and how they impact the function of a neuronal circuit. Therefore, in addition to connectivity analysis, scientists are interested in trends and correlations and looking at individual neuronal structures, synapses, and attributes.

2.2. Connectomics Pipeline

High-resolution connectomics relies on many different processing steps to go from the original tissue samples of neuronal data to the reconstructed and analyzed wiring diagram. This process is generally called the *Connectome pipeline* [LPS14, Seu12a] and is depicted in Fig. 1. Throughout this process, at each step, interactive and scalable visualization is key to helping scientists handle their large and complex datasets. This survey follows the individual steps of the connectomics pipeline and focuses on visualization methods and challenges in each step.

Data Acquisition. Data acquisition starts with a 3D tissue sample that is chemically preserved to lock proteins and molecules that

form neuronal structures. Next, the tissue sample is cut into very thin slices using a microtome and, subsequently, each slice is imaged with a microscope. Light microscopes can acquire images of a *xy* resolution of 200 nm. EM is necessary for higher resolutions of up to 4 nm in the *xy* plane and around 30 nm in the *z*-dimension. EM also densely captures details such as synapses.

Alignment & Registration. To image a large tissue slice, microscopes typically acquire image tiles of a fixed size (e.g., 12,000 × 12,000 pixels). In a post-processing step, these individual 2D image tiles need to be *aligned* and *stitched* to combine them into a single large 2D section. *Registration*, on the other hand, takes a stack of 2D sections as input and aligns them to reconstruct a 3D volume representing the original 3D tissue block.

Segmentation & Proofreading. Reconstructing the wiring diagram of all neurons in a tissue block requires labeling (i.e., segmentation) of cell membranes and synapses. The gold standard for segmentation is manual labeling, requiring expert users to mark individual pixels as belonging to certain structures. This approach, however, quickly becomes infeasible for large volumes with millions of neurons. Therefore, more and more semi-automatic and fully automatic segmentation methods have been developed recently. While automatically generated segmentations are becoming increasingly accurate, they still require *proofreading* by humans to correct mistakes and verify the reconstructed connectivity graph. Semi-automatic proofreading methods aim to streamline this process by pointing users to likely segmentation errors in the dataset.

Exploration & Analysis. The final steps in the connectomics pipeline consist of visual data exploration and analysis. Depending on the type of data available (e.g., light microscopy or EM, segmented or unsegmented), different visualization methods exist to explore the data in more detail. Visualization approaches range from the visual exploration of the raw imaging volumes to the analysis of abstract connectivity graphs or query-based visual analysis approaches that combine spatial data, connectivity data, and any labeled or extracted metadata.

3. Data Acquisition

Advances in high-resolution imaging technologies enable the acquisition of brain connectivity information across multiple temporal and spatial resolutions. Based on the scope of this survey, we provide an account of the *micro-* and *nano-* scale modalities used for brain data acquisition. For macroscale modalities that capture neural fibers and their connectivity information at centimeter and millimeter resolutions, we refer the reader to detailed surveys by Pfister et al. [PKB^{*}12], and Chen et al. [CSC18].

3.1. Sample Preparation

Steps for sample preparation differ based on the imaging modality. Brain tissue samples are tagged using various labeling techniques for optical imaging to capture the structural information of individual neuronal cell types or their projective trajectory. Specifically, neurons are labeled using single or multi-colored stains or by breeding transgenic subjects to produce photophysical fluorescent proteins that express different colors on the exposure of

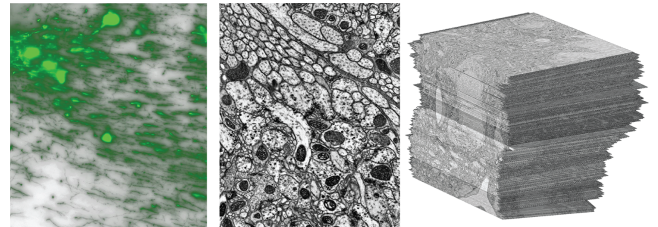


Figure 4: Left to right: Widefield (WF) microscopy slice, EM slice, and registered EM volume showing 2D image sections.

light [LLS08]. Additionally, to capture relationships between organization and function of neural circuits, specimens are injected with viruses, such as Rabies [CL15], that spread selectively between synaptically connected neurons.

For imaging nanoscale structures using EM, tissue samples are embedded in plastic to prevent its destruction during slicing. Next, the sample is stained with heavy metals that interact with electrons in ways that electron microscopes can detect. After staining, the tissue sample is either first physically cut into thin slices using a microtome and then imaged [HMS^{*}14], or the microscope images and destroys thin sections of the sample progressively [TKH^{*}12].

3.2. Microscale Brain Imaging

Light microscopy has been used to map and study neuronal circuits at a micrometer scale for a long time. Neuroscientist Cajal was able to identify connectivity patterns of Golgi stained neuronal circuits for the first time [Val70] using microscopic resolution sufficient to image single neurons.

Wide Field Microscopy. The choice of the microscope is greatly dependent on sample thickness and signal-to-noise tolerance. Wide-field (WF) microscopy exposes a whole tissue sample to a light source before capturing the image [BJA^{*}19]. With its large field of view, WF can image a sample in a short time, albeit for thin, sectioned slices (< 30 μm). It collects light emitted from the focal plane and illuminated layers above and below the focal plane. As a result, the acquired images suffer from a degraded contrast between foreground and background due to out-of-focus light swamping and low signal-to-noise ratio (see Fig. 4, left). Image processing techniques aim to resolve the blur and focus (see Section 3.4).

Confocal Laser Scanning Microscopy. In contrast to WF, a confocal laser scanning microscope utilizes laser units as the light source to excite the fluorescent stains of a sectioned sample (30–70 μm) and acquires the resulting image following a pinhole design principle [Pad00]. As such, the confocal system can block out any out-of-focus light. Although this produces sharp images, some information is lost due to the pinhole blocking out-of-focus photons that may have originated from the focal plane.

Both confocal and fluorescence WF microscopy systems produce raw 3D data by sequentially changing the focal plane along the *z* direction (that is, along with the depth of the sample) and stack the generated 2D images atop each other. Typically, modern super-resolution microscopy systems can achieve a lateral *xy* resolution of around 200 nm and an axial resolution of around 600 nm [Wil].

Advanced Methods. Sectioning a brain specimen into thinner samples increases the probability of the structures being severed at multiple points across consecutive slices. Advanced microscopy technologies, such as light-sheet and two-photon tomography, allow imaging of thicker or whole-brain samples. Light-sheet microscopy is a modification to wide-field fluorescence technology such that it has intrinsic optical sectioning capabilities by automatically moving the sample through a single plane sheet of light [DLS*07].

Serial two-photon tomography [RKV*12] is an ex-vivo imaging technique that combines serial imaging and sectioning. The simultaneous absorption of molecules by two photons allows optical sectioning without absorption above and below the plane of focus. This eliminates the need for a pinhole. Though this method offers increased depth penetration, the custom addition of a built-in vibrating blade microtome creates undisturbed images within the same space, as the sectioning occurs after the imaging. Finally, with the advancement of “super-resolution” microscopy, optical examinations of nanometer-scale phenomena using light microscopy is now possible (e.g., [HW94, SEG15]).

While the mentioned modalities have resolutions that are not sufficient to resolve synapses, expansion microscopy (ExM) physically expands brain tissues to overcome the resolution limitation of light microscopy [CTB15, WZB19]. Additionally, imaging neurons at a micrometer scale facilitates capturing functional networks of neuronal systems [WTY*15, RHC20], trace synaptic circuits [LWK*07], and analyze its geometry and functional connectivity across disease and aging [BMA*21]. Moreover, light microscopy has also been used recently for the connectivity analysis of defined cell types by using spectral connectomics [SHW*20].

3.3. Nanoscale Brain Imaging

EM is the only modality that can densely image biological tissues at a nanometer scale (see Fig. 4). Short wavelengths of high-energy electrons provide sufficient resolution for EM to capture the finest details of synaptic connections and organelle structure.

The main challenge to imaging large brain volumes using EM include throughput time, alignment, and contrast. Early technologies require a sample to be sectioned into ultrathin slices, which are then aligned on a tape and imaged at a pixel resolution of 4×4 nanometers [LPS14]. Transmission electron microscopy (TEM) [BLK*11] utilizes camera arrays that allow a fine lateral resolution, aiding in the identification of fine structural details. Newer techniques, such as serial-blockface scanning EM (SEM) [DH04] and focused ion-beams (FIB-SEM) [KMWL08] are block-face methods that successively image and section each layer of the sample block. This allows better alignment, thus saving computation time. Specifically, FIB-SEMs are designed to section the sample automatically. Multi-beam scanning electron microscopes (mSEM) [EMS*15, HPJ*20] image larger fields of view, enabling the acquisition of big tissue samples in a reasonable amount of time. For instance, Shapson-Coe et al. [SCJB*21] used an mSEM with 61 ion beams to image $10,000 \mu\text{m}^2$ simultaneously as a hexagonal shape. Overlapping image tiles are then stitched together for larger fields of view.

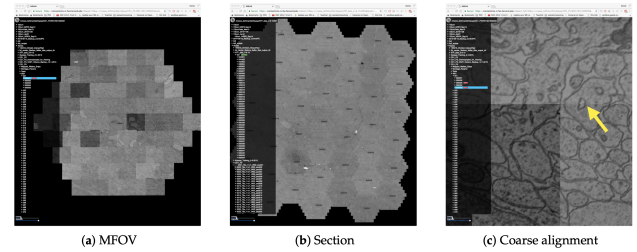


Figure 5: Visualization of multi-beam SEM acquisition and alignment with *MBeam viewer* [HHM*17]. a) 61 image tiles per multi-beam field of view (MFOV). Each individual image is $3,128 \times 2,724$ pixels in size, resulting in roughly $30k \times 26k$ pixels for each MFOV. b) 55 MFOVs are stitched together into one $200k \times 170k$ pixel section. c) zoomed-in view to evaluate coarse alignment.

3.4. Visualization for Data Acquisition

Image quality assurance is essential in preparing a digital tissue volume. *MBeam viewer* [HHM*17] is a web-based visual tool to assess imaging quality and contrast during data acquisition of EM images. EM collects multiple tiles per imaging section that need to be stitched together, and stitching greatly depends on the image quality and a uniform contrast across the tiles. Typical quality problems are the inconsistent vertical position of the sample (primarily in ATUM-SEM), unfocused images due to slice height variations, and external particles on the imaging specimen. *MBeam viewer* allows immediate and remote inspection of the image tiles by juxtaposing them on a 2D canvas. On-the-fly mipmapping enables interactive zoom and pan and the rapid assessment of the image tiles’ quality (see Fig. 5). Modern EM [EZ18] software, such as for the Zeiss SEM, integrates visualization for browsing and filtering the image collection and can even create 3D scans of a sample.

Since EM imaging produces roughly a petabyte of image data per cubic millimeter, data storage poses a significant cost factor and a limitation for volume visualization algorithms. Therefore, it is desirable to compress imaging volumes as much as possible without losing details needed in the rest of the connectomics pipeline. Minnen et al. [MJB*21] present a machine learning-based denoising approach for EM images. Compressing the denoised images leads to a 17-fold data size reduction with no loss in segmentation and negligible loss in synapse prediction accuracy. They use a UNET architecture with residual connections to learn a denoising model.

4. Alignment and Registration

Raw microscopy data needs to be processed to recover the 3D volume of the specimen. Challenges during data acquisition, such as slicing and deformation, and a limited field-of-view only allow the imaging of small image tiles. Mosaicing describes the alignment and stitching of individual imaged tiles acquired in the lateral directions (i.e., xy -plane). This is followed by the axial registration (i.e., z -direction) of sections through the sample volume. Image registration is well studied, using either intensity- or feature-based techniques. In this section, we focus on methods specialized for processing brain volumes imaged with optical and EM modalities.

4.1. 2D Alignment and Stitching

High-resolution microscopes have lenses with a small field of view. Thus, large biological tissues are imaged by laterally acquiring smaller image tiles in the xy plane, with partial overlap. Alignment techniques aim to resolve these overlapping tiles and stitch them to reconstruct a complete 2D image section. In the literature, this step is also often referred to as *mosaicing* or *montaging*. Algorithms for alignment and stitching address two important challenges. First, high-resolution microscopy generates a large amount of data. A single 2D image slice imaged using light microscopy is in the order of tens of gigabytes, while a slice imaged using EM is hundreds of gigabytes. Therefore, alignment algorithms need to be highly optimized or parallelized to recover the transformation parameters for all image tiles in a reasonable amount of time. Second, the sample preparation and imaging workflow are fallible. Often there are tears, folds, or other deformities in the mounted sample. As a result, these algorithms need to consider missing information, artifacts, and inconsistent lighting and contrast conditions.

Broadly, the following general steps are adopted to align and stitch a grid of image tiles: (1) identify tile pairs and their overlapping region, (2) estimate candidate displacement values between adjacent tiles, (3) apply fine adjustment optimizations to reduce errors in the stitched image, (4) stitch tiles to produce the mosaic, and in some works, (5) post-process the component images together to yield a seamless final result. The literature identifies two main approaches for aligning and stitching image tiles.

Feature-based approaches [CHP^{*}06, SCHT10] identify matching features in adjacent tiles to compute image translations. This approach can be sensitive to feature sparsity in the overlapping regions of adjacent tiles. Thus, some methods make assumptions about the data, e.g., for aligning blob-like structures [BAS^{*}96], fine-filaments [AKCL^{*}03], or contours [BLLF06].

(Pixel) correlation techniques [Gre09, ERP^{*}09, TKG^{*}10, BI12, CMB^{*}17] can be more general as they utilize domains such as image frequency by applying Fourier transforms, or pixel intensity by applying cross-correlation or mutual information. Similarly, this approach assumes that images have enough pixels with unique frequency or intensity components in the overlapping areas. As such, the choice of method depends on the overall image content and the characteristics of matching features.

Hybrid approaches [ERP^{*}09, TLB^{*}11] make use of both feature-based and pixel correlation methods for a coarse-to-fine alignment. Using this approach, Tsai et al. [TLB^{*}11] have improved the accuracy, robustness, and scalability in aligning light microscopy image tiles. They determine potential tile pairs by extracting features such as corners and edges from 2D maximum-intensity projection (MIP) images [Low04] and find pair matches using the Dual-Bootstrap Iterative-Closest Point algorithm (DB-ICP) [YSST07]. An affine transformation between tile pairs is computed to account for spatial distortion between pairs. Finally, to stitch the tile pairs into a single volume, they employ pixel-based normalized cross-correlation (NCC) minimization and a global consistency approach [CSRT02].

Preparing brain samples often cause tears or folds, creating gaps in the image continuity. As a result, an overlap between image pairs

can not always be guaranteed. To address this challenge, Yigitsoy and Navab [YN13] have introduced an approach based on structural continuity beyond image boundaries. A tensor voting on the orientation and saliency properties of the extracted structures is used to infer artificial overlaps in the extended regions. The inferred aligned structures are then used to estimate multi-scale transformations for the optimal alignment between the tiles.

Tools for 2D Alignment and Stitching are designed to minimize the overall computational workload of large image volumes while also keeping track of tile-pair alignment quality and allowing manual intervention.

XuvTools [ERP^{*}09] is an automatic 3D stitching software that adopts a coarse-to-fine strategy, combining both feature and pixel correlation techniques. Assuming no information about the tile sequence, *XuvTools* uses a multi-scale phase-only correlation to estimate a coarse position of the tiles. Using a GUI, users manually position the tiles in a grid layout. For fine-scale alignment, it detects salient points that would appear in the overlap region and maximizes NCC coefficients of multiple smaller patches around the salient points. Once tiles pairs are determined, absolute tile positions are computed by globally minimizing the displacement values. Finally, artifacts due to changing intensities at the border of the tiles are alleviated by applying bleaching correction to each tile pair. While this process is fully automated, *XuvTools* displays the progress of alignment and stitching at every iteration. If a stitching error is identified, users can adjust parameters for the correlation threshold and the size and search radius of correlation windows to recompute the fine alignment step.

TeraStitcher [BI12] is designed to stitch tera-sized tiled microscopy images on consumer hardware. To efficiently estimate the relative displacement of tile pairs, adjacent tile pairs are divided into user-defined substacks, and 2D maximum intensity projections of the tiles along the three dimensions are used to compute the NCC coefficients. For the optimal global placement of tile pairs, a minimum spanning tree approach by Yu and Peng [YP11] is employed. Finally, overlapping regions are blended using two phase-shifted sinusoidal functions for a complete mosaic. To further improve processing and stitching time, Bria et al. [BBGI19] use a CUDA multi-process parallelization strategy. *TeraStitcher* allows manual intervention to refine stitching metadata by providing (1) a preview feature to stitch user-selected portions of data and (2) graphical metadata models for a more comprehensive analysis. Users can detect and locate abnormalities by inspecting the stack borders using the preview.

Although some microscopes typically provide approximate tile locations, in practical settings translation stages can still exhibit inaccuracies. To this end, Hörl et al. [HRRP^{*}19] have developed *BigStitcher*, designed specifically for gigapixel light-sheet microscopy datasets that solves for tile pairs in non-regular grids containing empty images and multiple independent samples. Using downsampled image tiles, all possible shifts for overlapping pairs are first calculated using phase correlation, called links. In the optimization step, an additional attribute of *strong* (confirmed) and *weak* (estimated) links is introduced to solve for the global optimal tile placement. By optimizing both link types, strongly linked regions are accurately aligned, while an optimal alignment is de-

terminated for weakly linked groups of tiles. The entire process is interactively displayed, enabling users to verify, interact and potentially guide the proper alignment of complicated datasets.

In studying the alignment workflow of pairwise displacement followed by global placement, Chalfoun et al. [CMB^{*}17] found that residual errors can be introduced when the raw data has sparse features or information for feature-based and intensity correlation methods, respectively. To address this, they have introduced *Microscopy Image Stitching Tool (MIST)*, a grid stitching technique that minimizes stitching errors by estimating the microscope mechanical stage model parameters and using them to improve the search space of the global tile placement optimization step. MIST uses a multicore hybrid CPU/GPU implementation to handle terabytes of microscopy data.

Simply warping one tile onto another using the displacement transformation can introduce artificial deformations in the final stitched output. To this end, Saalfeld et al. [SFCT12] have introduced a technique for EM images that aligns corresponding key points and formulates an elasticity constraint on local neighborhoods to solve for a nonrigid deformation. The elasticity constraint is implemented by representing image tiles as a triangular mesh of a spring-connected particle system. Each vertex of the spring mesh searches for corresponding key-point locations in the adjacent tile using pairwise block-matching, and the springs tend to maintain a rigid transformation across the overlapping tiles, penalizing distortions. Such a constraint allows the alignment of arbitrarily large image tiles without propagating transformation errors. Haehn et al. [HHM^{*}17] have developed a visualization tool for this process, called *RHAligner*, which provides an abstracted visualization of stitched sections and allows for quick assessment of the alignment process. *RHAligner* expands the algorithm to solve for a hexagonal grid and optimizes it by adopting a parallel implementation.

4.2. 3D Registration

Brain specimens have to be physically sectioned into a series of slices for most imaging modalities. Thus, to extract 3D structural and functional information, the serial sections need to be registered along the z -direction (or imaging direction). However, the process of physical sectioning severs structures at the slicing interface, destroying continuity between consecutive sections and resulting in tissue deformation. In contrast, modalities that adopt a block face approach do not suffer from this information loss [HXL^{*}15].

Some rudimentary approaches to simplify registration include introducing intrinsic or imposed fiducial markers in the sample [HML^{*}95, BMV05, PYD04], defining anatomical landmarks [SPB^{*}15], or attaching additional imaging modalities [J^{*}09] to be used as a priori information.

Beyond an a priori approach, 3D registration techniques are designed to recover a volume that results in the natural progression of features through successive sections [JWC^{*}06]. Within the scope of optical microscopy, Lee and Bajcsy [LB08] have proposed registering sections by tracking the trajectory of salient cylindrical structures in each section and across adjacent slices.

Tools for 3D Registration. Peng et al. [PCL^{*}11] have developed *BrainAligner* for registering light microscopy image slices

that first perform robust global affine registration by transforming them into a common coordinate system using a predefined brain atlas [BIP15], followed by nonlinear local alignments using predefined landmarks. For local alignment, predefined landmarks are used to generate a thin-plate-spline warping field [Boo89]. Furthermore, *BrainAligner* allows adding custom landmarks to help optimize or improve critical alignments.

Some studies [HPJ^{*}11, DWG^{*}09, LFP11] have suggested using traced neurons for registration. Essentially, the process of neuron tracing (see Sec. 5.2) generates a concise and less noisy representation of neuron morphology compared to using the raw microscopy volume for registration. The *Filament Editor* [DHO14] and *NeuronStitcher* [CldC^{*}17] are two widely used interactive registration and alignment tools that assemble adjacent microscopy sections using traced neurons and allow fine-tuning by providing a visualization of complicated neuron fragments.

NeuroConstruct [GBM^{*}21] adopts a hybrid approach of using intensity correlation (for coarse registration) and feature-based alignment (for fine tuning) to register segmented light microscopy brain volumes. Following global registration, similar to Yigitsoy and Navab [YN13], a tensor-based method is used to propagate and register exiting/entering neurites across adjacent sections. Finally, the reconstructed volume can be interactively fine-tuned by clicking on corresponding entering/exiting neurites.

In the EM domain, Fialia [Fia05] has developed *Reconstruct*, to perform both manual and automatic registration on serial section EM slices. For manual registration, users can progressively define and adjust transformation parameters (translation and rotation). Results are visualized by blending or flickering adjacent sections. For automatic registration, *Reconstruct* treats neuron traces in sections as fiducial markers and computes the transformation that minimizes the distance between the centroids of the traces in section pairs. Users can view the registration result and make manual edits to fix misalignments or distortions. Adjustments made to one section pair are then propagated to the rest of the series.

TrakEM2, developed by Cardona et al. [CSS^{*}12], is a widely used open-source software for neural circuit reconstruction from terascale EM serial sections. For its automated registration pipeline, sections are registered by first extracting SIFT features [Low99] to estimate a linear transformation, followed by elastic alignment [SFCT12] to compensate for non-linear distortion. Alternatively, for manual registration, feature correspondences are assigned using a GUI interface. Local alignment and transformation errors are interactively fixed using point-click-and-drag manipulation aided by transparent overlays of section pairs. Brain volumes are viewed either as low-resolution images of large fields of view or as high-resolution images for user-defined areas of interest.

In addition to mosaicing, the elastic registration technique [SFCT12] discussed in Sec. 4.1 can also be used for registering adjacent section series. The block matching algorithm explores transformation parameters in all sections of a local neighborhood of each vertex of the defined spring mesh. Using this, Haehn et al. [HHM^{*}17] have developed a plugin named *RHAligner* for their Butterfly middleware that registers EM sections and provides a visualization to monitor, debug, assess, and fine-tune the results. Since identifying features incorrectly can result in the failure of all

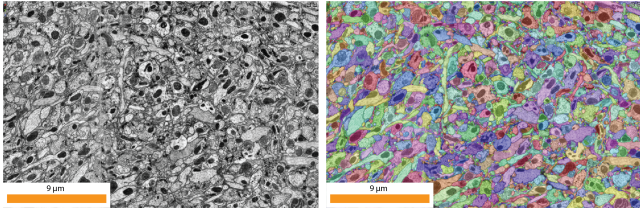


Figure 6: EM slice (left) and dense segmentation overlay (right).

successive steps, the extracted SIFT features are shown to the user for debugging by overlaying them on top of the original image. Once registered, users can visualize and identify incorrect registrations by scrolling through a 2D representation of the stack. In case of a failed registration, the tool visualizes the displacement of blocks using color-coded arrows representing vector fields based on the direction of each displacement according to its angle. Due to the uniqueness of each dataset, debugging the misalignments is designed to be a manual process.

Lindow et al. [LBD*21] have developed a software-assisted algorithm for the alignment and matching of filamentous structures in serial-section EM tomography. It provides visualization and interaction tools for each registration and reconstruction process to guarantee a real-time response. More recently, deep learning techniques are being investigated due to their advantage of improving performance and improved accuracy and robustness to learn features in the sample for registration [YHT*17, Jai17].

5. Segmentation

Once a 3D volume is recovered from the raw microscopy data, individual neuronal structures need to be segmented to enable the detailed study and visualization of separate structures and their connectivity. A dense segmentation of an EM slice is shown in Figure 6. A full survey of the state of the art in semantic and instance segmentation of biomedical images is out of scope for this paper. Therefore, we point the reader to recent surveys on deep learning for image analysis and segmentation [MBK*19, LRL*21] and focus on approaches targeting connectomics and neuroscience.

5.1. Automatic Segmentation Approaches

While the ultimate goal for segmentation in the connectomics pipeline is to extract relevant structural and connectivity information from large microscopy volumes, the techniques employed vary based on the imaging scale, image resolution, and modality. Microscale segmentation approaches capture larger structural shapes in microscopy images, such as cell bodies and neurites. On the other hand, nanoscale segmentation approaches work on high-detail image cross-sections that include individual cell organelles and synapses. Both approaches, however, have to overcome data challenges, such as low signal-to-noise ratio, imaging artifacts, foreground blurring, or slice mis-alignment [SCJB*21].

Microscale Segmentation. At the microscale, segmentation focuses on tracing the path of a neuronal structure along its centerline and determining its starting point (typically cell bodies) and

termination. Current techniques aim to identify intensity distribution features and determine the tracing direction for branching neuronal morphologies. Methods to address these goals include optimal seed-points path finding [PLM11, LBA11, QZL*16], model fitting [WNTR11, LQX*19], fast marching [BR14, YHL*19], distance-tree hierarchical pruning [XP13], and deep learning-based automatic approaches [CIdC*17, LZPJ17, ZKPL18, FPA*20].

Nanoscale Segmentation. Automatic segmentation methods for EM data mainly perform dense segmentation (i.e., every pixel in an image is assigned a label) based on deep learning. Recently published large EM connectomics datasets [SCJB*21, XJL*20] use flood filling networks (FFN) [JKL*18] for segmentation. FFNs add recurrent pathways to convolutional neural networks (CNN), which helps maintain the neuron shape prediction over multiple steps of the segmentation process. FFN based architectures [JKL*18] outperform other state-of-the-art methods [ZWJ17, LZL*17, FTG*17] by producing fewer merge and split errors. Since hyper-parameter configuration, network architecture, and other attributes of the learning pipeline largely depend on the data size and available hardware, efforts toward a self-configuring pipeline have been made [IJK*21]. More recently, Lin et al. [LWLP21] have developed an open-source deep-learning framework for the semantic and instance segmentation of volumetric microscopy images built on PyTorch. 3D segmentation also comes with the challenge of tracking 2D slice segmentations through the imaging stack. Cross-classification clustering (3C) [MMS*19] solves this task specifically for EM connectomics, where multiple complicated, intertwined neurons need to be tracked. All these approaches require labeled microscopy imaging data. Lauenburg et al. [LLZ*22] recently presented a method for 3D instance segmentation of unlabeled images from the expansion microscopy domain by leveraging labeled images from the EM domain via a cyclic segmentation GAN (CySGAN). Other segmentation approaches include local shape descriptors (LSDs) [SND*21], dense voxel embeddings [LLLS21], or FusionNet [QHJ21]. To scale segmentation up to petascale imaging volumes, *Chunkflow* [WSLS21] allows distributing computational tasks over the cloud and local resources.

5.2. Interactive Segmentation Approaches

Currently, deep learning is the state-of-the-art method for image segmentation. However, complex programming setups, imperfect segmentation results, and limited access to data and computing resources often make it difficult for neuroscientists, primarily non-programmers, to take advantage of the recent advances. Therefore, manual and semi-automatic approaches remain valuable to neuroscientists in practice, as well as interactive methods for fine-tuning of deep learning models.

Model Fine-Tuning for ML-based Segmentation. Haberl et al. [HCT*18] propose a plug-and-play cloud-based image segmentation framework for biomedical images of different imaging modalities. They build on the DeepEM3D model [ZWJ17], which was specifically designed for the segmentation of anisotropic EM imaging volumes. Users can access their service through a [website](#), where they can retrain existing models with their training data or run DeepEM3D [ZWJ17] on a set of provided data set. The Uni-EM tool [UBK*19] helps to make automatic deep learning segmen-

tation algorithms more accessible through a visual interface, making it usable for non-programmers. Users can generate ground truth data with a paint tool in Uni-EM and use it for network training. They also integrated *Dojo* [HKBR^{*}14] for proofreading segmentation results (see Sec. 6.2). However, due to the design as a desktop application, users are limited by local hardware and can not access cloud-computing resources. Ghahremani et al. [GBM^{*}21] propose a workflow that helps users interactively annotate a small set of neuronal structures by drawing over 2D cross-sectional views. A preliminary model is trained using a small annotation set. Consequently, instead of manually generating a sufficiently large dataset of annotations, the preliminary model is used to create draft annotations, which they can fine-tune. The training of the preliminary model can also be iterative to reduce the fine-tuning effort.

Semi-automatic Segmentation. *Ilastik* [SSKH11, BKK^{*}19] is a tool for the semi-automatic segmentation of microscopy image volumes. It uses a random forest classifier to infer a segmentation from label inputs provided by the user. The features are learned from 3D neighborhoods of pixels. Users can refine segmentation outputs interactively and are guided by a segmentation uncertainty map pointing them to ambiguous segmentation regions. Roberts et al. [RJVR^{*}11] propose another semi-automatic segmentation technique that uses sparse scribbles to generate accurate segmentation in EM image volumes. First, the user scribbles into a neuron’s cross-section in each volume slice. 2D segmentations for each slice are then predicted by minimizing a variational segmentation energy function. These 2D segmentations are the fixpoints for generating a 3D volumetric segmentation shape. *NeuroTrace* [WBH^{*}10] suggest segmentation masks using multiphase level sets [VRMP09] and integrates a scalable volume viewer. *TrakEM* [CSS^{*}12] also offers semi-automatic reconstruction, synapse labeling, and skeleton extraction. *VAST* [BSL18] is also a widely used program for manual and semi-automatic labeling and segmentation of large microscopy image volumes. Users can annotate the volume at different resolution levels to speed up segmentation. By outlining closed contours of cells, *VAST* automatically fills the selected region.

Manual Segmentation. *Neurolucida* [GG90] is an early tool developed primarily as a manual computer-assisted tracing system for light microscopy systems. The specialty of this software is its integration with the microscopy system to superimpose both image data and system control functions for manual tracing. Given that *Neurolucida* is not freely available, alternative manual segmentation tools [PHK04, PLM11, MCV17] are available. *3D Slicer* [PHK04] is a widely adopted user interface integrating *ITK* segmentation functionalities. *Catmaid* [SCHT09] and *Viking Viewer* [AMG^{*}11] are multi-user collaborative environments for manual segmentation of large datasets. *Catmaid* additionally allows synchronized inspection of multiple registered datasets, such as comparing EM and light microscopy volumes. Scalability in these systems is achieved through a tiled image pyramid, enabling the browser only to load relevant data pieces into working memory. Many of the manual and semi-automatic segmentation tools also support proofreading, such as *VAST* [BSL18], *Catmaid* [SCHT09], and the *Viking Viewer* [AMG^{*}11]. We outline their proofreading capabilities in Section 6.

Immersive Neuron Tracing. Studying the complex circuits of neu-

rons on a 2D computer screen requires projecting their 3D shape into 2D. Spatial understanding can only be done by interacting with the data. Virtual reality (VR) provides an immersive viewing and navigation interface for 3D data, enabling more intuitive interactions with complex spatial structures.

Boges et al. [BCM^{*}19, BAS^{*}20] leverage this advantage by proposing a new approach to creating, proofreading, and exploring skeletons of neuronal structures in VR. Representing neurons using skeletons is often more efficient than storing surface meshes due to reduced data sizes while preserving important topological information. Their environment is designed to generate skeletons of neuronal structures represented by surface meshes, quick correction of errors (e.g., branching errors), and efficient quantitative analysis by measuring distances and topological features. They immerse the user in an endoscopic view inside the neuron. A path stabilizing feature automatically places skeleton nodes and edges while navigating through the neuron. Their evaluation reported that the path stabilizer could reduce the number of interactions needed to generate a full skeleton compared to manual skeleton placement.

Usher et al. [UKF^{*}18] present a design study leveraging VR to trace neurons more effectively. Instead of tracing neurons slice by slice in the imaging volume, their tool visualizes segmentation suggestions in 3D. It allows for correcting segmentation merge and split errors using intuitive 3D navigation. Their method applies state-of-the-art data management and large-scale visualization techniques to support data sizes exceeding RAM capacity enabling the use of consumer-level VR hardware. Users reported that fine-tuning segmentations is still challenging in VR. Additionally, the authors observed that tracing errors occurred because users forgot to navigate back to branching points of neurons. McDonald et al. [MUM^{*}21] extend this strategy by adding topological features for user guidance. Their semi-automatic technique computes multiple potential paths that follow a neuron using the Morse-Smale complex (MSC) [GBHP08]. Based on this set of paths, users select a subset that contains the actual path of the neuron. This approach makes neuron tracing more automatic while preserving the advantages of 3D navigation in VR.

5.3. Connectivity Extraction

EM-based imaging remains the gold standard for connectivity analysis. In principle, EM allows the identification of individual synapses, making connectivity analysis more accurate and more data-intensive. However, detecting synapses in EM data is still a significant challenge that needs to be tackled to generate reliable connectivity information. Light microscopy often cannot resolve individual synapses due to limitations in imaging resolution, giving rise to methods that estimate the connectivity between neurons based on statistical rules.

Synapse Annotation. Several segmentation and proofreading tools support the annotation of synapses, where users have to manually or semi-automatically set the location of a synapse and mark their connecting structures [SCHT09, BSL18, ZOYP18]. Additionally, several automatic synapse detection methods have been proposed recently. Huang et al. [HSP18] use a UNET CNN to detect presynaptic structures and a multilayer perceptron (MLP) to find postsynaptic structures. Parag et al. [PBK^{*}18] detect synapse location

and the direction of connectivity simultaneously. A 3D U-net is used for synapse detection and a 3D CNN for result pruning. Lin et al. [LWJ^{*}20] employ an active learning approach to suggest the most informative synapse instances in the unlabeled data given an annotation budget. Other recent automatic synapse detection approaches were proposed by Berning et al. [BBH15], Dorkenwald et al. [DSK^{*}17], and Buhmann et al. [BSMM^{*}21].

All previously presented methods studying brain connectivity rely on many intermediate steps to generate connectivity data. Roncal et al. [GRKV^{*}15] present the first end-to-end pipeline that takes a microscopy image volume as input and outputs a graph of connectivity information. They combine a set of state-of-the-art algorithms for graph extraction. Their pipeline starts by detecting the membranes of neuronal structures [CGGS12]. Next, they create a three dimensional neuron segmentation using Rohana [KVRKB^{*}15], Gala [NIKP^{*}13], or a simple watershed-based algorithm [BM00]. This set of segmentation algorithms computes the nodes (neurons) of the connectivity graph. To find the link between the nodes (synapses), they use a Random Forrest classifier [RPKF^{*}14] to detect synapses in the data set. To optimize their results, they performed a hyperparameter grid search for all used algorithms. They evaluated 1,856 graphs and published the parameter configuration for the best graph obtained when they tested their pipeline on the Kasthuri dataset [KHB^{*}15] (see Table 8.2 for a list of open-source datasets). All parts of the presented pipeline introduce errors that propagate throughout the process. Especially, small spine segmentation errors can lead to larger inaccuracies in the connectivity graphs. To quantify these errors, Roncal et al. [GRKV^{*}15] present two graph quality assessment measures based on the dual graph, called the line graph. Synapses are represented as nodes in the line graph, and neurons indicate edges. First, the Frobenius norm [GVL96] is used to measure the error between the line graph of the ground truth and the line graph of the estimated graph. This measure, however, is unbound and increases with the graph size, which can result in misleading interpretations. The second quality metric leverages the F1 score between the edges of the estimated line graph and the edges of the ground truth line graph. Using this method, true positive edges are represented in the estimated and ground-truth graphs. False positives are only shown in the estimated graph, and false negatives are missing in the estimated graph.

Approximate Connectivity Prediction. In some cases, the resolution of imaging techniques is too low to resolve individual synapses between neurons, such as in light microscopy. In that case, it is harder to make reliable statements about neuron connectivity. Scientists use Peters' rule [RMA17] to predict connections. This rule states that proximity between neurons increases their chance of forming synapses. Swoboda et al. [SMB^{*}14, SMB^{*}17] build on this assumption by proposing a tool that studies connectivity by visually analyzing neuron arborization overlaps. Since displaying all branches of the overlap directly in 3D would lead to a cluttered visualization, they only render glyphs (i.e., small dots color-coding the amount of overlap). Hovering over the glyphs reveals more information about the particular overlap. Arborization overlaps between neurons are computed upon startup of the application within a few seconds. Other research has found that Peters' rule is not accurate and, therefore, proximity between neurons is not enough to predict synaptic connectivity [KHB^{*}15].

Motif Discovery. One way to extract information from large connectivity graphs is to search for common motifs in them [UHM^{*}21]. A graph motif is a recurrent and statistically significant subgraph or pattern of a larger graph and, applied to brain circuits, could give insights into the biological principles of the brain. Optimally, motif discovery techniques should be performed on dense brain tissue reconstructions to ensure that all connections between cells are considered.

Motif discovery algorithms can be categorized in *network-centric* and *motif-centric* approaches [RPS^{*}19]. Network-centric approaches use subgraph enumeration techniques such as the Kavosh algorithm [KAE^{*}09] to list all subgraphs of a certain size in a graph. This approach is computationally expensive but allows identifying common subgraphs without having a prior hypothesis. On the other hand, motif-centric approaches such as *DotMotif* [MRJ^{*}21] require the user to sketch a specific motif first. Then the algorithm searches the graph for instances of that motif. We refer the reader to detailed surveys on graph theory, motif discovery, and subgraph enumeration techniques [RPS^{*}19, YFZ^{*}20].

Song et al. [SSR^{*}05] were among the first to study small motifs in the visual cortex of a rat. Specifically, their network-centric approach investigates how random graphs differ from biological circuits. They apply a statistical motif detection algorithm where a motif is found if its count is higher than the expected count in a random graph. They identify small motifs such as many bidirectional connections in two-neuron circuits. Furthermore, they found an overrepresentation of triangular patterns in three-neuron circuits.

Neuroscientists believe that some psychiatric diseases originate in specific brain wiring patterns [LLS08, BB09]. Vogelstein et al. [VRVP13] propose a method that can help identify these malfunctioning connections and study them in more detail. They study graph classification theoretically and apply their findings to connectomics. Given a set of graphs and their labels, they want to predict a classification for a new unlabeled label graph. By finding so-called *signal-subgraphs*, their method can identify the differences between two graphs by highlighting unique edges. This method enables the comparison of invertebrate brain graphs of different individuals of the same species, such as the *C. elegans*.

Ideally, motif discovery is performed on large subsets of the brain. In that way, motifs spanning different areas of the brain can be identified, and neurons do not get truncated. Scheffer et al. [SXJ^{*}20] present a study of a large portion of the brain of a fruit fly. They study both big and small motifs. They found overrepresented reciprocal connections in small motifs and cliques (i.e., graph structures where every node is connected to every other node) as the most common large motifs.

6. Proofreading

Reconstructing a connectome from high-resolution EM images of brain tissue requires extensive human effort to proofread automatically generated segmentation and synapses. Current automatic segmentation algorithms can handle large and complex datasets that would be infeasible to segment manually with relatively high accuracy. However, these automated methods are still less accurate than

manual expert segmentations. Therefore, during proofreading, scientists identify and correct errors in the automatic reconstruction of their data, a requirement for subsequently extracting the wiring diagram. Even a few incorrect labels or missing synapses could otherwise change the connectivity diagram significantly.

The proofreading workflow can roughly be categorized into three steps [HKBR^{*}14]: First, searching and identifying structures that contain segmentation errors or missing segmentation; second, modifying and correcting the existing segmentation; and third, confirming and verifying the correctness of the modified segmentation.

The most common errors in automatic segmentation data in connectomics are merge errors, split errors, and missing synapse labels. *Merge errors* occur when two separate structures are incorrectly connected and merged into a single segment (i.e., under-segmentation). *Split errors* occur when a single structure is incorrectly split into two separate segments (i.e., over-segmentation). Split errors are typically faster to correct than merge errors, as only the look-up table from segment labels to actual biological structures needs to be updated so that two segment labels correspond to a single biological structure. Therefore, many automatic segmentation algorithms are tuned to slightly over-segment the data (rather than under-segment) to speed up subsequent proofreading. In addition to split- and merge errors, the third type of errors are *missing or incorrect synapse annotations*. This error occurs when synapses are either not detected at all or marked at an incorrect position. Synapse annotations are typically not part of the segmented data but stored as tabular metadata, including the synapse's spatial position, the two structures it connects, and optional data such as inferred synapse strength.

Some proofreading approaches only support the correction of merge and split errors, while other tools focus more on correcting the connectivity based on synapse annotations. In the following, we outline current proofreading approaches, starting with purely manual methods (Sec. 6.1), before outlining semi-automatic (Sec. 6.2) and automatic proofreading approaches (Sec. 6.3), as well as crowdsourced proofreading (Sec. 6.4).

6.1. Manual Proofreading

Manual proofreading tools allow users to change incorrect segmentations. However, they do not offer any automatic support or guidance. This means that all manual segmentation tools discussed in Section 5.2 that allow the user to draw on individual image slices to segment structures in the image can also be used for proofreading (e.g., *Catmaid* [SCHT09], *Viking Viewer* [AMG^{*}11], *WebKnossos* [BBB^{*}17], and *VAST* [BSL18]). In the following, we focus explicitly on their proofreading capabilities. A downside of purely manual approaches is that they neither support the user in finding errors nor do they provide methods to fix erroneous segmentation with minimal user input semi-automatically.

VAST [BSL18] is a widely used segmentation and proofreading tool for EM data that does pixel-per-pixel segmentations. It allows users to draw segmentation masks on top of the displayed slice image and, more recently, even offers support for fixing split- and merge errors. *VAST* is a single-user tool that focuses on voxel-based segmentation masks and manual painting.

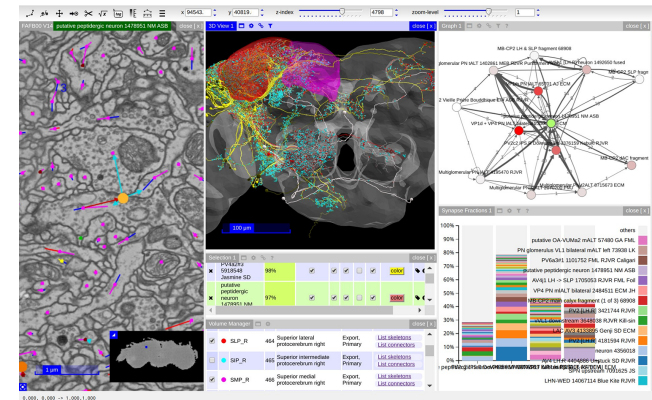


Figure 7: The skeleton tracing interface of *Catmaid* [SCHT09] includes a slice view for adding skeleton elements, a 3D viewer, and an abstract connectivity view.

Instead of working on voxel-based dense segmentations, where every voxel is assigned to a label, several tools focus on quickly reconstructing and proofreading connectivity data. *Catmaid* [SCHT09] is an open-source web-based tool for terabyte-scale image data browsing that also supports collaborative microcircuit reconstruction and annotation. *Catmaid*'s approach focuses on letting users trace skeletons of neurons instead of doing a full pixel-per-pixel segmentation (see Fig. 7). It supports synapse annotation to reconstruct neuronal connectivity and offers several graph views. The *Viking Viewer* [AMG^{*}11] is similarly a collaborative annotation environment for extracting skeletons in terabyte-sized datasets. It supports multi-channel data and creates graphs to display neuronal circuits.

Boges et al. [BCM^{*}19, BAS^{*}20] focus on skeleton-based proofreading in immersive and virtual environments. Users can create or proofread skeletons that were automatically generated by the Mean Curvature Flow (MCS) [TAOZ12] and Centerline Tree (CLT) [SBB^{*}00] algorithm. Proofreading tasks include identifying the main skeleton branch, removing duplicate nodes in highly detailed skeletons, and deleting branching artifacts in the soma area.

6.2. Semi-automatic Proofreading

Semi-automatic proofreading aims to minimize required user input and to speed up and simplify the proofreading process. Most methods focus on the second part of the proofreading workflow, where users correct and adjust merge and split errors (after the errors have been identified).

Mojo [KBRK^{*}13] is one of the earlier proofreading tools for large EM datasets that supports the fast correction of split and merge errors. *Mojo* was superseded by *Dojo* [HKBR^{*}14], which also supports the fast correction of split and merge errors but also offers a web-based multi-user interface to scale up the proofreading process. *Dojo* focuses on simplifying the required user interactions. Split errors can be corrected by simply clicking on the segments that should be merged in the slice view. To correct merge errors, users have to draw the boundary line between the two structures,

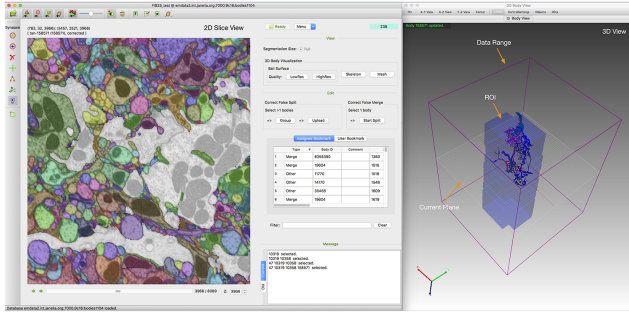


Figure 8: *NeuTu* [ZOYP18] supports the correction of split and merge errors in 2D, while showing an overview of the edits in 3D.

and *Dojo* automatically splits the segmentation into two separate segments by computing a watershed algorithm.

Several tools have been introduced that combine scalable visualization, segmentation, and proofreading. *WebKnossos* [BBB^{*}17] is a web-based framework for visualizing, segmenting, and proofreading large 3D volumes. The tool includes manual brushing and painting and a merger-mode to correct over-segmentation. It supports voxel-based segmentation as well as skeletons and includes task- and project management features akin to *Neuroblocks* [AABH^{*}16] (see Sec. 6.5). *WebKnossos* also offers paid services for annotation, segmentation, and dataset alignment. *NeuTu* [ZOYP18] is an open-source multi-user tool for neuron reconstruction, proofreading, and visualization. *NeuTu* supports the correction of split and merge errors and the annotation of synapses (see Fig. 8). They use a distributed, versioned, image-oriented data service (DVID) [KP19] for fast data access and simultaneous proofreading of multiple users on the same dataset.

6.3. Guided & Automatic Proofreading

In addition to semi-automatic proofreading methods, some guided and automatic methods have recently been proposed. Guided methods identify where segmentation errors are most likely, and help the user find and identify errors quickly. Automatic methods then compute corrections for the identified errors.

Sicat et al. [SHM13] use auto-corrections combined with manual proofreading. The method takes a graph-based approach to compute the midpoints of each segment in each slice and visualize how the midpoint locations propagate through the volume. Spatial outliers are marked as errors and corrected via automatic interpolation and manual proofreading. This simple approach works well for some merge errors but does not account for split errors. For split errors, focused proofreading [Pla16] uses a region adjacency graph across slices to compute affinity scores, leading to a list of potential split errors that can be presented to the proofreader. It builds upon *NeuroProof* [Far20] as its agglomerator and is open source.

Haehn et al. [HKT^{*}18] identify split and merge errors by using a classifier based on a traditional CNN architecture. However, they additionally use a suggestion system to speed up and simplify proofreading. The system loops over potential merge and split error regions that were detected by the classifier. Every error is presented

to the user as a simple binary decision to accept or reject a correction. In a user study, this guided proofreading approach performed better than focused proofreading [Pla16] and semi-automatic proofreading in *Dojo* [HKBR^{*}14].

As opposed to the above approaches that focus on automatic proofreading of voxel-based segmentation, the recently proposed *VICE* system [GWB^{*}21] aims to correct connectivity-related errors. *VICE* helps users recover connectivity pathways by focusing on proofreading local circuits of individual cells. The method uses heuristics derived from actual proofreading scenarios to compute likely connectivity errors by considering predicted synapse locations and presenting the detected error locations to the user in a scalable 3D view. The user can then manually correct these errors.

RLCorrector [NJJ21] takes a completely automated approach to proofreading based on reinforcement learning. The tool can efficiently manage a combination of merge and split errors concurrently by modeling the human decision process in proofreading using a reinforcement agent and combining multiple reinforcement learning agents in a hierarchical manner. Quantitative results indicate that *RLCorrector* is better at correcting split errors than the guided proofreading approach by Haehn et al. [NJJ21], but that Haehn et al. is better at correcting merge errors.

Summarizing, fully automatic proofreading approaches rely on effective automatic error detection and subsequent correction. Several automatic error detection methods have been published in recent years, however, many of them still need to be integrated into larger proofreading frameworks. Current error detection methods rely either on predictions from image data [HKT^{*}18, ZTLS17, RMP^{*}17], skeletonization and graph-based methods [SHM13, Pla16, DPM^{*}18], or biological constraints and heuristics [GWB^{*}21, MHZ^{*}19].

6.4. Crowdsourced Proofreading

Even with semi-automatic and guided methods, proofreading requires extensive human effort for today’s large and high-resolution EM datasets. Crowd-sourced approaches aim to mobilize gamers and citizen scientists worldwide to proofread large datasets. *Eyewire* [Seu12b] was the first crowd-sourced gamified proofreading system. Users are tasked with creating 3D reconstructions of neurons by improving an initial segmentation generated by a deep convolutional network. Users trace each neuron and rack up points based on speed, skill, and accuracy. A leader board compares activities between users and encourages them to compete with other community members. The platform also provides an interactive tutorial to make the onboarding of new users easier. It attracted over 200,000 gamers and led to follow-up studies that investigated player motivation for participating in a community-based science project [TLRSH17].

FlyWire [DMM^{*}22] is a similar crowd-sourced platform that aims to create an open community dedicated to proofreading the neural circuits in a *Drosophila melanogaster* (i.e., fruit fly) brain (see Fig. 9). However, compared to *Eyewire*, which targets non-experts and the general public, *FlyWire* is geared towards a slightly more experienced and knowledgeable audience. Both *Eyewire* and *FlyWire* provide extensive training material for onboarding new

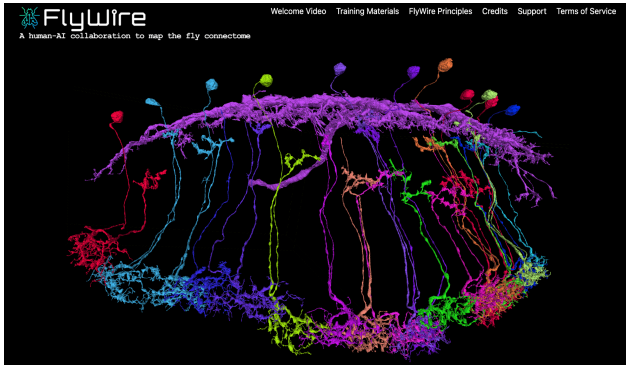


Figure 9: Flywire [DMM^{*}22] is a crowd-sourced and gamified proofreading platform for a fruit fly dataset.

users and proofreaders. *FlyWire* is designed to make edit operations fast and traceable in a many-user environment and ultimately scale up to whole-brain connectomics. *FlyWire* represents the segmentation as a graph of supervoxels. A supervoxel is an atomic group of voxels that is never split. Therefore, merge and split operations can be represented as adding or removing nodes in that graph.

Similar approaches to crowd-sourcing will be necessary to proofread recently acquired large human connectome datasets containing more than a hundred million synapses [SCJB^{*}21].

6.5. Segmentation Provenance and Project Tracking

Manual and semi-automatic segmentation approaches and proofreading of automatic segmentations need considerable human effort. Depending on the data size and user experience, it might take weeks to months to get to a fully segmented and proofread dataset. Since mapping neuronal circuits is time-consuming, it is often done collaboratively. Accordingly, tools like *NeuroBlocks* [AABH^{*}16] help to coordinate these efforts by offering a visualization system for tracking the state, progress, and evolution of very large volumetric segmentation data in neuroscience. Similarly, *WebKnossos* [BBB^{*}17], an open-source annotation, proofreading, and visualization tool, incorporates an annotation task and project management interface and versioning system for user-created annotations. DVID [KP19] is also a cloud-based versioning system for large-scale connectomics segmentation images. Versioning is particularly important when updating automatic segmentations during proofreading.

7. Visual Exploration & Analysis

Imaging and segmentation of connectomics datasets reveal extremely complicated neuronal shapes and neuronal circuits. Automated analysis methods alone are not enough to capture their full complexity and to translate the data into insights for neuroscientists. Therefore, visualization tools are essential to make sense of the available information. These tools need to scale to vast amounts of data and, at the same time, find a good balance between enabling complex analysis while limiting mental load.

In the following, we briefly review essential data structures

specifically designed for organizing heterogeneous image stacks, segmentation data, and metadata for fast data access (Sec. 7.1). We then describe methods for spatial exploration (Sec. 7.2) and connectivity exploration (Sec. 7.3). We categorize spatial data exploration approaches based on segmentation availability and how the segmented data is represented, either as geometry or as volume data. In Sec. 7.4 we describe interactive visualization-based analysis approaches, including neuron shape analysis, spatial neighborhood analysis, as well as visual query systems that combine spatial and connectivity analysis. Finally, we describe current visualization approaches for connectomics that focus on communication and presentation purposes (Sec. 7.5).

7.1. Data Structures for Connectomics

Nowadays, some connectomics data sets already exceed petabytes in size [SCJB^{*}21, YBB^{*}20]. Therefore, visual analysis ultimately depends on efficient and sophisticated data management methods to access imaging and connectivity data.

Data Compression and Multi-Resolution Data Structures. For efficient data storage and access, segmentation volumes can be compressed by exploiting large homogenous segment regions with no natural relationship between segment ids [MHL^{*}17]. This method can reduce data storage of low-frequency segmentation volumes by a factor of 600-2,200x. In addition, efficient rendering of meshes and volumes depends on multi-resolution data structures that reduce the required GPU memory and allow for adaptive resolution changes based on the viewers' distance. For that, either mesh compression techniques [GHS^{*}22], multi-resolution data structures [DFM02, HBWP12] or adaptive rendering methods can be used [GCBM^{*}17].

Connectivity Data. Large connectivity graphs often exceed the size of consumer hardware working memory. Connectivity analysis tools like *NeuPrint* [CDU^{*}20] (see Sec. 7.4.3) build on existing technologies like neo4j's graph querying language *Cypher* [FGG^{*}18], for analyzing neuronal connectivity graphs. Custom data structures for combining connectomics connectivity data with other data modalities have also been proposed. Ganglberger et al. [GKHB20] present a data structure for querying large-scale connectivity matrices. They store voxel-wise connectivity in a spatially organized way using space-filling Hilbert curves [Hil35]. Voxel-wise connectivity represents a single voxel's cumulative connectivity with a volume of interest (VOI). Additionally, connectivity matrices are stored at multiple resolutions. For instance, a single matrix element in a four times downsampled connectivity matrix corresponds to four voxels in the image volume. Connectivity matrices can also be aggregated by brain regions so that one element in the matrix corresponds to all voxels of a brain parcellation. The matrix can be further compressed by only taking non-zero values into account, exploiting sparseness.

Cloud-based Data Stores. The open connectome project (OCP) [BKK^{*}13] provides a scalable database cluster for the analysis of large connectome data sets that is widely used in the connectomics community. The database supports the storage of large-scale imaging volumes, spatially registered image annotations, and metadata. Scalability is achieved by partitioning the volume into cuboids, which are processed on multiple physical nodes.

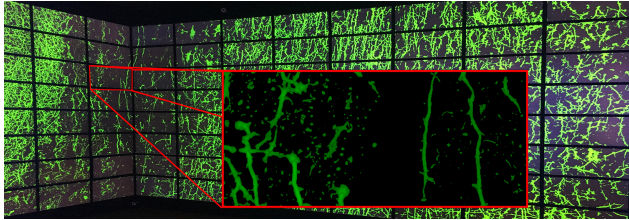


Figure 10: Immersive visualization of a large wide field microscope volume [BJA^{*}19]. © 2018 IEEE. Reprinted, with permission.

Morton-order space-filling curves assign a unique index to each cuboid to ensure similar indices for contiguous regions. Additionally, they store a multi-resolution hierarchy for each volume. The current level of the resolution hierarchy determines the size of the cuboids and the cluster workload. OCP offers an interface to the data through a RESTful API, making the data accessible through web services. GET-requests can extract an arbitrary subvolume from the database and download it to the client for local analysis. The OCP cluster also supports simple metadata queries and is widely used as the data backend in different connectomics applications [VPF^{*}18]. The brain observatory storage service and database (BossDB) [HKG^{*}22] is a newer generation cloud-based data access system for petascale neuroscience imaging datasets. Their spatial database implements a storage hierarchy that manages data transfer between affordable, persistent data storage and an in-memory data storage like Redis. Finally, many modern connectomics research projects [VMH^{*}16, SXJ^{*}20, CBB^{*}21, SCJB^{*}21] opt to store their large datasets in established cloud services such as Google Cloud Storage or Amazon Webservices. For example, CloudVolume [SCK^{*}21] is a serverless client python interface that enables random access to precomputed arbitrarily large image volumes, segmentations, and mesh data.

7.2. Spatial Exploration

Before performing a detailed analysis, scientists often want to get an overview of the available imaging and segmentation data and the structures they contain. This includes looking at slices (cross-sections) or volume visualizations of unsegmented data, or viewing the segmented structures in 3D using either surface meshes or voxel segmentation data. To help users understand the complex spatial shapes of neurons, 3D visualization is essential. Table 7.2.1 gives a summary of different spatial exploration methods.

7.2.1. Unsegmented Data

After data acquisition and registration, connectomics data are not (yet) segmented. In some cases, segmentations are hard to compute due to a lack of sufficient training data, or alternatively labeling structures manually would take too much effort. In other cases, a segmentation is not even needed, and experts prefer exploring the raw imaging data. In these cases, spatial exploration tools for unsegmented volume data are used, where volume rendering typically employs the concept of transfer functions, mapping raw data values to optical properties in order to distinguish different structures.

Light Microscopy Volume Exploration. *FluoRender* [WOCH12,

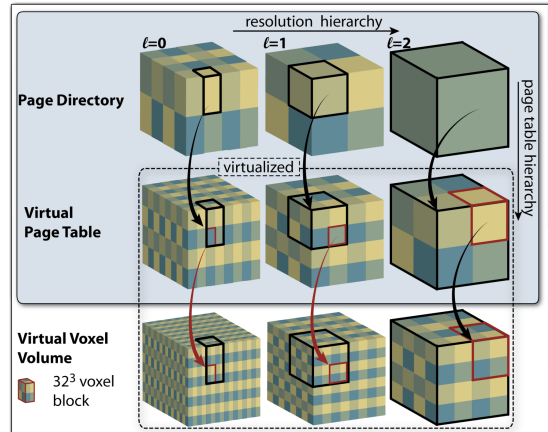


Figure 11: Virtual GPU memory hierarchy [HBWP12] for petascale volume rendering, combining a hierarchy of resolution levels (horizontal axis) with a hierarchy of page tables (vertical axis). © 2012 IEEE. Reprinted, with permission.

[WOH^{*}17] is a framework for visualizing multichannel fluorescence microscopy data that has been used to render neuronal tissue. Structures imaged in up to 100 channels are visualized by exploiting multi-dimensional transfer functions and sophisticated capabilities for channel intermixing. *FluoRender* also provides the possibility for users to perform freehand segmentation guided by the interactive visualization. Boorboor et al. [BJA^{*}19] have introduced a technique to visualize neuronal structures in large light microscopy raw images without the need to apply computationally and performance-wise expensive image deconvolution processing algorithms. Moreover, they maximize visual acuity for visualizing massive brain datasets by deploying their visualizations on an immersive gigapixel-resolution facility [PPKM15] (see Fig. 10).

Large-Scale Volume Visualization. There are several differences that distinguish volume visualization approaches for connectomics EM datasets in comparison to other applications of volume rendering: First, the size of large EM volumes necessitates highly scalable approaches relying on multi-resolution data structures and efficient rendering techniques. Second, EM datasets are often very anisotropic with the *z* dimension being at a much lower resolution than the *xy* plane, which needs special consideration for efficient data storage and to reduce artifacts during rendering.

Hadwiger et al. [HBWP12] tackle the size of petascale volume data via a virtual GPU memory architecture for multi-resolution volume data. Multiple levels of page tables provide full scalability, by also virtualizing the page tables themselves, while supporting output-sensitive multi-resolution rendering via a fully virtualized 3D mipmap structure (see Fig. 11). This basic architecture is more efficient than standard octrees for highly anisotropic datasets such as EM data. Further, the authors propose a visualization-driven pipeline where data loading and rendering is triggered on-the-fly during the ray-casting pass, depending on the current view. Volume bricks are only uploaded to the GPU if the ray-caster requests a missing brick. Furthermore, this approach supports dynamic acquisition of microscope data, as data bricks needed for rendering can be reconstructed at runtime.

Table 1: Visualization approaches for spatial exploration of connectomics data. We classify tools based on data modality, their support for volume rendering (Vol Ren) and whether they display segmentation data as volumes (Vol) or meshes (Mesh).

| | Data | | Vol Ren | Segmentation | | Notes |
|-----------|------|----|------------|--------------|------|---|
| | LM | EM | | Vol | Mesh | |
| [WOH*17] | • | | • | | | general purpose tool |
| [BJA*19] | • | | • | | | enhanced visualization of WF microscopy images |
| [PRL*10] | • | | • | | • | early system for neuron tracing |
| [GBM*21] | • | | • | • | | hybrid rendering for uncertainty of segmentation |
| [WBH14] | • | • | | | • | 3D viewer for SWC skeleton files |
| [MSBS*21] | • | • | | | • | widely used, scalable slice and 3D mesh view |
| [TRFE*16] | | • | | | • | analysis and comparison of pyramidal neurons |
| [HBWP12] | | • | • | | | handles large anisotropic data |
| [BHAA*13] | | • | • | • | | scalable volume rendering for segmented volumes |
| [BAAK*13] | | • | • | • | | interactive visual queries |
| [HAAB*18] | | • | • | • | | efficient empty-space skipping for tubular structures |
| [BMA*19] | | • | • | • | | scalable culling for segmentation volumes |

In addition to standard GPU-based approaches on workstations or GPU clusters, recent web technologies are starting to make terascale visualization within web browsers feasible. Usher and Pasucci have shown that, in principle, a high-performance terascale framework can be built using WebAssembly and WebGPU [UP20]. They combine data streaming and caching, on-the-fly decompression, isosurface extraction from volume data, as well as point cloud rendering into an interactive tool that is able to tackle terascale data sets, including connectomics data.

7.2.2. Segmented Data

Segmented datasets allow targeted inspection of individual neuronal structures and circuits. Therefore, neuroscientists most commonly segment their data to increase analysis and visualization quality. Segmented data is typically stored on a per-voxel basis, resulting in an additional segmentation (or label) volume that stores the segment ID for each voxel. Visualization algorithms can either directly use the labeled voxel data or, alternatively, use pre-computed surface meshes of each labeled structure in the segmentation volume. The advantage of voxel-based segmentations is that they can be easily integrated into the volume rendering pipeline, enabling scientists to glance inside segmented structures and e.g., see cell organelles within segmented neurons. On the other hand, surface meshes are much more compact to store and more efficient to render but only give insight into the outside (i.e., the surface) of a segmented structure. Below, we group different approaches based on whether they (mainly) work on voxel-based segmentation data, surface meshes, or use a combination depending on structure type.

Volumetric (Voxel) Segmentation Data. To handle large, segmented EM data, Beyer et al. [BHAA*13] extended their previous

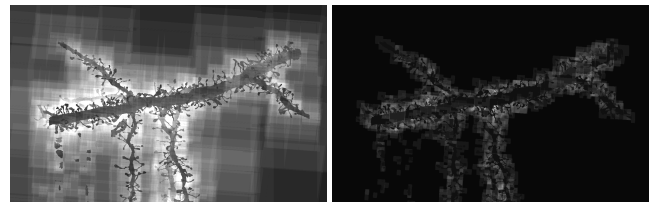


Figure 12: The depth complexity (number of space skipping operations) of standard octree empty space skipping (left) vs. SparseLeap [HAAB*18] (right). Brighter is slower (more operations). © 2018 IEEE. Reprinted, with permission.

virtual memory architecture for raw (unsegmented) petascale volume data [HBWP12] to include petascale segmentation volumes, by adding an additional voxel cache for integer segmentation data.

ConnectomeExplorer [BAAK*13] extends the above frameworks for petascale volume visualization [HBWP12, BHAA*13] with additional metadata for neuronal structures, synapses, and connectivity information. A visual query language then leverages this metadata for the interactive, semantic specification, and visual analysis of correlations between structures of interest. More details of this visual query interface are given in Section 7.4.3.

More recent works aim to further optimize volume rendering performance of large segmented EM datasets by optimizing culling and empty-space skipping strategies. Segmented petascale volumes often contain millions of segmented structures, typically resulting from machine learning algorithms. This large number of labels makes efficient querying and rendering structures of interest challenging. To tackle this problem, Beyer et al. [BMA*19] present a scalable culling architecture that combines probabilistic and deterministic data structures for efficient hierarchical culling (filtering) of segmented connectomics data sets comprising millions of segmented structures. The culling data structure is hierarchical and data-adaptive, choosing the most suitable approach for data representation locally, depending on actual data characteristics, e.g., the number and distribution of integer label values. For fast, output-sensitive culling for visualization, the hierarchical space subdivision also incorporates down-sampled multi-resolution data.

In addition to the large number of objects, connectomics data contain many finely detailed and thin structures, such as axons and dendrites. Rendering these structures fast enough is a tremendous challenge, because traditional empty space skipping techniques for ray-casting incur significant overhead for data lacking large contiguous areas of empty space. To alleviate performance problems due to a fine-grained fragmentation of space caused by fine structures, the *SparseLeap* [HAAB*18] method for empty space skipping combines fast GPU rasterization, modern GPU features introduced for order-independent transparency, and volume ray-casting to achieve better scalability for the visualization of highly-detailed, segmented connectomics data (see Fig. 12). *SparseLeap* interactively adapts to changes in the selected set of neuronal structures, for example due to interactive query evaluation as in the *ConnectomeExplorer* [BAAK*13] framework.

In summary, volume rendering methods for segmented EM datasets all focus on computationally scalable approaches. They

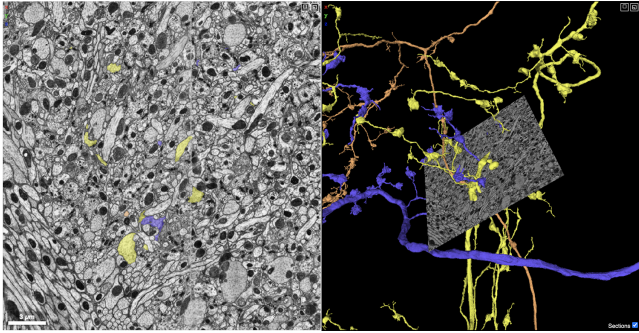


Figure 13: WebGL-based rendering in *Neuroglancer* [MSBS^{*}21] of the FlyEM hemibrain dataset [SXJ^{*}20] showing an EM slice and three out of 25,000 segmented neurons.

build on multi-resolution data structures and visualization-driven pipelines and techniques such as efficient culling and empty space skipping to achieve interactive framerates for rendering datasets containing millions of finely segmented objects.

Mesh Segmentation Data. Displaying segmented connectomics structures as surface meshes is often coupled with slice views of the raw image data, to give users a better context of the data. *Neuroglancer*, for example, is an open-source, web-based viewer for volumetric microscopy and segmentation data built upon WebGL (see Fig. 13). A tile-based architecture supports multi-scale visualization of petascale imaging and segmentation volumes, making it one of the most scalable web-based viewers for connectomics data. Large data sets and segmentation volumes can be stored in cloud services such as Google Cloud Storage. The *Neuroglancer* client subsequently downloads small chunks of the data set for visualization. *Neuroglancer* overlays cross-sectional views of microscopy images with multi-scale 3D surface meshes and skeletons. It is currently one of the most widely used visualization software for large connectomics data sets. However, *Neuroglancer* is designed purely for data viewing and currently does not support any analysis functionality natively. *Sharkviewer* [WBH14] is a minimalistic, web-based interactive visualization library to visualize neuronal skeletons. It is used as a plugin for *NeuPrint* [CDU^{*}20]. Segmentation meshes are the data type of choice for many visual analysis tools in connectomics, as meshes are smaller and easier to handle than segmentation volumes. We will describe these visual analysis tools and their visualization capabilities in more detail in Sec. 7.4.

Mesh and Volumetric Segmentation Data. Several approaches use both, a volumetric and mesh representation of segmentation data, mainly for light microscopy data. *V3D* [PRL^{*}10] was one of the first frameworks for the visualization of gigabyte-scale light microscopy image stacks. It is designed as an extensible software framework, that can be adapted to address different biological problems. The paper demonstrates the configuration of a *V3D* plugin designed to reconstruct neurons. This work was one of the first visual analysis tools for connectomics data that implicitly addressed scalability to data size. They render a lower-resolution representation of the volume once the user interacts with the 3D navigation. Their approach is still limited by the memory size of the GPU but already adds features to increase rendering efficiency. On the other

hand, they contribute a usable way to select an x-y-z location directly from the 3D visualization using only a few mouse clicks. The user must select the desired point in the 3D visualization from two different viewing angles.

More recently, *NeuroConstruct* [GBM^{*}21] has leveraged a hybrid rendering technique to visualize the uncertainty of CNN segmentation results in light microscopy images. It renders areas of high segmentation confidence as isosurfaces, while uncertain segmentations are visualized by direct volume rendering.

7.3. Connectivity Exploration

Since the ultimate goal of connectomics is to reconstruct the complete wiring diagram of a brain to map structure to function, it is essential to provide visual tools for analyzing connectivity information. Connectivity can be studied at multiple levels of detail and in many different ways. Many visualization approaches display a connectivity graph as a node-link diagram where information about neuron shape is lost (e.g., [SCJB^{*}21]), while other approaches still take the morphology of neurons into account (e.g., [AABS^{*}14]). In this section, we focus on visualization methods for neuronal connectivity graphs. We summarize the different methods in Table 7.3.

Node-Link Views. The most straightforward approach to visualizing the reconstructed connectivity is to show the resulting graph. In a neuronal connectivity graph, neurons are represented as nodes, and synapses are abstracted to edges between nodes. Abstracting the imaging data into graphs helps reduce the size of tera- and petabyte data sets. However, any information about cell morphology and spatial relations is lost.

Several tools support node-link diagrams for displaying neuronal connectivity information (e.g., [BAAK^{*}13, AMG^{*}11, SCHT09]). However, these graphs quickly get visually overloaded when the data size increases. Recently, Shapson-Coe et al. [SCJB^{*}21] have imaged one cubic millimeter of human brain tissue at nanoscale resolution, leading to 1.4 petabytes of imaging data. They render the connectivity of specific cells as a simple node-link diagram. The displayed graph is extremely dense, and efficient connectivity analysis remains an open problem at this scale. In addition, humans have proofread only a small subset of neurons, and, therefore, connectivity errors remain. This shows the importance of effective crowd-sourced proofreading (Sec. 6.4).

Many approaches studying neuron connectivity are limited to small but densely segmented subvolumes of the brain. This limits the analysis by considering incomplete reconstructions of neurons that were truncated by the bounds of the volume. Kunst et al. [KLM^{*}19] present the first brain-wide wiring diagram at cellular resolution for vertebrates. Specifically, they acquired over 2,000 sparsely individually labeled neurons and gene expression data in a reference atlas of zebrafish larvae brains. They visualize neuronal connectivity with node-link diagrams and an adjacency matrix. It incorporates features to search for morphologically similar neurons using *NBLAST* [CMO^{*}16] (see Sec. 7.4.1), query neurons based on their trajectory through brain regions, and access metadata of individual neurons.

Other connectivity analysis approaches include diverse imaging

Table 2: Connectivity visualization approaches. We classify tools based on data modality, visualization method, and whether the visualization displays morphological (i.e., structural) information for neurons (Morph. shown). Note, that many tools for neuron tracing or segmentation also include node-link diagrams, but have not been included in this table for brevity.

| | Data | | Vis Method | Morph. shown | Notes |
|-----------|------|----|---|-----------------|--|
| | LM | EM | | | |
| [GSF*19] | • | | node-link | | connectivity queries in multimodal data |
| [SBS*13] | • | | circuit wiring diagram | • | connections based on arborization overlap |
| [MPL*17] | • | | mosaic matrices, mirror glyphs, Kiviat diagrams | | temporal connectivity visualization |
| [BAAK*13] | | • | node-link | | interactive (connectivity) queries |
| [SCJB*21] | | • | node-link | | connectivity graph of 1 cubic millimeter of human brain tissue |
| [KLM*19] | | • | node-link, adjacency matrix | | inter-region connectivity matrix with clustering of similar regions. |
| [CDU*20] | | • | adjacency matrix | | adj. matrix between brain regions |
| [AABS*14] | | • | 2D subway line metaphor | • | multi-scale connectivity exploration and visualization |

modalities to augment connectivity information. For example, spatial gene expression shows the influence of particular genes on specific brain regions. To study the correlations between gene expression and neuron connectivity, Ganglberger et al. [GSF*19] developed *BrainTrawler*. This interactive web application allows querying and analyzing connectivity and gene expression data. Combining these with heterogeneous data sources helps correlate spatial gene expressions to local connectivity patterns. *BrainTrawler* organizes connectivity information at different levels of scale. While neuron-based connectivity helps to understand circuits at the lowest level, analyzing connectivity between brain regions is also supported. A custom data structure [GKHB20] maintains interactivity and fast querying of multiscale and multimodal data (see Sec. 7.1).

Abstract Connectivity Views. In contrast to standard node-link views, several visualization approaches have looked at brain connectivity from different angles.

For instance, *Neurolines* [AABS*14] uses a subway map metaphor to simplify connectivity analysis in the connectome (see Fig. 14). The complex shapes of neurons make connectivity analysis in 3D complicated due to visual clutter. Therefore, *Neurolines* projects the 3D skeleton of neurons into 2D while preserving neuron topology and relative distances. Hovering over synapses on the skeleton reveals additional information, such as a view of the original EM data and the abstracted skeleton of the connecting neuron. To enable a scalable analysis of connectivity in large brain volumes, *Neurolines* offers multiple levels of abstraction in different views.

Based on confocal light microscopy images, *NeuroMap* [SBS*13] has employed circuit wiring diagrams to represent all possible connections of neurons in the fruit fly (*Drosophila melanogaster*) brain. The more overlap the arboriza-

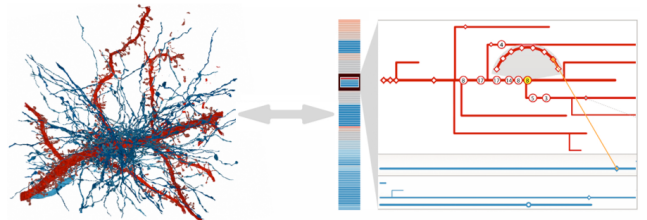


Figure 14: *Neurolines* [AABS*14] projects the complex topology of neurons and their connections to 2D using a subway map metaphor. © 2014 IEEE. Reprinted, with permission.

tions of two neurons have, the more likely it is that they form a synapse between them [BS13]. *Neuromap* abstracts the different elements of neurons, such as the cell body, arborizations, and projections, into a graph structure. This graph is then used to visualize the overlap of arborizations in a modified node-link diagram, which is further augmented by highlighting different brain regions and allowing details on demand. *RemBrain* [MPL*17] also operates on light microscopy data but tracks temporal connectivity by using mosaic matrices, Kiviat diagrams, and glyphs. *RemBrain* is based on the previous visualization method *Swordplots* [MFL*16].

Finally, matrix views showing the connectivity between brain regions are heavily popular in macro-scale connectomics. For nanoscale EM data, *NeuPrint* [CDU*20] employs a matrix view for visualizing the connectivity between brain regions in the fruitfly brain. Generally, matrix views and abstract connectivity views scale better to large graphs than node-link diagrams. However, interactive querying and analysis tools for large graphs are essential to explore and understand the data in detail, which will be discussed in the following section.

7.4. Visualization-Focused Analysis

One of the final steps in the connectomics pipeline consists of the visual and quantitative analysis of the initially explored data. This step relies on the combined spatial data analysis in correlation to connectivity data. Furthermore, this step requires interactive means for querying the data to enable neuroscientists to generate and test hypotheses in petabyte-scale data more efficiently. We summarize methods for visualization-focused analysis in Table 7.4.1.

7.4.1. Neuron Analysis

Neuron Quantification. In addition to displaying the raw spatial data, some tools augment visualizations with numerical features for a more quantitative analysis of the complicated 3D structure of neurons. Several proposed works quantify neurons and neuronal shapes or compute pairwise comparisons between neurons.

For instance, Al-Thelaya et al. [ATAG*21] use a shape descriptor to quantify and classify 2D/3D nuclei shapes. Their descriptor measures the discrete curvature along closed and resampled contours of the shape. In addition, it is invariant to translation, rotation, and parameterization. They use 3D meshes of brain cell nuclei to compute a feature vector to evaluate the performance and train a support vector machine (SVM) using radial basis functions to predict cell types. They found that neuron nuclei form different

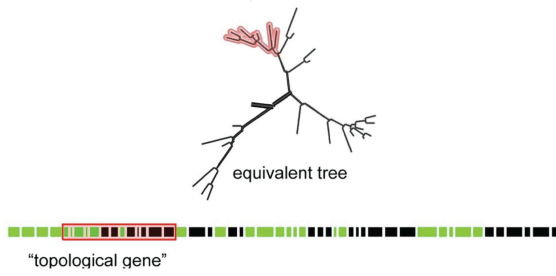


Figure 15: 1D "barcode" visualization of the hierarchical tree layout of neurons [CFBH10]. Black segments refer to terminal segments, while green segments start and end at a branching point.

clusters per cortical layer, making it hard to generalize cell type classification for all neurons.

Instead of only characterizing soma, *NBLAST* [CMO*16] is a technique for the quantitative pairwise comparison of full neurons. It uses spatial location and branching patterns to compute a similarity score. *NBLAST* divides the query and target neuron into small segments, each storing a spatial location and a tangent vector. For each segment, the nearest neighboring segment is found (using the Euclidean distance), and their tangent vectors are compared. *NBLAST* uses both Euclidean distance and the dot product of the tangent vectors to compute the similarity score. *NBLAST* can identify biologically meaningful neuronal clusters among different data modalities and has been used to identify the same neuron in light microscopy and EM datasets. Furthermore, a similarity score can be computed efficiently on consumer-level hardware without training time. Schubert et al. [SDJ*19] use cellular morphology networks (CMNs) for the automatic quantification of neuronal shapes. Their method creates morphology embeddings (Neuron2Vec), which were used to detect glia cells in high-resolution EM data and to identify segmentation errors.

Interactive Neuron Analysis & Visualization. While the above approaches for neuron quantification aim to automatically provide results such as similarity scores or cell type predictions, a different, more user-centric approach is followed by interactive, visual neuron analysis tools. Recently, *ZeVis* [CHM*21] has made the interactive visual analysis of cell nuclei morphology and their distributions possible. EM segmentations of nuclei can be compared interactively and filtered by brain region or specific shape attributes. They visualize nuclei distributions using 3D histograms and their locations using 2D multi-axis views. For the purpose of nuclei analysis and model training, Lin et al. [LWP*21] and Mu et al. [MYT*21] provide a dataset containing around 170,000 nuclei segmentations.

Instead of the analysis of cell nuclei, *PyramidalExplorer* [TRFE*16] focuses on the visual analysis of pyramidal neurons, a specific neuron type. Pyramidal neurons [DF92] exhibit long branches spanning multiple cortical areas. *PyramidalExplorer* not only has data viewing capabilities but also supports morphological data analysis. For instance, numerous quantitative attributes for each spine are extracted, such as volume, surface area, position, and maximal diameter. Spines can be color-coded according to selected morphological features. They can also be inspected in detail in a separate 3D view. *PyramidalExplorer* implements a

content-based information retrieval system (CBIR). A signature is computed based on a user-defined data selection and used to compare different data selections. For instance, a neuron signature is a numerical score based on spine attributes. This helps to query the data set for similar pyramidal neurons.

In comparison, Pastor et al. [PBB*21] use more high-level and natural features to quantify the spatial shapes of neurons. They build on a set of existing tools [PMT*15, GCBM*17, TRFE*16] to develop a unified framework for morphological neuron analysis at different levels of abstraction. Their framework provides high-level abstract representations of the trajectory of neurons through different cortical layers. When studying neuronal morphology in greater detail, the tool allows for comparing quantitative features of small neuronal structures, such as dendritic spines. For instance, users can visualize juxtaposed 3D models of spines and sort them based on spine length, volume, surface area, or any other feature that has been extracted from the data in a preprocessing step. In comparison, *NeuroMorphoVis* [AHE*18] supports a broader set of tasks from morphological skeleton and soma analysis to neuron data handling and generation of high-quality renderings. Cuntz et al. [CFBH10] propose a method to summarize the neuronal branching pattern in a 1D "barcode" visualization (see Fig. 15). They use the hierarchical tree structure of neurons and identify all branching and terminal points of the skeleton. Each segment of the tree is visualized as one section in the barcode. The length of the section directly relates to the length of the segment in the skeleton. Green sections start and end at branching points, and the black sections indicate a terminal segment. The neuron analysis & visualization (*Navis*) python library [SBJ*21] builds on top of *natverse* [BMJ*20] is designed to analyze and visualize neuron morphology. It implements state-of-the-art algorithms such as pairwise neuron comparison with *NBLAST* [CMO*16], neuron simplification tools, and advanced neuron plotting algorithms. By labeling branches in the neuron trees by their distances to the soma, simplified 2D versions of neurons skeletons are visualized. *Navis* functionality is based on an interface for programmatic access to the FlyEM [XJL*20] data set. Neuron skeletons used in *Navis* can be generated using the *kimimaro* python library [SBLW21]. *Kimimaro* rapidly generates skeletons from dense segmentation volumes. It implements a TEASAR-derived algorithm [SBB*00]. *Neuromorph* [JNC*15, JBK18] also supports the morphological analysis of neurons, but instead of a programmatic python interface, it is integrated into the 3D modeling software Blender. Therefore, users have a visual interface for extracting distances or labeling parts of neurons such as spines.

While previous approaches [SBJ*21, CMO*16, SCK*21, JBK18] focus on specific properties of neuronal morphology, *SNT* [AGE*21] generates streamlined connectivity diagrams and combines multiple quantitative attributes of neurons to study how they broadcast information between brain regions. For instance, they extracted the normalized cable length and the number of axonal endings in the MouseLight database [WBF*19] to identify the number of brain areas innervated by a particular cell.

7.4.2. Neighborhood Analysis

Spatially imaging the brain at a high resolution lets researchers conclude about connectivity between neurons and helps them understand the interactions of neurons with other cell types. This is

Table 3: Visualization-focused analysis approaches. We classify tools based on data modality and the type of analysis they support: Neuron Analysis (Neur. A.), Neighborhood Analysis (Nbh. A.) or Interactive Queries (Qu.).

| | Data | | Neur. A. | Nbh. A. | Qu. | Notes |
|-----------|------|----|-------------|------------|-----|---|
| | LM | EM | | | | |
| [AGE*21] | • | | • | | | quantification of neuronal anatomy |
| [AHE*18] | • | | • | | | morphology analysis of neuronal skeletons |
| [TRFE*16] | • | | • | | • | visual analysis of pyramidal neurons |
| [BSG*09] | • | | | • | • | semantic, spatial & neighborhood queries |
| [ATAG*21] | • | • | • | | | Shape descriptor for cellular nuclei |
| [PBB*21] | • | • | • | | | multilevel navigation |
| [CFBH10] | • | • | • | | | 1D barcode visualization of neurons |
| [SBJ*21] | • | • | • | | • | neuron plotting and morphological analysis |
| [SBLW21] | • | • | • | | | neuron skeletonization |
| [CMO*16] | | • | • | | | pairwise neuron similarity computation without training |
| [SDJ*19] | | • | • | | | neuron morphology embeddings |
| [CHM*21] | | • | • | | | cell nuclei analysis |
| [JBK18] | | • | • | • | | neuron analysis in Blender |
| [MAAB*18] | | • | | • | | glia and neuron interactions |
| [TCG*22] | | • | | • | | scalable comparison of neuronal spatial neighborhoods |
| [ACA*19] | | • | | • | | interactive glycogen absorption analysis |
| [CBH*15] | | • | | • | | immersive analysis of glycogen clusters |
| [ABG*18] | | • | | • | | immersive analysis of metabolic processes |
| [CDU*20] | | • | • | | • | interactive queries of the FlyEM hemibrain |
| [BAAK*13] | | • | • | | • | query algebra for large EM data volumes |

important because support cells and the location and size of cell organelles like mitochondria also influence neuronal function. Most spatial neighborhood analysis focuses on the relationship between glia cells and neurons. Glia cells spatially surround and insulate neurons and support them. Mohammed et al. [MAAB*18] propose *Abstractocyte*, a visual tool to study the interaction between astrocytes and neurites in EM volumes interactively. Astrocytes are special star-shaped glia cells. The tool allows for the interactive abstraction of astrocytes and neurites to simplify their complex shapes. The user interactively sets a point in a 2D abstraction panel to select the abstraction level for neurons and astrocytes. The horizontal coordinate determines the abstraction of the neurite, while the vertical axis sets the astrocyte abstraction. In addition, *Abstractocyte* allows for spatial queries and clustering of glycogen granules. While *Abstractocyte* focuses on the visual exploration of interactions between astrocytes and neurites only, Troidl et al. [TCG*22] propose a more general method to explore spatial neighborhoods of neuronal structures. Their tool, *Barrio*, integrates a scalable approach for comparing multiple spatial neighborhoods using juxtaposed spatial 3D views and abstract 2D InfoVis views.

Similarly, Agus et al. [ACA*19] study the energy metabolism in

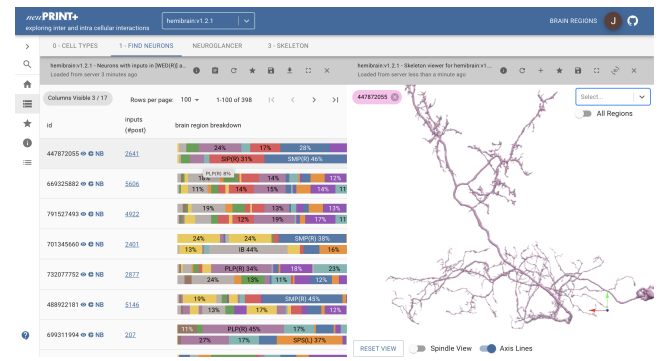


Figure 16: The NeuPrint web application [CDU*20]. The left column shows neurons with inputs from brain region A and outputs from brain region B. Two stacked bar charts are displayed for each neuron, visualizing the distribution of brain regions from the inputs (top chart) and outputs (bottom chart). The right column shows an interactive 3D rendering of a neuron skeleton.

neuronal tissue using astrocytic glycogen granules, visible in high-resolution EM images. They follow a more quantitative approach than [MAAB*18] and model energy absorption with a glycogen absorption map. This map stores potentially absorbed energy for each position in the volume. They augment connectivity information shown as a node-link diagram with the energy absorption map and incorporate it into a 3D volume rendering view.

Immersive Neighborhood Analysis. Neighborhood analysis also suffers from limitations of the 2D screen to display complex spatial structures. Therefore, researchers have experimented with immersive technologies to offer a more intuitive perspective on spatial data. Cali et al. [CBH*15] use VR to study the distribution of glycogen granules inside astrocytes. The cloud of glycogen granules seemed random when looking at conventional 3D renderings on 2D screens. However, VR helped them to identify clusters in the distribution of glycogen, which they later could automatically detect using the DBSCAN-algorithm [EKS*96]. Based on this observation, they conducted a quantitative analysis of the spatial relationship with the clusters to pre- or postsynaptic elements using the *Neuromorph* Blender integration [JNC*15, JBK18].

To study the metabolic support of astrocytic glycogen granules on neurites in even greater detail, Agus et al. [ABG*18] compute a glycogen-derived lactate absorption map (GLAM). The amount of absorbed energy depends on the size of the glycogen granule and its distance to the neurite. They experiment with displaying the absorption maps combined with 3D reconstructions of neurites in a VR environment. In evaluating their method, the authors report that users find analyzing GLAM-based visualization in VR at least as valuable as using a desktop setup. Especially when analyzing color-mapped data, users preferred the VR setup over a standard visualization on a 2D screen.

7.4.3. Visual Query Interfaces

Interactive analysis and query systems are essential for investigating today's large connectomics datasets. Neuronal datasets and connectivity graphs are so large and complex that looking at all

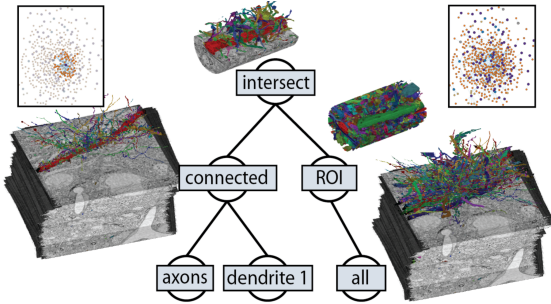


Figure 17: *ConnectomeExplorer* [BAAK^{*}13] enables interactive queries on petascale volumes, using a set-based algebra and hierarchical queries. © 2014 IEEE. Reprinted, with permission.

parts of the data is quickly becoming infeasible. Therefore, scientists need ways to find interesting areas in their data, filter quickly, and query data to test their hypotheses.

NeuPrint [CDU^{*}20] is an analysis ecosystem that uses existing graph databases such as neo4j to organize connectivity graph data at different abstraction levels. *NeuPrint* tightly integrates an interactive web application for viewing and querying connectomics data. It shows an adjacency matrix to visualize the connectivity between brain regions. Each element in the matrix shows the number of connections between brain region A and brain region B. By selecting a matrix element, users see detailed information about the neurons connecting these two brain regions (see Fig. 16). Individual neurons can be selected, and their skeletons are visualized in 3D. Additionally, *NeuPrint* displays an overview for each neuron, showing from which brain region input neurons (top row) come and to which brain regions outputs (bottom row) go, as two stacked bar charts (see Fig. 16). *NeuPrint* users can also query connectivity information using the established Cypher language [FGG^{*}18].

In comparison, *BrainGazer* [BSG^{*}09] focuses more on querying neuronal structures based on spatial features instead of connectivity information. It combines a direct volume rendering (DVR) approach with three types of visual queries in the fruit fly's brain. Semantic queries are initiated by clicking on an object, and if objects are occluded, clicking multiple times flips through all of them. Object queries allow searching the proximity of neuronal structures for interesting features. To do so, *BrainGazer* computes the closest distances between all objects and allows filtering the neighborhood of a specific object for other close objects. Finally, path queries select an arbitrary region in the brain using a freehand drawing selection tool. The selected region, including all selected objects, is loaded into a view. This querying method allows for more accurate capturing of anatomical areas than rectangular or circular selection tools. *BrainGazer* precomputes lookup volumes and distances tables to efficiently access close objects. Data used in *BrainGazer* was reconstructed from confocal microscopy images.

ConnectomeExplorer [BAAK^{*}13] combines both spatial and connectivity queries with a high-performance 3D interactive visualization framework of segmented EM volumes. It implements a query algebra that allows users to filter and search the data interactively, using efficient hierarchical query evaluation (see Fig. 17). The tool supports three types of queries: *Spatial queries* allow

searching neighborhoods of neuronal structures in a region of interest (ROI), *topological queries* help study neuronal connectivity, and *attribute queries* allow searching automatically or manually labeled attributes of neurons, such as the number of spines or the number of ventricles in a cell. To efficiently query large volumes of brain tissue interactively, *ConnectomeExplorer* uses hierarchical and multi-resolution data structures.

7.5. Visualization for Communication

Most visualization tools for connectomics focus on proofreading, exploration, and analysis of the data. However, initial research has been done on visualization for communication purposes in connectomics in recent years. *Brainrender* [CTP^{*}21] is a python-based open-source interactive 3D viewer for anatomically registered data. *Brainrender* aims to generate publication-ready, high-quality illustrative visualizations with minimal programming requirements. The main goal is to support the visualization of data registered to any anatomical atlas. This is achieved by tightly integrating the tool with the BrainGlobe Atlas [CPT^{*}20], which provides a unified interface to many publicly available reference atlases. Visualization with *Brainrender* is not limited to microscale data of single neurons but combines data of different scales and imaging modalities.

8. Public Data Sets and Open Source Tools

Connectomics relies heavily on open science [Fre15]. Data acquisition, storage, and processing requires tremendous efforts and resources, which is only feasibly for some larger research labs and their industrial partners. Therefore, other researchers depend on publicly accessible data and tools to test their own hypotheses. This section gives an overview of the most relevant data sets and open-source tools developed and maintained by the scientific community.

8.1. Data Sets

We summarize openly available connectomics data sets and their key characteristics in the following. All datasets are listed in Table 8.2. Furthermore, the Open Connectome Project [BKK^{*}13], the Neuro Data Register [Neu], and BossDB [HKG^{*}22] host a number of different connectomics datasets, both for light microscopy and EM. Similarly, the website NeuroMorpho [Uni] hosts digitally reconstructed neurons and glia associated with peer-reviewed publications. Bonney et al. [BCSH^{*}22] recently surveyed publicly available EM datasets to study microvascular structures in the brain.

Light Microscopy. While light microscope data sets require much less memory space than EM and often do not have extensive segmentation masks, they still provide a valuable resource for neuroscientists. The DIADEM challenge [BBC^{*}11] has produced six online available light microscope data sets, each imaging a few neurons. They were intended as training data for neuron segmentation algorithms. Here, we explain two of these data sets in more detail. The cerebral climbing fiber dataset contains three image stacks of neurons in a rat brain, and the rat hippocampal CA3 interneuron data set includes two neurons each in an imaging stack. Weiler et al. [WCV^{*}14] used fluorescence microscopy to image over six million cubic microns of cortical mouse brain tissue, stained with

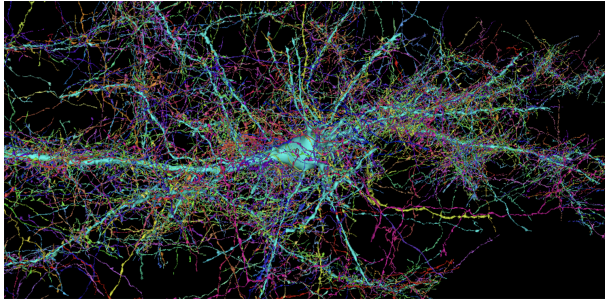


Figure 18: 4k incoming connections on a pyramidal cell in the H01 dataset [SCJB*21] visualized in Neuroglancer [MSBS*21].

synaptic proteins and at synaptic resolution. Bloss et al. [BCK*16] used both light microscopy and array tomography to image synaptic connectivity between interneurons and pyramidal cell dendrites.

EM. Recently, Shapson-Coe et al. [SCJB*21] released the H01 data set, which covers one cubic millimeter of human brain tissue imaged with EM (see Fig. 18). The data set is densely segmented, including approximately 100 proofread cells. With 1.4 petabytes of data, it is the largest connectomics data set published so far. Still, the data set only covers a small fraction of the human brain. Larger brain volumes are required to fully capture neuronal circuits that span over long distances, especially for motif discovery.

The FlyEM hemibrain [XJL*20] data set covers approximately half of the fruit fly brain and includes segmentations. Compared to the H01 [SCJB*21] data set, it contains more proofread cells. Therefore, it is currently considered the data set of choice for motif discovery. Similarly, Zheng et al. [ZLP*18] imaged the whole brain of the fruit fly with initially only a small subcircuit segmented. However, this data set is currently in the process of being completely segmented and proofread using the crowdsourced *FlyWire* platform [DMM*22]. The FANC dataset [PHG*21] is a sparse connectome of an adult fruit fly. All neurons and synapses involved in controlling leg and wing movement have been reconstructed. The MICrONS data set [CBB*21] contains one cubic millimeter of brain tissue of a mouse. It combines EM images with functional recordings of visual stimuli of 75,000 neurons, making it the largest multimodal connectomics data set so far. Its smaller predecessor data set is also available online [SMBC*20, DTM*21]. In 2015, Kasthuri et al. [KHB*15] collected 660 GB of EM images of a mouse’s neocortex with partial segmentation. Wei and Lin [WLFB*20, WLL*21, LWP*21] made proofread segmentation volumes for axons, mitochondria and cell nuclei publicly available.

8.2. Open Source Software Tools

Table 8.2 lists the most relevant open source software tools for connectomics and also links to related Github repositories, websites and documentation. We focus on open-source and ready-to-use tools and software packages.

9. Future Research Directions

Connectomics research is a young subfield of neuroscience currently entering an exciting phase. The size of new data sets is grow-

ing continuously every year, allowing insights into larger and larger subvolumes of the brain. Even a full connectome reconstruction of a fly brain is now within reach [DMM*22].

From here, a plethora of opportunities for novel visualization research arises. Below, we highlight the areas that we think would benefit most from novel visualization approaches, including scalable and combined proofreading and visual query systems, multi-scale connectivity analysis, visual functional pathway exploration, and the visual fusion of multimodal data and living tissue data.

9.1. Scalability

Connectomics data sets have increased from terascale to petascale within the last decade due to advances in image acquisition. Neuroscientists even predict that a full brain connectome of a mouse will likely be reconstructed within a decade [SCJB*21, ABC*20]. Therefore, scalability will remain the main research focus for each step in the connectomics pipeline, including visualization.

Many of today’s large data sets are stored remotely on the cloud, and users download only small chunks on demand. However, to support interactive web-based visualization and analysis applications, scalable data formats are needed that support compressed storage and interactive access and provenance tracking of segmentations and concurrent multi-user access. These features will allow researchers to integrate proofreading and subsequent updating of the segmentation data into large-scale visual query and analysis systems and further streamline the connectomics pipeline.

Furthermore, to make the segmentation and proofreading of even larger datasets feasible, new approaches are needed that are inherently scalable. Segmentation algorithms will continue to be imperfect, therefore, better human-AI collaboration is the way forward to create usable connectome reconstructions. Dorkenwald et al. [DMM*22] present the first step in this direction, where an automatically generated segmentation is continuously updated through crowd-sourced human proofreading. New segmentation algorithms should also be aware of their limits and forward complex cases automatically to a human proofreader [JKL*18]. Likewise, visualization research should consider how to design these human-AI interactions to support the reconstruction of large volumes in a reasonable amount of time.

9.2. Large Connectivity Graph Exploration

Connectomics data allows researchers to evaluate actual wiring diagrams and discover the fundamental principles in neural circuit architectures. However, the community is still in dire need of connectivity analysis methods that explore neuronal connectivity at different scales, ranging from small, local synaptic motifs to higher-level connectivity patterns involving neurons in several cortical layers. This should be approached as a multi-scale problem, where different solutions are needed for varying levels of detail in the data.

Tools for motif querying for these data sets are just beginning to be developed [MRJ*21], and currently, all require an intuition about a particular type of motif. Subgraph enumeration techniques provide a promising direction to find connectivity motifs without any prior hypotheses. Visualization research can help find ways to

Table 4: Commonly used and publicly available connectomics data sets.

| Name | Sample | Modality | Physical Size | #Neurons | Synapses | Reference | |
|-----------------|-------------------|----------------------------------|---|-------------------------------|--------------------------------|-------------------|----------|
| Climbing Fibers | Rat | LM | 200 μm^3 | 3 | not imaged | [BBC*11] | |
| CA3 interneuron | Rat | LM | 200 μm^3 | 2 | not imaged | [BBC*11] | |
| Weiler et al. | Mouse | LM | $6 \times 10^7 \mu\text{m}^3$ | not imaged | stained with synaptic proteins | [WCV*14] | |
| Bloss et al. | Mouse | array tomography TEM | $1 \times 10^6 \mu\text{m}^3$ | immunolabeled | immunolabeled | [BCK*16] | |
| H01 | Human | mSEM | 1mm ³ | 57K | 133.7 M | [SCJB*21] | |
| MICrONS 1 | Mouse | two-photon calcium imaging & TEM | $1.4 \times .87 \times .84 \text{ mm}^3$ | 120K | 523 M | [CBB*21] | |
| MICrONS 2 | Mouse | two-photon calcium imaging & TEM | $250 \times 140 \times 90 \mu\text{m}^3$ | 334 | 3.2 M | [DTM*21, SMBC*20] | |
| Kasthuri et al. | Mouse | SEM | 1500 μm^3 | 1897 | 1700 | [KHB*15] | |
| Fly Hemibrain | Fruit Fly | FIB-SEM | $250 \times 250 \times 250 \mu\text{m}^3$ | 25K | 20 M | [XJL*20] | |
| FAFB | Fruit Fly | TEM camera array (TEMCA) | $8 \times 10^7 \mu\text{m}^3$ | 120 | only small subset segmented | [ZLP*18] | |
| Neuromorpho | 16 species | various | various | various | various | [Uni] | |
| OpenConnectome | various | various | various | various | various | [BKK*13] | |
| DIADEM | various | various | various | various | various | [BBC*11] | |
| MitoEM | Rat & Human | multibeam SEM | $2 \times 30 \mu\text{m}^3$ | 40K mitochondria | not segmented | [WLFB*20] | |
| AxonEM | Rat & Human | EM | $2 \times 30 \mu\text{m}^3$ | various | 18K axons | not segmented | [WLL*21] |
| NucMM | Zebrafish & Mouse | EM & micro-CT | 0.1mm ³ 0.25mm ³ | 170.000 nuclei & 7.000 nuclei | not segmented | [LWP*21] | |
| FANC | Fruit Fly | TEM | 0.023 mm ³ | >1000 motor & sensory neurons | | [PHG*21] | |

intuitively specify complex connectivity motifs and visualize them effectively in both abstracted form and 3D. Visualization research can help find interactive and scalable ways to reduce the complexity and dimensionality of connectivity motifs. Future research also needs to investigate integrating more complex attributes into motif queries such as cell shape, brain region, and other topological information. Furthermore, how to query large sets of connectivity subgraphs for meaningful motifs remains an open question.

In addition, more visualization research is needed to develop methods for the interactive exploration and analysis of large neural wiring diagrams, supporting multi-scale connectivity analysis, and the combined analysis of highly detailed spatial image data and large-scale connectivity data. Furthermore, with novel datasets that contain pre- and post-synaptic information, the visual exploration of functional connectivity is now becoming possible. Therefore, the visual analysis of synaptic chains in the data based on morphological image features such as synapse strengths and the underlying synaptic network is important for future research.

9.3. Multimodal Data Sources

Both optical imaging and EM come with specific drawbacks. EM requires complex staining and can only image dead tissue, while light microscopy is limited in its resolution. Both imaging technologies complement each other, and it is beneficial to use the best of both worlds. Functional data has been combined with EM [CBB*21], and also saturated reconstructions of living brain tissue at nanoscale resolution has succeeded recently [VMM*22].

These advances raise exciting questions, also for the data visualization community. How can we visually augment large brain circuits with functional data? And how can we display changing connectivity patterns in living tissue over time? Combining multiple data modalities will lead to new research in registration algorithms, e.g., when combining the same tissue imaged with optical microscopes and EM. When imaging living tissue in high resolution, neurons and cell organelles move through the volume. Computer scientists will need to develop new methods to identify interesting regions of change and to track structures over time. Finally, how can we interrogate these multimodal and multidimensional connectomics datasets efficiently? Domain-specific query languages [BAAK*13] and techniques for intuitive visual user guidance are promising approaches and could allow neuroscientists to bridge the gap between visual analytics and hypothesis generation.

10. Discussion and Conclusions

Connectomics data provide potential answers to many questions about neural circuits that were not addressable previously. However, the challenge of approaching these questions is that connectomics data is not readily amenable to analysis, given its size and complexity. Until connectomics data began to be generated, neuroscientists would propose neuron structures and circuit architectures drawn as simple cartoon diagrams. Invariably, however, these models are vastly oversimplified compared to actual neurites and synapses in large-scale connectomics data. In this sense, large-scale connectomics data offers a paradigm shift by giving researchers, for the first time, the opportunity to evaluate actual wiring diagrams

Table 5: Open source tools for connectomics. We categorize each tool’s focus as either A & R (Alignment & Registration), SEG (Segmentation), EXP (Exploration), or ANL (Analysis). We report on multi-user support (MU) and link to each tools’ website and source code.

| Name | Focus | | | | | MU | Details | Source Code | Reference |
|----------------|-------|-----|----|-----|-----|----|--|----------------------------|-----------|
| | A&R | SEG | PR | EXP | ANL | | | | |
| BigStitcher | • | | | | | | large scale image alignment + rendering | Github | [HRRP*19] |
| TeraStitcher | • | | | | | | large scale image stitching | Github | [BI12] |
| MIST | • | | | | | | stitching of large 2D image grids | Github | [CMB*17] |
| TrakEM2 | • | • | • | | | | image registration, annotation & segm. | Github | [CSS*12] |
| Vaa3D | • | • | | • | • | | visualization assisted analysis | Github | [BIP15] |
| FluoRender | • | | • | • | | | confocal microscopy data analysis | Github | [WOH*17] |
| Kimimaro | | • | | | | | automated skeleton extraction | Github | [SBLW21] |
| Ilastik | | • | | | | | object classification, counting & tracking | Github | [BKK*19] |
| NeuTu | | • | • | • | | • | neuron reconstruction & visualization | Github | [ZOYP18] |
| Paintera | | • | • | • | | | neuron segm., reconstr. & proofreading | Github | [ZOYP18] |
| WebKnossos | | • | • | • | | • | cloud-based 3D annotation | Github | [BBB*17] |
| VikingViewer | | • | • | • | | • | terascale annotation | Github | [AMG*11] |
| CatMaid | | • | • | • | | • | collaborative annotation | Github | [SCHT09] |
| VAST | | • | • | • | | | volume annotation & segmentation | Executable | [BSL18] |
| PyTC | | • | | | | | deep learning-based neuron, synapse and organelle segmentation | Github | [LWLP21] |
| FlyWire | | | • | | | • | crowd sourced proofreading | Github | [DMM*22] |
| Dojo | | | • | | | • | semi-automatic collaborative proofreading | Github | [HHM*17] |
| Neuromorph | | | | | • | | proximity analysis & center line extraction | Github | [JBK18] |
| DotMotif | | | | | • | | neuronal motif search | Github | [MRJ*21] |
| NeuPrint | | | | • | • | | connectivity exploration & analysis | Github | [CDU*20] |
| Brainrender | | | | | • | | data communication | Github | [CTP*21] |
| Neuroglander | | | | | • | | large scale volume visualization | Github | [MSBS*21] |
| NeuVid | | | | | • | | video generation | Github | [Hub22] |
| SharkViewer | | | | • | • | | 3D skeleton viewing | Github | [WBH14] |
| NaVis | | | | • | • | | Neuron comparison & visualization | Github | [SBJ*21] |
| natverse | | | | • | • | | Neuroanatomical data analysis | Github | [BMJ*20] |
| NeuroMorphoVis | | | | • | • | | Neuroanatomical data analysis | Github | [AHE*18] |

and discover the fundamental principles at play in neuron structures and circuit architectures. Visualization researchers now have the rare opportunity to develop interactive frameworks that allow neuroscientists to make sense of these data sets with tens of thousands of cells and hundreds of millions of synapses.

This report presented the state of the art of data visualization for high-resolution connectomics data. We grouped related work along the common connectomics pipeline. While most visualization approaches cluster towards the end of the pipeline, interesting visualization work has also been done in the early parts of the pipeline. This work intends to summarize the field for both new visualization researchers and experts in the area. We also compiled a list of the latest and most commonly used publicly available data sets and open-source tools in the field, highlighting the recent push for open science. Connectomics research, in particular, relies heavily on sharing data and expertise among research groups. This report also reflects the interdisciplinarity of the field. Neuroscientists, machine learning experts, and visualization researchers need to collaborate closely. We argue that human-AI collaboration will play an increasing role in translating the vast amounts of imaging data into

comprehensible knowledge. In turn, we hope that research findings in connectomics will help incorporate more biologically-inspired architectures into deep learning models.

We hope this review provides visualization and connectomics researchers with a better overview of the different visualization methods currently available for each step along the connectomics pipeline. However, connectomics is a constantly evolving field with many open visualization challenges. We hope to inspire future research in this exciting field with our survey. Tackling these challenges has the potential to bring us one step closer to the ultimate goal of understanding the workings of the human brain.

Acknowledgements

We thank Z. Lin for his feedback. This research was supported by the National Science Foundation (NSF) Award Number IIS-1901030, NCS-FO-2124179, CNS1650499, OAC1919752, ICER1940302, IIS2107224, an IBM-SUNY-IBM grant 2106 and the King Abdullah University of Science & Technology (KAUST).

References

- [AABH*16] AL-AWAMI A., BEYER J., HAEHN D., KASTHURI N., LICHTMAN J. W., PFISTER H., HADWIGER M.: NeuroBlocks – Visual Tracking of Segmentation and Proofreading for Large Connectomics Projects. *IEEE Transactions on Visualization and Computer Graphics* 22, 1 (Jan. 2016), 738–746. URL: <http://ieeexplore.ieee.org/document/7192653/>, doi:10.1109/TVCG.2015.2467441. 12, 13
- [AABS*14] AL-AWAMI A., BEYER J., STROBELT H., KASTHURI N., LICHTMAN J. W., PFISTER H., HADWIGER M.: NeuroLines: A Subway Map Metaphor for Visualizing Nanoscale Neuronal Connectivity. *IEEE Transactions on Visualization and Computer Graphics* 20, 12 (Dec. 2014), 2369–2378. URL: <https://ieeexplore.ieee.org/document/6875935/>, doi:10.1109/TVCG.2014.2346312. 16, 17
- [ABC*20] ABBOTT L. F., BOCK D. D., CALLAWAY E. M., DENK W., DULAC C., FAIRHALL A. L., FIETE I., HARRIS K. M., HELMSTAEDTER M., JAIN V., OTHERS: The mind of a mouse. *Cell* 182, 6 (2020), 1372–1376. Publisher: Elsevier. URL: <https://www.sciencedirect.com/science/article/pii/S00092867420310011.21>
- [ABG*18] AGUS M., BOGES D., GAGNON N., MAGISTRETTI P. J., HADWIGER M., CALÍ C.: GLAM: Glycogen-derived Lactate Absorption Map for visual analysis of dense and sparse surface reconstructions of rodent brain structures on desktop systems and virtual environments. *Computers & Graphics* 74 (Aug. 2018), 85–98. URL: <https://linkinghub.elsevier.com/retrieve/pii/S0009784931830058X>, doi:10.1016/j.cag.2018.04.007. 19
- [ACA*19] AGUS M., CALÌ C., AL-AWAMI A., GOBBETTI E., MAGISTRETTI P., HADWIGER M.: Interactive Volumetric Visual Analysis of Glycogen-derived Energy Absorption in Nanometric Brain Structures. *Computer Graphics Forum* 38, 3 (2019), 427–439. URL: <https://onlinelibrary.wiley.com/doi/abs/10.1111/cgf.13700>, doi:<https://doi.org/10.1111/cgf.13700.19>
- [AGE*21] ARSHADI C., GÜNTHER U., EDDISON M., HARRINGTON K. I. S., FERREIRA T. A.: SNT: a unifying toolbox for quantification of neuronal anatomy. *Nature Methods* 18, 4 (Apr. 2021), 374–377. URL: <http://www.nature.com/articles/s41592-021-01105-7>, doi:10.1038/s41592-021-01105-7. 18, 19
- [AHE*18] ABDELLAH M., HERNANDO J., EILEMANN S., LAPERE S., ANTILLE N., MARKRAM H., SCHÜRMANN F.: NeuroMorphoVis: a collaborative framework for analysis and visualization of neuronal morphology skeletons reconstructed from microscopy stacks. *Bioinformatics* 34, 13 (July 2018), i574–i582. URL: <https://academic.oup.com/bioinformatics/article/34/13/i574/5045775>, doi:10.1093/bioinformatics/bty231. 18, 19, 23
- [AKCL*03] AL-KOFAHI O., CAN A., LASEK S., SZAROWSKI D. H., TURNER J. N., ROYSAM B.: Algorithms for accurate 3D registration of neuronal images acquired by confocal scanning laser microscopy. *Journal of Microscopy* 211, 1 (2003), 8–18. URL: <https://onlinelibrary.wiley.com/doi/abs/10.1046/j.1365-2818.2003.01196.x>, doi:10.1046/j.1365-2818.2003.01196.x. 6
- [AMG*11] ANDERSON J., MOHAMMED S., GRIMM B., JONES B., KOSHEVOY P., TASDIZEN T., WHITAKER R., MARC R.: The Viking viewer for connectomics: scalable multi-user annotation and summarization of large volume data sets. *Journal of Microscopy* 241, 1 (Jan. 2011), 13–28. URL: <https://www.ncbi.nlm.nih.gov/pmc/articles/PMC3017751/>, doi:10.1111/j.1365-2818.2010.03402.x. 9, 11, 16, 23
- [ATAG*21] AL-THELAYA K., AGUS M., GILAL N. U., YANG Y., PINTORE G., GOBBETTI E., CALÌ C., MAGISTRETTI P. J., MIFSUD W., SCHNEIDER J.: InShaDe: Invariant Shape Descriptors for visual 2D and 3D cellular and nuclear shape analysis and classification. *Computers & Graphics* 98 (2021), 105–125. URL: <https://www.sciencedirect.com/science/article/pii/S0097849321000790>, doi:<https://doi.org/10.1016/j.cag.2021.04.037>. 17, 19
- [BAAK*13] BEYER J., AL-AWAMI A., KASTHURI N., LICHTMAN J. W., PFISTER H., HADWIGER M.: ConnectomeExplorer: Query-Guided Visual Analysis of Large Volumetric Neuroscience Data. *IEEE Transactions on Visualization and Computer Graphics* 19, 12 (Dec. 2013), 2868–2877. URL: <http://ieeexplore.ieee.org/document/6634132/>, doi:10.1109/TVCG.2013.142. 15, 16, 17, 19, 20, 22
- [BAS*96] BECKER D. E., ANCIN H., SZAROWSKI D. H., TURNER J. N., ROYSAM B.: Automated 3-D montage synthesis from laser-scanning confocal images: Application to quantitative tissue-level cytological analysis. *Cytometry: The Journal of the International Society for Analytical Cytology* 25, 3 (1996), 235–245. URL: [https://doi.org/10.1002/\(SICI\)1097-0320\(19961101\)25:3<235::AID-CYTO4>3.0.CO;2-E](https://doi.org/10.1002/(SICI)1097-0320(19961101)25:3<235::AID-CYTO4>3.0.CO;2-E). 6
- [BAS*20] BOGES D., AGUS M., SICAT R., MAGISTRETTI P. J., HADWIGER M., CALÌ C.: Virtual reality framework for editing and exploring medial axis representations of nanometric scale neural structures. *Computers & Graphics* 91 (Oct. 2020), 12–24. URL: <https://linkinghub.elsevier.com/retrieve/pii/S0097849320300789>, doi:10.1016/j.cag.2020.05.024. 9, 11
- [BB09] BASSETT D. S., BULLMORE E. T.: Human brain networks in health and disease. *Current Opinion in Neurology* 22, 4 (Aug. 2009), 340–347. URL: <https://journals.lww.com/00019052-200908000-00003>, doi:10.1097/WCO.0b013e32832d93dd. 10
- [BB12] BRIGGMAN K. L., BOCK D. D.: Volume electron microscopy for neuronal circuit reconstruction. *Current Opinion in Neurobiology* 22, 1 (Feb. 2012), 154–161. URL: <https://www.sciencedirect.com/science/article/pii/S0959438811001887>, doi:10.1016/j.conb.2011.10.022. 1
- [BBB*17] BOERGENS K. M., BERNING M., BOCKLISCH T., BRÄUNLEIN D., DRAWITSCH F., FROHNHOFEN J., HEROLD T., OTTO P., RZEPKA N., WERKMEISTER T., WERNER D., WIESE G., WISSLER H., HELMSTAEDTER M.: webKnossos: efficient online 3D data annotation for connectomics. *Nature Methods* 14, 7 (July 2017), 691–694. URL: <https://www.nature.com/articles/nmeth.4331>, doi:10.1038/nmeth.4331. 11, 12, 13, 23
- [BBC*11] BROWN K. M., BARRIONUEVO G., CANTY A. J., DE PAOLA V., HIRSCH J. A., JEFFERIS G. S., LU J., SNIPPE M., SUGIHARA I., ASCOLI G. A.: The DIADEM data sets: representative light microscopy images of neuronal morphology to advance automation of digital reconstructions. *Neuroinformatics* 9, 2 (2011), 143–157. URL: <https://link.springer.com/article/10.1007/s12021-010-9095-5>. 20, 22
- [BBDGI19] BRIA A., BERNASCHI M., GUARRASI M., IANNELLO G.: Exploiting Multi-Level Parallelism for Stitching Very Large Microscopy Images. *Frontiers in Neuroinformatics* 13 (2019). URL: <https://www.frontiersin.org/article/10.3389/fninf.2019.00041.6>
- [BBH15] BERNING M., BOERGENS K., HELMSTAEDTER M.: SegEM: Efficient Image Analysis for High-Resolution Connectomics. *Neuron* 87, 6 (Sept. 2015), 1193–1206. URL: <https://linkinghub.elsevier.com/retrieve/pii/S0896627315007606>, doi:10.1016/j.neuron.2015.09.003. 10
- [BCK*16] BLOSS E. B., CEMBROWSKI M. S., KARSH B., COLONELL J., FETTER R. D., SPRUSTON N.: Structured dendritic inhibition supports branch-selective integration in CA1 pyramidal cells. *Neuron* 89, 5 (2016), 1016–1030. URL: <https://doi.org/10.1016/j.neuron.2016.01.029>. 21, 22

- [BCM*19] BOGES D., CALÌ C., MAGISTRETTI P. J., HADWIGER M., SICAT R., AGUS M.: Immersive Environment for Creating, Proofreading, and Exploring Skeletons of Nanometric Scale Neural Structures. *Smart Tools and Apps for Graphics - Eurographics Italian Chapter Conference* (2019), 10 pages. URL: <https://digilib.eg.org/handle/10.2312/stag20191360>, doi: 10.2312/STAG.20191360. 9, 11
- [BCSH*22] BONNEY S. K., COELHO-SANTOS V., HUANG S.-F., TAKENO M., KORNFIELD J., KELLER A., SHIH A. Y.: Public volume electron microscopy data: An essential resource to study the brain microvasculature. preprint, Neuroscience, Feb. 2022. URL: <http://biorkxiv.org/lookup/doi/10.1101/2022.02.20.481154>. 20
- [BHAA*13] BEYER J., HADWIGER M., AL-AWAMI A., WON-KI JEONG, KASTHURI N., LICHTMAN J. W., PFISTER H.: Exploring the Connectome: Petascale Volume Visualization of Microscopy Data Streams. *IEEE Computer Graphics and Applications* 33, 4 (July 2013), 50–61. URL: <http://ieeexplore.ieee.org/document/6562713/>, doi: 10.1109/MCG.2013.55. 15
- [BHP15] BEYER J., HADWIGER M., PFISTER H.: State-of-the-Art in GPU-Based Large-Scale Volume Visualization. *Computer Graphics Forum* 34, 8 (Dec. 2015), 13–37. URL: <http://doi.org/10.1111/cgf.12605>, doi: 10.1111/cgf.12605. 2
- [BII12] BRIA A., IANNELLO G.: TeraStitcher - A tool for fast automatic 3D-stitching of teravoxel-sized microscopy images. *BMC Bioinformatics* 13, 1 (Nov. 2012), 316. URL: <https://doi.org/10.1186/1471-2105-13-316>. 6, 23
- [BIP15] BRIA A., IANNELLO G., PENG H.: An open-source VAA3D plugin for real-time 3D visualization of terabyte-sized volumetric images. In *2015 IEEE 12th International Symposium on Biomedical Imaging (ISBI)* (Apr. 2015), pp. 520–523. doi: 10.1109/ISBI.2015.7163925. 7, 23
- [BJA*19] BOORBOOR S., JADHAV S., ANANTH M., TALMAGE D., ROLE L., KAUFMAN A.: Visualization of Neuronal Structures in Wide-Field Microscopy Brain Images. *IEEE Transactions on Visualization and Computer Graphics* 25, 1 (Jan. 2019), 1018–1028. doi: 10.1109/TVCG.2018.2864852. 4, 14, 15
- [BKK*13] BURNS R., KASTHURI N., KAZHDAN M., SMITH S. J., KLEISSAS D., PERLMAN E., CHUNG K., WEILER N. C., LICHTMAN J., SZALAY A. S., VOGELSTEIN J. T., LILLANEY K., VOGELSTEIN R. J., BERGER D. R., GROSENICK L., DEISSEROTH K., REID R. C., RONCAL W. G., MANAVALAN P., BOCK D. D.: The open connectome project data cluster: scalable analysis and vision for high-throughput neuroscience. In *Proceedings of the 25th International Conference on Scientific and Statistical Database Management - SSDBM* (2013), ACM Press, p. 1. URL: <http://dl.acm.org/citation.cfm?doid=2484838.2484870>, doi: 10.1145/2484838.2484870. 13, 20, 22
- [BKK*19] BERG S., KUTRA D., KROEGER T., STRAEHLE C. N., KAUSLER B. X., HAUBOLD C., SCHIEGG M., ALES J., BEIER T., RUDY M., OTHERS: Ilastik: interactive machine learning for (bio) image analysis. *Nature Methods* 16, 12 (2019), 1226–1232. URL: <https://doi.org/10.1038/s41592-019-0582-9>. 9, 23
- [BLK*11] BOCK D. D., LEE W.-C. A., KERLIN A. M., ANDERMANN M. L., HOOD G., WETZEL A. W., YURGENSON S., SOUCY E. R., KIM H. S., REID R. C.: Network anatomy and in vivo physiology of visual cortical neurons. *Nature* 471, 7337 (Mar. 2011), 177–182. URL: <http://www.nature.com/articles/nature09802>, doi: 10.1038/nature09802. 5
- [BLLF06] BAJCSY P., LEE S.-C., LIN A., FOLBERG R.: Three-dimensional volume reconstruction of extracellular matrix proteins in uveal melanoma from fluorescent confocal laser scanning microscope images. *Journal of Microscopy* 221, 1 (2006), 30–45. URL: <https://onlinelibrary.wiley.com/doi/abs/10.1111/j.1365-2818.2006.01539.x>, doi: 10.1111/j.1365-2818.2006.01539.x. 6
- [BM00] BIENIEK A., MOGA A.: An efficient watershed algorithm based on connected components. *Pattern Recognition* 33, 6 (2000), 907–916. URL: <https://www.sciencedirect.com/science/article/pii/S0031320399001545>, doi: [https://doi.org/10.1016/S0031-3203\(99\)00154-5](https://doi.org/10.1016/S0031-3203(99)00154-5). 10
- [BMA*19] BEYER J., MOHAMMED H., AGUS M., AL-AWAMI A. K., PFISTER H., HADWIGER M.: Culling for Extreme-Scale Segmentation Volumes: A Hybrid Deterministic and Probabilistic Approach. *IEEE Transactions on Visualization and Computer Graphics* 25, 1 (Jan. 2019), 1132–1141. URL: <https://ieeexplore.ieee.org/document/8444102/>, doi: 10.1109/TVCG.2018.2864847. 15
- [BMA*21] BOORBOOR S., MATHEW S., ANANTH M., TALMAGE D., ROLE L. W., KAUFMAN A. E.: NeuRegenerate: A Framework for Visualizing Neurodegeneration. *IEEE Transactions on Visualization and Computer Graphics* (2021), 1–1. doi: 10.1109/TVCG.2021.3127132. 5
- [BMJ*20] BATES A. S., MANTON J. D., JAGANNATHAN S. R., COSTA M., SCHLEGEL P., ROHLING T., JEFFERIS G. S.: The natverse, a versatile toolbox for combining and analysing neuroanatomical data. *Elife* 9 (2020). URL: [10.7554/eLife.53350](https://doi.org/10.7554/eLife.53350). 18, 23
- [BMV05] BUSSOLATI G., MARCHIÒ C., VOLANTE M.: Tissue arrays as fiducial markers for section alignment in 3-D reconstruction technology. *Journal of Cellular and Molecular Medicine* 9, 2 (Apr. 2005), 438–445. URL: <https://www.ncbi.nlm.nih.gov/pmc/articles/PMC6740281/>, doi: 10.1111/j.1582-4934.2005.tb00368.x. 7
- [Boo89] BOOKSTEIN F.: Principal warps: thin-plate splines and the decomposition of deformations. *IEEE Transactions on Pattern Analysis and Machine Intelligence* 11, 6 (June 1989), 567–585. doi: 10.1109/34.24792. 7
- [BR14] BASU S., RACOCEANU D.: Reconstructing neuronal morphology from microscopy stacks using fast marching. In *2014 IEEE International Conference on Image Processing (ICIP)* (Oct. 2014), pp. 3597–3601. ISSN: 2381-8549. doi: 10.1109/ICIP.2014.7025730. 8
- [BS13] BRAITENBERG V., SCHÜZ A.: *Cortex: statistics and geometry of neuronal connectivity*. Springer Science & Business Media, 2013. 17
- [BSG*09] BRUCKNER S., SOLTESZOVA V., GROLLER E., HLADUVKA J., BUHLER K., YU J. Y., DICKSON B. J.: BrainGazer - Visual queries for neurobiology research. *IEEE Transactions on Visualization and Computer Graphics* 15, 6 (2009), 1497–1504. doi: 10.1109/TVCG.2009.121. 20
- [BSL18] BERGER D., SEUNG H. S., LICHTMAN J. W.: VAST (Volume Annotation and Segmentation Tool): Efficient Manual and Semi-Automatic Labeling of Large 3D Image Stacks. *Frontiers in Neural Circuits* 12 (2018). URL: [https://www.frontiersin.org/articles/10.3389/fncir.2018.00088/](https://www.frontiersin.org/articles/10.3389/fncir.2018.00088/full). 9, 11, 23
- [BSMM*21] BUHMANN J., SHERIDAN A., MALIN-MAYOR C., SCHLEGEL P., GERHARD S., KAZIMIERS T., KRAUSE R., NGUYEN T. M., HEINRICH L., LEE W.-C. A., WILSON R., SAALFELD S., JEFFERIS G. S. X. E., BOCK D. D., TURAGA S. C., COOK M., FUNKE J.: Automatic detection of synaptic partners in a whole-brain Drosophila electron microscopy data set. *Nature Methods* 18, 7 (July 2021), 771–774. URL: <http://www.nature.com/articles/s41592-021-01183-7>, doi: 10.1038/s41592-021-01183-7. 10
- [CBB*21] CONSORTIUM M., BAE J. A., BAPTISTE M., BODOR A. L., BRITTAINE D., BUCHANAN J., BUMBARGER D. J., CASTRO M. A., CELII B., COBOS E., COLLMAN F., COSTA N. M. D., DORKENWALD S., ELABBADY L., FAHEY P. G., FLISS T., FROUDARAKIS E., GAGER J., GAMLIN C., HALAGERI A., HEBDITCH J., JIA Z., JORDAN C., KAPNER D., KEMNITZ N., KINN S., KOOLMAN S., KUEHNER K., LEE K., LI K., LU R., MACRINA T., MAHALINGAM G., MCREYNOLDS S., MIRANDA E., MITCHELL E., MONDAL S. S., MOORE M., MU S., MUHAMMAD T., NEHORAN

- B., OGEDENGBE O., PAPADPOULOS C., PAPADPOULOS S., PATEL S., PITKOW X., POPOVYCH S., RAMOS A., REID R. C., REIMER J., SCHNEIDER-MIZELL C. M., SEUNG H. S., SILVERMAN B., SILVERSMITH W., STERLING A., SINZ F. H., SMITH C. L., SUCKOW S., TAKENO M., TAN Z. H., TOLIAS A. S., TORRES R., TURNER N. L., WALKER E. Y., WANG T., WILLIAMS G., WILLIAMS S., WILLIE K., WILLIE R., WONG W., WU J., XU C., YANG R., YATSENKO D., YE F., YIN W., YU S.-C.: *Functional connectomics spanning multiple areas of mouse visual cortex*. Tech. rep., Aug. 2021. URL: <https://www.biorxiv.org/content/10.1101/2021.07.28.454025v2>. 1, 14, 21, 22
- [CBH*15] CALÌ C., BOGES D., HOLST G., KRESHUK A., HAMPRECHT F., SRINIVASAN M., LEHVASLAHO H., MAGISTRETTI P.: Ultrastructural analysis of glycogen in hippocampal astrocytic processes using 3D virtual reality. In *Front. Neurosci. Conference Abstract: 11th National Congress of the Belgian Society for Neuroscience*. doi: 10.3389/conf.fnins (2015), vol. 5. URL: https://www.frontiersin.org/10.3389/conf.fnins.2015.89.00005/event_abstract. 19
- [CDU*20] CLEMENTS J., DOLAFI T., UMAPYAM L., NEUBARTH N. L., BERG S., SCHEFFER L. K., PLAZA S. M.: *neuPrint: Analysis Tools for EM Connectomics*. Tech. rep., Jan. 2020. URL: <https://www.biorxiv.org/content/10.1101/2020.01.16.909465v1>. 13, 16, 17, 19, 20, 23
- [CFBH10] CUNTZ H., FORSTNER F., BORST A., HÄUSSER M.: One Rule to Grow Them All: A General Theory of Neuronal Branching and Its Practical Application. *PLOS Computational Biology* 6, 8 (Aug. 2010). URL: <https://journals.plos.org/ploscompbiol/article?id=10.1371/journal.pcbi.1000877>, doi: 10.1371/journal.pcbi.1000877. 18, 19
- [CGGS12] CIREŞAN D. C., GIUSTI A., GAMBARDELLA L. M., SCHMIDHUBER J.: Deep neural networks segment neuronal membranes in electron microscopy images. In *Proceedings of the 25th International Conference on Neural Information Processing Systems - Volume 2* (Dec. 2012), pp. 2843–2851. URL: <https://citeserx.ist.psu.edu/viewdoc/download?doi=10.1.1.367.3014&rep=rep1&type=pdf>. 10
- [CHM*21] CHOI J., HILDEBRAND D. G. C., MOON J., QUAN T. M., TUAN T. A., KO S., JEONG W.-K.: ZeVis: A Visual Analytics System for Exploration of a Larval Zebrafish Brain in Serial-Section Electron Microscopy Images. *IEEE Access* 9 (2021), 78755–78763. URL: <https://ieeexplore.ieee.org/document/9440958/>, doi: 10.1109/ACCESS.2021.3084066. 18, 19
- [CHP*06] CHOW S. K., HAKOZAKI H., PRICE D. L., MACLEAN N. A. B., DEERINCK T. J., BOUWER J. C., MARTONE M. E., PELTIER S. T., ELLISMAN M. H.: Automated microscopy system for mosaic acquisition and processing. *Journal of Microscopy* 222, 2 (2006), 76–84. URL: <https://onlinelibrary.wiley.com/doi/abs/10.1111/j.1365-2818.2006.01577.x>, doi: 10.1111/j.1365-2818.2006.01577.x. 6
- [CIIdC*17] CHEN H., IASCOME D. M., DA COSTA N. M., LEIN E. S., LIU T., PENG H.: Fast assembling of neuron fragments in serial 3D sections. *Brain Informatics* 4, 3 (Sept. 2017), 183–186. URL: <http://link.springer.com/10.1007/s40708-017-0063-9>, doi: 10.1007/s40708-017-0063-9. 7, 8
- [CL15] CALLAWAY E. M., LUO L.: Monosynaptic Circuit Tracing with Glycoprotein-Deleted Rabies Viruses. *Journal of Neuroscience* 35, 24 (June 2015), 8979–8985. URL: <https://www.jneurosci.org/content/35/24/8979>, doi: 10.1523/JNEUROSCI.0409-15.2015. 4
- [CMB*17] CHALFOUN J., MAJURSKI M., BLATTNER T., BHADRIRAJU K., KEYROUZ W., BAJCSY P., BRADY M.: MIST: Accurate and Scalable Microscopy Image Stitching Tool with Stage Modeling and Error Minimization. *Scientific Reports* 7, 1 (July 2017), 4988. URL: <https://www.nature.com/articles/s41598-017-04567-y>, doi: 10.1038/s41598-017-04567-y. 6, 7, 23
- [CMO*16] COSTA M., MANTON J. D., OSTROVSKY A. D., PROHASKA S., JEFFERIS G. S.: NBLAST: rapid, sensitive comparison of neuronal structure and construction of neuron family databases. *Neuron* 91, 2 (2016), 293–311. 16, 18, 19
- [CPT*20] CLAUDI F., PETRUCCO L., TYSON A. L., BRANCO T., MARGRIE T. W., PORTUGUES R.: BrainGlobe Atlas API: a common interface for neuroanatomical atlases. *Journal of Open Source Software* 5, 54 (Oct. 2020), 2668. URL: <https://joss.theoj.org/papers/10.21105/joss.02668>, doi: 10.21105/joss.02668. 20
- [CSC18] CHEN W., SHI L., CHEN W.: A Survey of Macroscopic Brain Network Visualization Technology. *Chinese Journal of Electronics* 27, 5 (2018), 889–899. URL: <https://onlinelibrary.wiley.com/doi/abs/10.1049/cje.2018.04.007>, doi: 10.1049/cje.2018.04.007. 2, 4
- [CSRT02] CAN A., STEWART C., ROYSAM B., TANENBAUM H.: A feature-based technique for joint, linear estimation of high-order image-to-mosaic transformations: mosaicing the curved human retina. *IEEE Transactions on Pattern Analysis and Machine Intelligence* 24, 3 (Mar. 2002), 412–419. doi: 10.1109/34.990145. 6
- [CSS*12] CARDONA A., SAALFELD S., SCHINDELIN J., ARGANDA-CARRERAS I., PREIBISCH S., LONGAIR M., TOMANCAK P., HARTENSTEIN V., DOUGLAS R.: TrakEM2 Software for Neural Circuit Reconstruction. *PLoS One* 7, 6 (2012). URL: <https://journals.plos.org/plosone/article?id=10.1371/journal.pone.0038011>, doi: 10.1371/journal.pone.0038011. 7, 9, 23
- [CTB15] CHEN F., TILLBERG P. W., BOYDEN E. S.: Expansion microscopy. *Science* 347, 6221 (2015), 543–548. Publisher: American Association for the Advancement of Science. 5
- [CTP*21] CLAUDI F., TYSON A. L., PETRUCCO L., MARGRIE T. W., PORTUGUES R., BRANCO T.: Visualizing anatomically registered data with brainrender. *eLife* 10 (Mar. 2021), e65751. URL: <https://elifesciences.org/articles/65751>, doi: 10.7554/eLife.65751. 20, 23
- [DF92] DEFELIPE J., FARIÑAS I.: The pyramidal neuron of the cerebral cortex: Morphological and chemical characteristics of the synaptic inputs. *Progress in Neurobiology* 39, 6 (1992), 563–607. URL: <https://www.sciencedirect.com/science/article/pii/0301008292900157>, doi: [https://doi.org/10.1016/0301-0082\(92\)90015-7](https://doi.org/10.1016/0301-0082(92)90015-7). 18
- [DFM02] DE FLORIANI L., MAGILLO P.: Multiresolution mesh representation: Models and data structures. In *Tutorials on Multiresolution in Geometric Modelling*. Springer, 2002, pp. 363–417. URL: https://doi.org/10.1007/978-3-662-04388-2_13. 13
- [DH04] DENK W., HORSTMANN H.: Serial Block-Face Scanning Electron Microscopy to Reconstruct Three-Dimensional Tissue Nanostructure. *PLOS Biology* 2, 11 (Oct. 2004), e329. URL: <https://journals.plos.org/plosbiology/article?id=10.1371/journal.pbio.0020329>, doi: 10.1371/journal.pbio.0020329. 5
- [DHO14] DERCKSEN V. J., HEGE H.-C., OBERLAENDER M.: The Filament Editor: an interactive software environment for visualization, proof-editing and analysis of 3D neuron morphology. *Neuroinformatics* 12, 2 (Apr. 2014), 325–339. doi: 10.1007/s12021-013-9213-2. 7
- [DLS*07] DODT H.-U., LEISCHNER U., SCHIERLOH A., JÄHRLING N., MAUCH C. P., DEININGER K., DEUSSING J. M., EDER M., ZIEGLGÄNSBERGER W., BECKER K.: Ultramicroscopy: three-dimensional visualization of neuronal networks in the whole mouse brain. *Nature Methods* 4, 4 (Apr. 2007), 331–336. URL: <https://www.nature.com/articles/nmeth1036>, doi: 10.1038/nmeth1036. 5
- [DMM*22] DORKENWALD S., MCKELLAR C. E., MACRINA T., KEMNITZ N., LEE K., LU R., WU J., POPOVYCH S., MITCHELL E.,

- NEHORAN B., JIA Z., BAE J. A., MU S., IH D., CASTRO M., OGEDENGBE O., HALAGERI A., KUEHNER K., STERLING A. R., ASHWOOD Z., ZUNG J., BRITTAIN D., COLLMAN F., SCHNEIDER-MIZELL C., JORDAN C., SILVERSMITH W., BAKER C., DEUTSCH D., ENCARNACION-RIVERA L., KUMAR S., BURKE A., BLAND D., GAGER J., HEBDITCH J., KOOLMAN S., MOORE M., MOREJOHN S., SILVERMAN B., WILLIE K., WILLIE R., YU S.-C., MURTHY M., SEUNG H. S.: FlyWire: online community for whole-brain connectomics. *Nature Methods* 19, 1 (Jan. 2022), 119–128. URL: <https://www.nature.com/articles/s41592-021-01330-0>, doi: 10.1038/s41592-021-01330-0. 12, 13, 21, 23
- [DPM*18] DIMITRIEV K., PARAG T., MATEJEK B., KAUFMAN A., PFISTER H.: Efficient Correction for EM Connectomics with Skeletal Representation. In *British Machine Vision Conference (BMVC)* (2018). URL: <http://www.bmva.org/bmvc/2018/contents/papers/0064.pdf>. 12
- [DSK*17] DORKENWALD S., SCHUBERT P. J., KILLINGER M. F., URBAN G., MIKULA S., SVARA F., KORNFELD J.: Automated synaptic connectivity inference for volume electron microscopy. *Nature Methods* 14, 4 (Apr. 2017), 435–442. URL: <http://www.nature.com/articles/nmeth.4206>, doi: 10.1038/nmeth.4206. 10
- [DTM*21] DORKENWALD S., TURNER N. L., MACRINA T., LEE K., LU R., WU J., BODOR A. L., BLECKERT A. A., BRITAIN D., KEMNITZ N., SILVERSMITH W. M., IH D., ZUNG J., ZLATESKI A., TARTAVULL I., YU S.-C., POPOVYCH S., WONG W., CASTRO M., JORDAN C. S., WILSON A. M., FROUDARAKIS E., BUCHANAN J., TAKENO M., TORRES R., MAHALINGAM G., COLLMAN F., SCHNEIDER-MIZELL C., BUMBARGER D. J., LI Y., BECKER L., SUCKOW S., REIMER J., TOLIAS A. S., COSTA N. M. D., REID R. C., SEUNG H. S.: Binary and analog variation of synapses between cortical pyramidal neurons. Tech. rep., Dec. 2021. URL: <https://www.biorxiv.org/content/10.1101/2019.12.29.890319v2>. 21, 22
- [DWG*09] DERCKSEN V., WEBER B., GUNTHER D., OBERLAENDER M., PROHASKA S., HEGE H.-C.: Automatic alignment of stacks of filament data. In *2009 IEEE International Symposium on Biomedical Imaging: From Nano to Macro* (June 2009), pp. 971–974. ISSN: 1945-8452. doi: 10.1109/ISBI.2009.5193216. 7
- [EKS*96] ESTER M., KRIEGEL H.-P., SANDER J., XU X., OTHERS: A density-based algorithm for discovering clusters in large spatial databases with noise. In *kdd* (1996), vol. 96, pp. 226–231. Issue: 34. URL: https://www.aaai.org/Papers/KDD/1996/KDD96-037.pdf?source=post_page.19
- [EMS*15] EBERLE A., MIKULA S., SCHALEK R., LICHTMAN J., TATE M. K., ZEIDLER D.: High-resolution, high-throughput imaging with a multibeam scanning electron microscope. *Journal of Microscopy* 259, 2 (Aug. 2015), 114–120. URL: <https://onlinelibrary.wiley.com/doi/10.1111/jmi.12224>, doi: 10.1111/jmi.12224. 5
- [ERP*09] EMMENLAUER M., RONNEBERGER O., PONTI A., SCHWARB P., GRIFFA A., FILIPPI A., NITSCHKE R., DRIEVER W., BURKHARDT H.: XuvTools: free, fast and reliable stitching of large 3D datasets. *Journal of Microscopy* 233, 1 (2009), 42–60. URL: <https://onlinelibrary.wiley.com/doi/abs/10.1111/j.1365-2818.2008.03094.x>, doi: 10.1111/j.1365-2818.2008.03094.x. 6
- [EZ18] EBERLE A. L., ZEIDLER D.: Multi-Beam Scanning Electron Microscopy for High-Throughput Imaging in Connectomics Research. *Frontiers in Neuroanatomy* 12 (Dec. 2018), 112. URL: <https://www.frontiersin.org/article/10.3389/fnana.2018.00112/full>, doi: 10.3389/fnana.2018.00112. 5
- [Far20] FARM J.: NeuroProof, June 2020. Last accessed: 2/1/2022. URL: <https://github.com/janelia-flyem/NeuroProof>. 12
- [FGG*18] FRANCIS N., GREEN A., GUAGLIARDO P., LIBKIN L., LIN-DAAKER T., MARSAUT V., PLANTIKOW S., RYDBERG M., SELMER P., TAYLOR A.: Cypher: An Evolving Query Language for Property Graphs. In *Proceedings of the 2018 International Conference on Management of Data* (May 2018), pp. 1433–1445. URL: <https://doi.org/10.1145/3183713.3190657>, doi: 10.1145/3183713.3190657. 13, 20
- [FH20] FRANKE L., HAEHN D.: Modern Scientific Visualizations on the Web. *Informatics* 7, 4 (Sept. 2020), 37. URL: <https://www.mdpi.com/2227-9709/7/4/37>, doi: 10.3390/informatics7040037. 2
- [Fia05] FIALA J. C.: Reconstruct: a free editor for serial section microscopy. *Journal of Microscopy* 218, 1 (2005), 52–61. URL: <https://onlinelibrary.wiley.com/doi/abs/10.1111/j.1365-2818.2005.01466.x>, doi: 10.1111/j.1365-2818.2005.01466.x. 7
- [FPA*20] FRIEDMANN D., PUN A., ADAMS E. L., LUI J. H., KEB-SCHULL J. M., GRUTZNER S. M., CASTAGNOLA C., TESSIER-LAVIGNE M., LUO L.: Mapping mesoscale axonal projections in the mouse brain using a 3D convolutional network. *Proceedings of the National Academy of Sciences* 117, 20 (May 2020), 11068–11075. URL: <https://pnas.org/doi/full/10.1073/pnas.1918465117>, doi: 10.1073/pnas.1918465117. 8
- [Fre15] FREEMAN J.: Open source tools for large-scale neuroscience. *Current Opinion in Neurobiology* 32 (June 2015), 156–163. URL: <https://linkinghub.elsevier.com/retrieve/pii/S0959438815000756>, doi: 10.1016/j.conb.2015.04.002. 20
- [FTG*17] FUNKE J., TSCHOPP F. D., GRISAITIS W., SINGH C., SAALFELD S., TURAGA S. C.: A Deep Structured Learning Approach Towards Automating Connectome Reconstruction from 3D Electron Micrographs. URL: <https://arxiv.org/abs/1709.02974v2>. 8
- [GBHP08] GYULASSY A., BREMER P.-T., HAMANN B., PASCUCCI V.: A Practical Approach to Morse-Smale Complex Computation: Scalability and Generality. *IEEE Transactions on Visualization and Computer Graphics* 14, 6 (Nov. 2008), 1619–1626. doi: 10.1109/TVCG.2008.110. 9
- [GBM*21] GHAREMANI P., BOORBOOR S., MIRHOSSEINI P., GUD-ISAGAR C., ANANTH M., TALMAGE D., ROLE L. W., KAUFMAN A. E.: NeuroConstruct: 3D Reconstruction and Visualization of Neurites in Optical Microscopy Brain Images. *IEEE Transactions on Visualization and Computer Graphics* (2021), 1–1. doi: 10.1109/TVCG.2021.3109460. 7, 9, 15, 16
- [GCBM*17] GARCIA-CANTERO J. J., BRITO J. P., MATA S., BAYONA S., PASTOR L.: NeuroTessMesh: A Tool for the Generation and Visualization of Neuron Meshes and Adaptive On-the-Fly Refinement. *Frontiers in Neuroinformatics* 11 (2017). URL: <https://www.frontiersin.org/article/10.3389/fninf.2017.00038>. 13, 18
- [GG90] GLASER J. R., GLASER E. M.: Neuron imaging with neurolucida — A PC-based system for image combining microscopy. *Computerized Medical Imaging and Graphics* 14, 5 (Sept. 1990), 307–317. URL: <https://www.sciencedirect.com/science/article/pii/089561119090105K>, doi: 10.1016/0895-6111(90)90105-K. 9
- [GHS*22] GALLIGAN F., HEMMER M., STAVA O., ZHANG F., BRETTLE J.: Google/draco: a library for compressing and decompressing 3d geometric meshes and point clouds, 2022. Last accessed: 2/1/2022. URL: <https://github.com/google/draco>. 13
- [GKHB20] GANGLBERGER F. J., KACZANOWSKA J., HAUBENSAK W., BÜHLER K.: A Data Structure for Real-Time Aggregation Queries of Big Brain Networks. *Neuroinformatics* 18, 1 (Jan. 2020), 131–149. URL: <http://link.springer.com/10.1007/s12021-019-09428-9>, doi: 10.1007/s12021-019-09428-9. 13, 17
- [Gre09] GREG H.: AlignTK, 2009. URL: <https://mmbios.pitt.edu/aligntk-home.6>

- [GRKV*15] GRAY RONCAL W., KLEISSAS D., VOGELSTEIN J., MANAVALAN P., LILLANEY K., PEKALA M., BURNS R., VOGELSTEIN R., PRIEBE C., CHEVILLET M., HAGER G.: An Automated Images-to-Graphs Framework for High Resolution Connectomics. *Frontiers in Neuroinformatics* 9 (2015), 20. URL: <https://www.frontiersin.org/article/10.3389/fninf.2015.00020>, doi:10.3389/fninf.2015.00020. 10
- [GSF*19] GANGLBERGER F., SWOBODA N., FRAUENSTEIN L., KACZANOWSKA J., HAUBENSAK W., BÜHLER K.: BrainTrawler: A visual analytics framework for iterative exploration of heterogeneous big brain data. *Computers & Graphics* 82 (2019), 304–320. URL: <https://doi.org/10.1016/j.cag.2019.05.032>. 17
- [GVL96] GOLUB G. H., VAN LOAN C. F.: Matrix computations. Johns Hopkins studies in the mathematical sciences, 1996. 10
- [GWB*21] GONDA F., WANG X., BEYER J., HADWIGER M., LICHTMAN J., PFISTER H.: VICE: Visual Identification and Correction of Neural Circuit Errors. *Computer Graphics Forum* (2021). URL: <https://arxiv.org/abs/2105.06861>. 12
- [HAAB*18] HADWIGER M., AL-AWAMI A., BEYER J., AGUS M., PFISTER H.: SparseLeap: Efficient Empty Space Skipping for Large-Scale Volume Rendering. *IEEE Transactions on Visualization and Computer Graphics* 24, 1 (Jan. 2018), 974–983. URL: <https://ieeexplore.ieee.org/document/8017589/>, doi:10.1109/TVCG.2017.2744238. 15
- [HBWP12] HADWIGER M., BEYER J., WON-KI JEONG, PFISTER H.: Interactive Volume Exploration of Petascale Microscopy Data Streams Using a Visualization-Driven Virtual Memory Approach. *IEEE Transactions on Visualization and Computer Graphics* 18, 12 (Dec. 2012), 2285–2294. URL: <http://ieeexplore.ieee.org/document/6327233/>, doi:10.1109/TVCG.2012.240. 13, 14, 15
- [HCT*18] HABERL M. G., CHURAS C., TINDALL L., BOASSA D., PHAN S., BUSHONG E. A., MADANY M., AKAY R., DEERINCK T. J., PELTIER S. T., OTHERS: CDDeep3M—Plug-and-Play cloud-based deep learning for image segmentation. *Nature methods* 15, 9 (2018), 677–680. URL: <https://doi.org/10.1038/s41592-018-0106-z>. 8
- [HHM*17] HAEHN D., HOFFER J., MATEJEK B., SUISSA-PELEG A., AL-AWAMI A., KAMENTSKY L., GONDA F., MENG E., ZHANG W., SCHALEK R., WILSON A., PARAG T., BEYER J., KAYNIG V., JONES T., TOMPKIN J., HADWIGER M., LICHTMAN J., PFISTER H.: Scalable Interactive Visualization for Connectomics. *Informatics* 4, 3 (Aug. 2017), 29. URL: <http://www.mdpi.com/2227-9709/4/3/29>, doi:10.3390/informatics4030029. 1, 5, 7, 23
- [Hil35] HILBERT D.: Über die stetige Abbildung einer Linie auf ein Flächenstück. In *Dritter Band: Analysis-Grundlagen der Mathematik-Physik Verschiedenes*. Springer, 1935, pp. 1–2. 13
- [HKBR*14] HAEHN D., KNOWLES-BARLEY S., ROBERTS M., BEYER J., KASTHURI N., LICHTMAN J. W., PFISTER H.: Design and Evaluation of Interactive Proofreading Tools for Connectomics. *IEEE Transactions on Visualization and Computer Graphics* 20, 12 (Dec. 2014), 2466–2475. URL: <http://ieeexplore.ieee.org/document/6875931/>, doi:10.1109/TVCG.2014.2346371. 9, 11, 12
- [HKG*22] HIDER R., KLEISSAS D., GION T., XENES D., MATELSKY J., PRYOR D., RODRIGUEZ L., JOHNSON E. C., GRAY-RONCAL W., WESTER B.: The Brain Observatory Storage Service and Database (BossDB): A Cloud-Native Approach for Petascale Neuroscience Discovery. *Frontiers in Neuroinformatics* 16 (Feb. 2022), 828787. URL: <https://www.frontiersin.org/articles/10.3389/fninf.2022.828787/full>, doi:10.3389/fninf.2022.828787. 14, 20
- [HKT*18] HAEHN D., KAYNIG V., TOMPKIN J., LICHTMAN J., PFISTER H.: Guided proofreading of automatic segmentations for connectomics. In *Proceedings of the IEEE Conference on Computer Vision and Pattern Recognition* (2018), pp. 9319–9328. URL: <https://arxiv.org/abs/1704.00848v1>. 12
- [HML*95] HUMM J. L., MACKLIS R. M., LU X. Q., YANG Y., BUMP K., BERESFORD B., CHIN L. M.: The spatial accuracy of cellular dose estimates obtained from 3D reconstructed serial tissue autoradiographs. *Physics in Medicine and Biology* 40, 1 (Jan. 1995), 163–180. URL: <https://doi.org/10.1088/0031-9155/40/1/014>, doi:10.1088/0031-9155/40/1/014. 7
- [HMS*14] HAYWORTH K. J., MORGAN J. L., SCHALEK R., BERGER D. R., HILDEBRAND D. G. C., LICHTMAN J. W.: Imaging ATUM ultrathin section libraries with WaferMapper: a multi-scale approach to EM reconstruction of neural circuits. *Frontiers in Neural Circuits* 8 (2014). URL: <https://www.frontiersin.org/article/10.3389/fncir.2014.00068>. 4
- [HPJ*11] HOGREBE L., PAIVA A. R. C., JURRUS E., CHRISTENSEN C., BRIDGE M., KORENBERG J., TASDIZEN T.: Trace driven registration of neuron confocal microscopy stacks. In *2011 IEEE International Symposium on Biomedical Imaging: From Nano to Macro* (Mar. 2011). ISSN: 1945-8452. doi:10.1109/ISBI.2011.5872649. 7
- [HPJ*20] HAYWORTH K. J., PEALE D., JANUSZEWSKI M., KNOTT G. W., LU Z., XU C. S., HESS H. F.: Gas cluster ion beam SEM for imaging of large tissue samples with 10 nm isotropic resolution. *Nature Methods* 17, 1 (Jan. 2020), 68–71. URL: <https://www.nature.com/articles/s41592-019-0641-2>, doi:10.1038/s41592-019-0641-2. 5
- [HRRP*19] HÖRL D., ROJAS RUSAK F., PREUSSER F., TILLBERG P., RANDEL N., CHHETRI R. K., CARDONA A., KELLER P. J., HARZ H., LEONHARDT H., TREIER M., PREIBISCH S.: BigStitcher: reconstructing high-resolution image datasets of cleared and expanded samples. *Nature Methods* 16, 9 (Sept. 2019), 870–874. URL: <https://www.nature.com/articles/s41592-019-0501-0>, doi:10.1038/s41592-019-0501-0. 6, 23
- [HSP18] HUANG G. B., SCHEFFER L. K., PLAZA S. M.: Fully-Automatic Synapse Prediction and Validation on a Large Data Set. *Frontiers in Neural Circuits* 12 (Oct. 2018), 87. URL: <https://www.frontiersin.org/article/10.3389/fncir.2018.00087/full>, doi:10.3389/fncir.2018.00087. 9
- [Hub22] HUBBARD P.: neuVid, 2022. URL: <https://github.com/connectome-neuprint/neuVid>. 23
- [HW94] HELL S. W., WICHMANN J.: Breaking the diffraction resolution limit by stimulated emission: stimulated-emission-depletion fluorescence microscopy. *Optics Letters* 19, 11 (June 1994), 780–782. URL: <https://www.osapublishing.org/ol/abstract.cfm?uri=ol-19-11-780>, doi:10.1364/OL.19.000780. 5
- [HXL*15] HAYWORTH K. J., XU C. S., LU Z., KNOTT G. W., FETTER R. D., TAPIA J. C., LICHTMAN J. W., HESS H. F.: Ultrastructurally smooth thick partitioning and volume stitching for large-scale connectomics. *Nature Methods* 12, 4 (Apr. 2015), 319–322. URL: <https://www.nature.com/articles/nmeth.3292>, doi:10.1038/nmeth.3292. 7
- [IJK*21] ISENSEE F., JAEGER P. F., KOHL S. A., PETERSEN J., MAIER-HEIN K. H.: nnU-Net: a self-configuring method for deep learning-based biomedical image segmentation. *Nature methods* 18, 2 (2021), 203–211. URL: <https://doi.org/10.1038/s41592-020-01008-z>. 8
- [Jai17] JAIN V.: Adversarial Image Alignment and Interpolation. *arXiv:1707.00067 [cs]* (June 2017). arXiv: 1707.00067. URL: <https://arxiv.org/abs/1707.00067>. 8
- [JBK18] JORSTAD A., BLANC J., KNOTT G.: NeuroMorph: a software toolset for 3D analysis of neurite morphology and connectivity. *Frontiers in neuroanatomy* 12 (2018), 59. URL: <https://doi.org/10.3389/fnana.2018.00059>. 18, 19, 23
- [JKL*18] JANUSZEWSKI M., KORNFIELD J., LI P. H., POPE A., BLAKELY T., LINDSEY L., MAITIN-SHEPARD J., TYKA M., DENK W., JAIN V.: High-precision automated reconstruction of neurons

- with flood-filling networks. *Nature methods* 15, 8 (2018), 605–610. URL: <https://doi.org.ezp-prod1.hul.harvard.edu/10.1038/s41592-018-0049-4>. 8, 21
- [JNC*15] JORSTAD A., NIGRO B., CALI C., WAWRZYNIAK M., FU A., KNOTT G.: NeuroMorph: a toolset for the morphometric analysis and visualization of 3D models derived from electron microscopy image stacks. *Neuroinformatics* 13, 1 (2015), 83–92. Publisher: Springer. 18, 19
- [JWC*06] JU T., WARREN J., CARSON J., BELLO M., KAKADIAS I., CHIU W., THALLER C., EICHELE G.: 3D volume reconstruction of a mouse brain from histological sections using warp filtering. *Journal of Neuroscience Methods* 156, 1 (Sept. 2006), 84–100. URL: <https://www.sciencedirect.com/science/article/pii/S0165027006001282>, doi:10.1016/j.jneumeth.2006.02.020. 7
- [KAE*09] KASHANI Z. R. M., AHARABIAN H., ELAHI E., NOWZARI-DALINI A., ANSARI E. S., ASADI S., MOHAMMADI S., SCHREIBER F., MASOUDI-NEJAD A.: Kavosh: a new algorithm for finding network motifs. *BMC Bioinformatics* 10, 1 (Oct. 2009), 318. URL: <https://doi.org/10.1186/1471-2105-10-318>. doi:10.1186/1471-2105-10-318. 10
- [KBRK*13] KNOWLES-BARLEY S., ROBERTS M., KASTHURI N., LEE D., PFISTER H., LICHTMAN J.: Mojo 2.0: Connectome Annotation Tool. doi:10.3389/CONF.FNINF.2013.09.00060. 11
- [KHB*15] KASTHURI N., HAYWORTH K., BERGER D., SCHALEK R., CONCHELLO J., KNOWLES-BARLEY S., LEE D., VÁZQUEZ-REINA A., KAYNIG V., JONES T., ROBERTS M., MORGAN J., TAPIA J., SEUNG H., RONCAL W., VOGELSTEIN J., BURNS R., SUSSMAN D., PRIEBE C., PFISTER H., LICHTMAN J.: Saturated Reconstruction of a Volume of Neocortex. *Cell* 162, 3 (July 2015), 648–661. URL: <https://linkinghub.elsevier.com/retrieve/pii/S0092867415008247>, doi:10.1016/j.cell.2015.06.054. 10, 21, 22
- [KLM*19] KUNST M., LAURELL E., MOKAYES N., KRAMER A., KUBO F., FERNANDES A. M., FÖRSTER D., DAL MASCHIO M., BAIER H.: A cellular-resolution atlas of the larval zebrafish brain. *Neuron* 103, 1 (2019), 21–38. URL: <https://doi.org/10.1016/j.neuron.2019.04.034>. 16, 17
- [KMWL08] KNOTT G., MARCHMAN H., WALL D., LICH B.: Serial Section Scanning Electron Microscopy of Adult Brain Tissue Using Focused Ion Beam Milling. *Journal of Neuroscience* 28, 12 (Mar. 2008), 2959–2964. URL: <https://www.jneurosci.org/content/28/12/2959>, doi:10.1523/JNEUROSCI.3189-07.2008. 5
- [KP19] KATZ W. T., PLAZA S. M.: DVID: Distributed Versioned Image-Oriented Dataservice. *Frontiers in Neural Circuits* 13 (Feb. 2019), 5. URL: <https://www.frontiersin.org/article/10.3389/fncir.2019.00005/full>, doi:10.3389/fncir.2019.00005. 12, 13
- [KVRKB*15] KAYNIG V., VAZQUEZ-REINA A., KNOWLES-BARLEY S., ROBERTS M., JONES T. R., KASTHURI N., MILLER E., LICHTMAN J., PFISTER H.: Large-scale automatic reconstruction of neuronal processes from electron microscopy images. *Medical Image Analysis* 22, 1 (May 2015), 77–88. URL: <https://linkinghub.elsevier.com/retrieve/pii/S1361841515000286>, doi:10.1016/j.media.2015.02.001. 10
- [LB08] LEE S.-C., BAJCSY P.: Trajectory fusion for three-dimensional volume reconstruction. *Computer Vision and Image Understanding* 110, 1 (Apr. 2008), 19–31. URL: <https://www.sciencedirect.com/science/article/pii/S107731420700032X>, doi:10.1016/j.cviu.2007.02.005. 7
- [LBA11] LONGAIR M. H., BAKER D. A., ARMSTRONG J. D.: Simple Neurite Tracer: open source software for reconstruction, visualization and analysis of neuronal processes. *Bioinformatics* 27, 17 (Sept. 2011), 2453–2454. URL: <https://academic.oup.com/bioinformatics/article-lookup/doi/10.1093/bioinformatics/btr390>, doi:10.1093/bioinformatics/btr390. 8
- [LBD*21] LINDOW N., BRÜNING F. N., DERCKSEN V. J., FABIG G., KIEWISZ R., REDEMANN S., MÜLLER-REICHERT T., PROHASKA S., BAUM D.: Semi-automatic stitching of filamentous structures in image stacks from serial-section electron tomography. *Journal of Microscopy* 284, 1 (Oct. 2021), 25–44. doi:10.1111/jmi.13039. 8
- [LD11] LICHTMAN J. W., DENK W.: The Big and the Small: Challenges of Imaging the Brain's Circuits. *Science* 334, 6056 (Nov. 2011), 618–623. URL: <https://www.sciencemag.org/lookup/doi/10.1126/science.1209168>, doi:10.1126/science.1209168. 3
- [LFP11] LUZZATI F., FASOLO A., PERETTO P.: Combining Confocal Laser Scanning Microscopy with Serial Section Reconstruction in the Study of Adult Neurogenesis. *Frontiers in Neuroscience* 5 (2011). URL: <https://www.frontiersin.org/article/10.3389/fnins.2011.00070>. 7
- [LLS21] LEE K., LU R., LUTHER K., SEUNG H. S.: Learning and Segmenting Dense Voxel Embeddings for 3D Neuron Reconstruction. *IEEE Transactions on Medical Imaging* 40, 12 (Dec. 2021), 3801–3811. URL: <https://ieeexplore.ieee.org/document/9489304/>, doi:10.1109/TMI.2021.3097826. 8
- [LLS08] LICHTMAN J. W., LIVET J., SANES J. R.: A technicolour approach to the connectome. *Nature Reviews Neuroscience* 9, 6 (June 2008), 417–422. URL: <http://www.nature.com/articles/nrn2391>, doi:10.1038/nrn2391. 4, 10
- [LLZ*22] LAUENBURG L., LIN Z., ZHANG R., SANTOS M. D., HUANG S., ARGANDA-CARRERAS I., BOYDEN E. S., PFISTER H., WEI D.: Instance Segmentation of Unlabeled Modalities via Cyclic Segmentation GAN. *arXiv:2204.03082 [cs]* (Apr. 2022). arXiv: 2204.03082. URL: <http://arxiv.org/abs/2204.03082.8>
- [Low99] LOWE D.: Object recognition from local scale-invariant features. In *Proceedings of the Seventh IEEE International Conference on Computer Vision* (Sept. 1999), vol. 2, pp. 1150–1157 vol.2. doi:10.1109/ICCV.1999.790410. 7
- [Low04] LOWE D. G.: Distinctive Image Features from Scale-Invariant Keypoints. *International Journal of Computer Vision* 60, 2 (Nov. 2004), 91–110. URL: <https://doi.org/10.1023/B:VISI.0000029664.99615.94>, doi:10.1023/B:VISI.0000029664.99615.94. 6
- [LPS14] LICHTMAN J., PFISTER H., SHAVIT N.: The big data challenges of connectomics. *Nature Neuroscience* 17, 11 (Nov. 2014), 1448–1454. URL: <https://www.nature.com/articles/nn.3837>, doi:10.1038/nn.3837. 3, 5
- [LQX*19] LI S., QUAN T., XU C., HUANG Q., KANG H., CHEN Y., LI A., FU L., LUO Q., GONG H., ZENG S.: Optimization of Traced Neuron Skeleton Using Lasso-Based Model. *Frontiers in Neuroanatomy* 13 (2019). URL: <https://www.frontiersin.org/article/10.3389/fnana.2019.00018>. 8
- [LRL*21] LUCAS A. M., RYDER P. V., LI B., CIMINI B. A., ELICEIRI K. W., CARPENTER A. E.: Open-source deep-learning software for bioimage segmentation. *Molecular Biology of the Cell* 32, 9 (2021), 823–829. URL: <https://doi.org/10.1091/mbc.E20-10-0660>. 2, 8
- [LWJ*20] LIN Z., WEI D., JANG W.-D., ZHOU S., CHEN X., WANG X., SCHALEK R., BERGER D., MATEJEK B., KAMENTSKY L., OTHERS: Two stream active query suggestion for active learning in connectomics. In *European Conference on Computer Vision* (2020), Springer, pp. 103–120. 10
- [LWK*07] LIVET J., WEISSMAN T. A., KANG H., DRAFT R. W., LU J., BENNIS R. A., SANES J. R., LICHTMAN J. W.: Transgenic strategies for combinatorial expression of fluorescent proteins in the nervous system. *Nature* 450, 7166 (Nov. 2007), 56–62. URL: <http://www.nature.com/articles/nature06293>, doi:10.1038/nature06293. 5

- [LWLP21] LIN Z., WEI D., LICHTMAN J., PFISTER H.: PyTorch Connectomics: A Scalable and Flexible Segmentation Framework for EM Connectomics. *arXiv:2112.05754* (Dec. 2021). arXiv: 2112.05754. URL: <https://arxiv.org/abs/2112.05754>. 8, 23
- [LWP*21] LIN Z., WEI D., PETKOVA M. D., WU Y., AHMED Z., K K. S., ZOU S., WENDT N., BOULANGER-WEILL J., WANG X., DHANYASI N., ARGANDA-CARRERAS I., ENGERT F., LICHTMAN J., PFISTER H.: NucMM Dataset: 3D Neuronal Nuclei Instance Segmentation at Sub-Cubic Millimeter Scale. In *Medical Image Computing and Computer Assisted Intervention – MICCAI 2021*, de Bruijne M., Cattin P. C., Cotin S., Padov N., Speidel S., Zheng Y., Essert C., (Eds.), vol. 12901. Springer International Publishing, Cham, 2021, pp. 164–174. Series Title: Lecture Notes in Computer Science. URL: https://link.springer.com/10.1007/978-3-030-87193-2_16, doi:10.1007/978-3-030-87193-2_16. 18, 21, 22
- [LZL*17] LEE K., ZUNG J., LI P., JAIN V., SEUNG H. S.: Superhuman accuracy on the SNEMI3D connectomics challenge. URL: <https://arxiv.org/abs/1706.00120>. 8
- [LZPJ17] LI R., ZENG T., PENG H., JI S.: Deep Learning Segmentation of Optical Microscopy Images Improves 3-D Neuron Reconstruction. *IEEE Transactions on Medical Imaging* 36, 7 (July 2017), 1533–1541. URL: <http://ieeexplore.ieee.org/document/7874113/>, doi:10.1109/TMI.2017.2679713. 8
- [MAAB*18] MOHAMMED H., AL-AWAMI A. K., BEYER J., CALI C., MAGISTRETTI P., PFISTER H., HADWIGER M.: Abstractocyte: A Visual Tool for Exploring Nanoscale Astroglial Cells. *IEEE Transactions on Visualization and Computer Graphics* 24, 1 (Jan. 2018), 853–861. URL: <http://ieeexplore.ieee.org/document/8017643/>, doi:10.1109/TVCG.2017.2744278. 19
- [MBK*19] MOEN E., BANNON D., KUDO T., GRAF W., COVERT M., VAN VALEN D.: Deep learning for cellular image analysis. *Nature methods* 16, 12 (2019), 1233–1246. URL: eplearningforcellularimageanalysis.2.8
- [MCVA17] MAGLIARO C., CALLARA A. L., VANELLO N., AHLUWALIA A.: A Manual Segmentation Tool for Three-Dimensional Neuron Datasets. *Frontiers in Neuroinformatics* 11 (2017). URL: <https://www.frontiersin.org/article/10.3389/fninf.2017.00036.9>
- [MFL*16] MA C., FORBES A. G., LLANO D. A., BERGER-WOLF T., KENYON R. V.: SwordPlots: Exploring Neuron Behavior within Dynamic Communities of Brain Networks. *Electronic Imaging* 28, 16 (Feb. 2016), 1–13. URL: <https://library.imaging.org/ei/articles/28/16/art00051>, doi:10.2352/ISSN.2470-1173.2016.16.HVEI-134.17
- [MHJ*17] MATEJEK B., HAEHN D., LEKSCHAS F., MITZENMACHER M., PFISTER H.: Compresso: Efficient compression of segmentation data for connectomics. In *International Conference on Medical Image Computing and Computer-Assisted Intervention* (2017), Springer, pp. 781–788. URL: https://link.springer.com/chapter/10.1007/978-3-319-66182-7_89. 13
- [MHZ*19] MATEJEK B., HAEHN D., ZHU H., WEI D., PARAG T., PFISTER H.: Biologically-Constrained Graphs for Global Connectomics Reconstruction. doi:10.1109/CVPR.2019.00219. 12
- [MJB*21] MINNEN D., JANUSZEWSKI M., BLAKELY T., SHAPSON-COE A., SCHALEK R. L., BALLÉ J., LICHTMAN J. W., JAIN V.: Denoising-based Image Compression for Connectomics. Tech. rep., Dec. 2021. URL: <https://www.biorxiv.org/content/10.1101/2021.05.29.445828v2.5>
- [MKRE16] MWALONGO F., KRONE M., REINA G., ERTL T.: State-of-the-Art Report in Web-based Visualization. *Computer Graphics Forum* 35, 3 (June 2016), 553–575. URL: <https://onlinelibrary.wiley.com/doi/10.1111/cgf.12929>, doi:10.1111/cgf.12929. 2
- [MMS*19] MEIROVITCH Y., MI L., SARIBEKYAN H., MATVEEV A., ROLNICK D., SHAVIT N.: Cross-Classification Clustering: An Efficient Multi-Object Tracking Technique for 3-D Instance Segmentation in Connectomics. In *Proceedings of the IEEE/CVF Conference on Computer Vision and Pattern Recognition (CVPR)* (June 2019). 8
- [MPL*17] MA C., PELLOLIO F., LLANO D. A., STEBBINGS K. A., KENYON R. V., ELISABETA MARAI G.: RemBrain: Exploring Dynamic Biospatial Networks with Mosaic Matrices and Mirror Glyphs. *Journal of Imaging Science and Technology* 61, 6 (Nov. 2017), 60404–1–60404–13. URL: <https://library.imaging.org/jist/articles/61/6/art00005>, doi:10.2352/J.ImagingSci.Tech.2017.61.6.060404. 17
- [MRJ*21] MATELSKY J. K., REILLY E. P., JOHNSON E. C., STISO J., BASSETT D. S., WESTER B. A., GRAYRONCAL W.: DotMotif: an open-source tool for connectome subgraph isomorphism search and graph queries. *Scientific Reports* 11, 1 (June 2021), 13045. URL: <https://www.nature.com/articles/s41598-021-91025-5>, doi:10.1038/s41598-021-91025-5. 10, 21, 23
- [MSBS*21] MAITIN-SHEPARD J., BADEN A., SILVERSMITH W., PERLMAN E., COLLMAN F., BLAKELY T., FUNKE J., JORDAN C., FALK B., KEMNITZ N., TINGZHAO, ROAT C., CASTRO M., JAGANNATHAN S., MOENIGIN, CLEMENTS J., HOAG A., KATZ B., PARSONS D., WU J., KAMENTSKY L., CHERVAKOV P., HUBBARD P., BERG S., HOFFER J., HALAGERI A., MACHACEK C., MADER K., ROEDER L., LI P. H.: google/neuroglancer:, Oct. 2021. URL: <https://zenodo.org/record/5573294>, doi:10.5281/ZENODO.5573294. 15, 16, 21, 23
- [MUM*21] McDONALD T., USHER W., MORRICAL N., GYULASSY A., PETRUZZA S., FEDERER F., ANGELUCCI A., PASCUCCI V.: Improving the Usability of Virtual Reality Neuron Tracing with Topological Elements. *IEEE Transactions on Visualization and Computer Graphics* 27, 2 (Feb. 2021), 744–754. doi:10.1109/TVCG.2020.3030363. 9
- [MYT*21] MU S., YU S.-C., TURNER N. L., MCKELLAR C. E., DORKENWALD S., COLLMAN F., KOOLMAN S., MOORE M., MORE-JOHN S., SILVERMAN B., WILLIE K., WILLIE R., BLAND D., BURKE A., ASHWOOD Z., LUTHER K., CASTRO M., OGEDENGBE O., SILVERSMITH W., WU J., HALAGERI A., MACRINA T., KEMNITZ N., MURTHY M., SEUNG H. S.: 3D reconstruction of cell nuclei in a full *Drosophila* brain. preprint, Neuroscience, Nov. 2021. URL: <http://biorxiv.org/lookup/doi/10.1101/2021.11.04.467197>. 18
- [Neu] NEURODATA: Open Connectome Project. Last accessed: 2/1/2022. URL: <https://neurodata.io/project/ocp/>. 20
- [NIKP*13] NUNEZ-IGLESIAS J., KENNEDY R., PARAG T., SHI J., CHKLOVSKII D. B.: Machine Learning of Hierarchical Clustering to Segment 2D and 3D Images. *PLoS ONE* 8, 8 (Aug. 2013), e71715. URL: <https://dx.plos.org/10.1371/journal.pone.0071715>, doi:10.1371/journal.pone.0071715. 10
- [NJJ21] NGUYEN K. T., JANG G., JEONG W.-K.: RLCorrector: Reinforced Proofreading for Connectomics Image Segmentation. *arXiv:2106.05487 [cs]* (June 2021). arXiv: 2106.05487. URL: <https://arxiv.org/abs/2106.05487>. 12
- [Pad00] PADDOCK S. W.: Principles and practices of laser scanning confocal microscopy. *Molecular Biotechnology* 16, 2 (Oct. 2000), 127–149. URL: <https://doi.org/10.1385/MB:16:2:127>, doi:10.1385/MB:16:2:127. 4
- [PBB*21] PASTOR L., BAYONA S., BRITO J., CUEVAS M., FERNAUD I., GALINDO S., GARCÍA-CANTERO J., QUEVEDO F., MATA S., ROBLES O., RODRÍGUEZ A., TOHARIA P., ZDRAVKOVIC A.: A Unified Framework for Neuroscience Morphological Data Visualization. *Applied Sciences* 11, 10 (May 2021), 4652. URL: <https://www.mdpi.com/2076-3417/11/10/4652>, doi:10.3390/app11104652. 18, 19
- [PBK*18] PARAG T., BERGER D., KAMENTSKY L., STAFFLER B.,

- [WEI18] WEI D., HELMSTAEDTER M., LICHTMAN J. W., PFISTER H.: Detecting Synapse Location and Connectivity by Signed Proximity Estimation and Pruning with Deep Nets. *arXiv:1807.02739* (Oct. 2018). URL: <http://arxiv.org/abs/1807.02739>. 9
- [PCL*11] PENG H., CHUNG P., LONG F., QU L., JENETT A., SEEDS A. M., MYERS E. W., SIMPSON J. H.: BrainAligner: 3D registration atlases of Drosophila brains. *Nature Methods* 8, 6 (June 2011), 493–498. URL: <https://www.nature.com/articles/nmeth.1602>, doi:10.1038/nmeth.1602. 7
- [PHG*21] PHELPS J. S., HILDEBRAND D. G. C., GRAHAM B. J., KUAN A. T., THOMAS L. A., NGUYEN T. M., BUHNMANN J., AZEVEDO A. W., SUSTAR A., AGRAWAL S., LIU M., SHANNY B. L., FUNKE J., TUTHILL J. C., LEE W.-C. A.: Reconstruction of motor control circuits in adult Drosophila using automated transmission electron microscopy. *Cell* 184, 3 (Feb. 2021), 759–774.e18. URL: <https://linkinghub.elsevier.com/retrieve/pii/S0092867420316834>, doi:10.1016/j.cell.2020.12.013. 21, 22
- [PHK04] PIEPER S., HALLE M., KIKINIS R.: 3D Slicer. In *2004 2nd IEEE International Symposium on Biomedical Imaging: Nano to Macro* (Apr. 2004), pp. 632–635 Vol. 1. doi:10.1109/ISBI.2004.1398617. 9
- [PKB*12] PFISTER H., KAYNIG V., BOTHA C. P., BRUCKNER S., DERCKSEN V. J., HEDE H.-C., ROERDINK J. B. T. M.: Visualization in Connectomics. *arXiv:1206.1428* (Aug. 2012). URL: <http://arxiv.org/abs/1206.1428>. 2, 4
- [Pla16] PLAZA S.: Focused Proofreading to Reconstruct Neural Connectomes from EM Images at Scale. pp. 249–258. doi:10.1007/978-3-319-46976-8_26. 12
- [PLM11] PENG H., LONG F., MYERS G.: Automatic 3D neuron tracing using all-path pruning. *Bioinformatics* 27, 13 (July 2011), i239–i247. URL: <https://academic.oup.com/bioinformatics/article-lookup/doi/10.1093/bioinformatics/btr237>, doi:10.1093/bioinformatics/btr237. 8, 9
- [PMT*15] PASTOR L., MATA S., TOHARIA P., BAYONA S., BRITO J. P., GARCIA-CANTERO J. J.: NeuroScheme: Efficient Multi-scale Representations for the Visual Exploration of Morphological Data in the Human Brain Neocortex. URL: <https://digilib.eg.org:443/xmlui/handle/10.2312/ceig.20151208>, doi:10.2312/ceig.20151208. 18
- [PPKM15] PAPADOPoulos C., PETKOV K., KAUFMAN A. E., MUELLER K.: The Reality Deck—an Immersive Gigapixel Display. *IEEE Computer Graphics and Applications* 35, 1 (Jan. 2015), 33–45. doi:10.1109/MCG.2014.80. 14
- [PRL*10] PENG H., RUAN Z., LONG F., SIMPSON J. H., MYERS E. W.: V3D enables real-time 3D visualization and quantitative analysis of large-scale biological image data sets. *Nature biotechnology* 28, 4 (2010), 348–353. URL: <https://doi.org/10.1038/nbt.1612>. 15, 16
- [PYD04] PAPADIMITRIOU C., YAPIJAKIS C., DAVAKI P.: Use of truncated pyramid representation methodology in three-dimensional reconstruction: an example. *Journal of Microscopy* 214, 1 (2004), 70–75. URL: <https://onlinelibrary.wiley.com/doi/abs/10.1111/j.0022-2720.2004.01298.x>, doi:10.1111/j.0022-2720.2004.01298.x. 7
- [QHJ21] QUAN T. M., HILDEBRAND D. G. C., JEONG W.-K.: FusionNet: A Deep Fully Residual Convolutional Neural Network for Image Segmentation in Connectomics. *Frontiers in Computer Science* 3 (May 2021), 613981. URL: <https://www.frontiersin.org/articles/10.3389/fcomp.2021.613981/full>, doi:10.3389/fcomp.2021.613981. 8
- [QZL*16] QUAN T., ZHOU H., LI J., LI S., LI A., LI Y., LV X., LUO Q., GONG H., ZENG S.: NeuroGPS-Tree: automatic reconstruction of large-scale neuronal populations with dense neurites. *Nature Methods* 13, 1 (Jan. 2016), 51–54. URL: <https://www.nature.com/articles/nmeth.3662>, doi:10.1038/nmeth.3662. 8
- [RHC20] ROSSI L. F., HARRIS K. D., CARANDINI M.: Spatial connectivity matches direction selectivity in visual cortex. *Nature* 588, 7839 (Dec. 2020), 648–652. URL: <https://www.nature.com/articles/s41586-020-2894-4>, doi:10.1038/s41586-020-2894-4. 5
- [RJVR*11] ROBERTS M., JEONG W.-K., VÁZQUEZ-REINA A., UNGER M., BISCHOF H., LICHTMAN J., PFISTER H.: Neural process reconstruction from sparse user scribbles. *MICCAI International Conference on Medical Image Computing and Computer-Assisted Intervention* 14, Pt 1 (2011), 621–628. doi:10.1007/978-3-642-23623-5_78. 9
- [RKV*12] RAGAN T., KADIRI L. R., VENKATARAJU K. U., BAHLMANN K., SUTIN J., TARANDA J., ARGANDA-CARRERAS I., KIM Y., SEUNG H. S., OSTEN P.: Serial two-photon tomography for automated ex vivo mouse brain imaging. *Nature Methods* 9, 3 (Mar. 2012), 255–258. URL: <https://www.nature.com/articles/nmeth.1854>, doi:10.1038/nmeth.1854. 5
- [RMA17] REES C. L., MORADI K., ASCOLI G. A.: Weighing the evidence in Peters’ rule: does neuronal morphology predict connectivity? *Trends in neurosciences* 40, 2 (2017), 63–71. 10
- [RMP*17] ROLNICK D., MEIROVITCH Y., PARAG T., PFISTER H., JAIN V., LICHTMAN J., BOYDEN E., SHAVIT N.: Morphological Error Detection in 3D Segmentations. *ArXiv* (2017). URL: <https://arxiv.org/abs/1705.10882>. 12
- [RPKF*14] RONCAL W. G., PEKALA M., KAYNIG-FITTKAU V., KLEISSAS D. M., VOGELSTEIN J. T., PFISTER H., BURNS R., VOGELSTEIN R. J., CHEVILLET M. A., HAGER G. D.: Vesicle: volumetric evaluation of synaptic interfaces using computer vision at large scale. *arXiv preprint arXiv:1403.3724* (2014). URL: <https://arxiv.org/abs/1403.3724>. 10
- [RPS*19] RIBEIRO P., PAREDES P., SILVA M. E. P., APARICIO D., SILVA F.: A Survey on Subgraph Counting: Concepts, Algorithms and Applications to Network Motifs and Graphlets. *arXiv:1910.13011 [cs]* (Oct. 2019). arXiv: 1910.13011. URL: <http://arxiv.org/abs/1910.13011>. 2, 10
- [SBB*00] SATO M., BITTER I., BENDER M. A., KAUFMAN A. E., NAKAJIMA M.: TEASAR: Tree-Structure Extraction Algorithm for Accurate and Robust Skeletons. In *Proceedings of the 8th Pacific Conference on Computer Graphics and Applications* (2000), p. 281. URL: <https://ieeexplore.ieee.org/abstract/document/883951>. 11, 18
- [SBJ*21] SCHLEGEL P., BARNES C., JAGANNATHAN S., PEDIGO B., COURT R.: navis-org/navis: Version 1.1.0, Nov. 2021. URL: <https://zenodo.org/record/5710143>, doi:10.5281/ZENODO.5710143. 18, 19, 23
- [SBLW21] SILVERSMITH W., BAE J. A., LI P. H., WILSON A.: seung-lab/kimimaro: Zenodo Release v1, Sept. 2021. URL: <https://zenodo.org/record/5539913>, doi:10.5281/ZENODO.5539913. 18, 19, 23
- [SBS*13] SORGER J., BÜHLER K., SCHULZE F., LIU T., DICKSON B.: neuroMAP — Interactive graph-visualization of the fruit fly’s neural circuit. In *IEEE Symposium on Biological Data Visualization (BioVis)* (2013), pp. 73–80. URL: <http://ieeexplore.ieee.org/lpdocs/epic03/wrapper.htm?arnumber=6664349>, doi:10.1109/BioVis.2013.6664349. 17
- [SCHT09] SAALFELD S., CARDONA A., HARTENSTEIN V., TOMANČAK P.: CATMAID: collaborative annotation toolkit for massive amounts of image data. *Bioinformatics* 25, 15 (2009), 1984–1986. URL: <https://doi.org/10.1093/bioinformatics/btp266>. 9, 11, 16, 23
- [SCHT10] SAALFELD S., CARDONA A., HARTENSTEIN V., TOMANČAK P.: As-rigid-as-possible mosaicking and serial section registration of large ssTEM datasets. *Bioinformatics* 26, 12 (June 2010). URL: <https://academic.oup.com/bioinformatics/article/26/12/i57/286450>, doi:10.1093/bioinformatics/btq219. 6

- [SCJB*21] SHAPSON-COE A., JANUSZEWSKI M., BERGER D. R., POPE A., WU Y., BLAKELY T., SCHALEK R. L., LI P. H., WANG S., MAITIN-SHEPARD J., KARLUPIA N., DORKENWALD S., SJOSTEDT E., LEAVITT L., LEE D., BAILEY L., FITZMAURICE A., KAR R., FIELD B., WU H., WAGNER-CARENA J., ALEY D., LAU J., LIN Z., WEI D., PFISTER H., PELEG A., JAIN V., LICHTMAN J. W.: *A connectomic study of a petascale fragment of human cerebral cortex*. Tech. rep., Nov. 2021. URL: <https://www.biorxiv.org/content/10.1101/2021.05.29.446289v4>. 1, 3, 5, 8, 13, 14, 16, 17, 21, 22
- [SCK*21] SILVERSMITH W., COLLMAN F., KEMNITZ N., WU J., CASTRO M., FALK B., ROAT C., MACRINA T., PERLMAN E., SHANGMU, HALAGERI A., GUNN P., JAGANNATHAN S., HOAG A., TURNER N., DORKENWALD S.: seung-lab/cloud-volume: Zenodo Release v1, Nov. 2021. URL: <https://zenodo.org/record/5671443>, doi: 10.5281/ZENODO.5671443. 14, 18
- [SDJ*19] SCHUBERT P. J., DORKENWALD S., JANUSZEWSKI M., JAIN V., KORNFELD J.: Learning cellular morphology with neural networks. *Nature Communications* 10, 1 (Dec. 2019), 2736. URL: <http://www.nature.com/articles/s41467-019-10836-3>, doi: 10.1038/s41467-019-10836-3. 18, 19
- [SEG15] SAXENA M., ELURU G., GORTHI S. S.: Structured illumination microscopy. *Advances in Optics and Photonics* 7, 2 (June 2015), 241–275. URL: <https://www.osapublishing.org/aop/abstract.cfm?uri=aop-7-2-241>, doi: 10.1364/AOP.7.000241. 5
- [Seu12a] SEUNG H.: *Connectome: How the brain's wiring makes us who we are*. HMH, 2012. 1, 3
- [Seu12b] SEUNG S.: EyeWire. (accessed Oct 14, 2021). URL: <http://eyewire.org>. 12
- [SFCT12] SAALFELD S., FETTER R., CARDONA A., TOMANCAK P.: Elastic volume reconstruction from series of ultra-thin microscopy sections. *Nature Methods* 9, 7 (July 2012), 717–720. URL: <https://www.nature.com/articles/nmeth.2072>, doi: 10.1038/nmeth.2072. 7
- [SHM13] SICAT R., HADWIGER M., MITRA N.: Graph Abstraction for Simplified Proofreading of Slice-based Volume Segmentation. In *Eurographics* (2013). doi: 10.2312/conf/EG2013/short_077-080. 12
- [SHW*20] SHEN F. Y., HARRINGTON M. M., WALKER L. A., CHENG H. P. J., BOYDEN E. S., CAI D.: Light microscopy based approach for mapping connectivity with molecular specificity. *Nature Communications* 11, 1 (Sept. 2020), 4632. URL: <https://www.nature.com/articles/s41467-020-18422-8>, doi: 10.1038/s41467-020-18422-8. 5
- [SL16] SWANSON L. W., LICHTMAN J. W.: From Cajal to Connectome and Beyond. *Annual Review of Neuroscience* 39 (July 2016), 197–216. doi: 10.1146/annurev-neuro-071714-033954. 3
- [SMB*14] SWOBODA N., MOOSBURNER J., BRUCKNER S., YU J. Y., DICKSON B. J., BÜHLER K.: *Visual and Quantitative Analysis of Higher Order Arborization Overlaps for Neural Circuit Research*. The Eurographics Association, 2014. URL: <https://diglib.eg.org:443/xmlui/handle/10.2312/vcgbm.20141189.107-116>, doi: 10.2312/vcgbm.20141189.107-116. 10
- [SMB*17] SWOBODA N., MOOSBURNER J., BRUCKNER S., YU J. Y., DICKSON B. J., BÜHLER K.: Visualization and Quantification for Interactive Analysis of Neural Connectivity in Drosophila. *Computer Graphics Forum* 36, 1 (2017), 160–171. URL: <https://onlinelibrary.wiley.com/doi/abs/10.1111/cgf.12792>, doi: 10.1111/cgf.12792. 10
- [SMBC*20] SCHNEIDER-MIZELL C. M., BODOR A. L., COLLMAN F., BRITTAINE D., BLECKERT A. A., DORKENWALD S., TURNER N. L., MACRINA T., LEE K., LU R., WU J., ZHUANG J., NANDI A., HU B., BUCHANAN J., TAKENO M. M., TORRES R., MAHALINGAM G., BUMBARGER D. J., LI Y., CHARTRAND T., KEMNITZ N., SILVERSMITH W. M., IH D., ZUNG J., ZLATESKI A., TARTAVULL I., POPOVYCH S., WONG W., CASTRO M., JORDAN C. S., FROUDARAKIS E., BECKER L., SUCKOW S., REIMER J., TOLIAS A. S., ANASTASSIOU C., SEUNG H. S., REID R. C., COSTA N. M. D.: *Chandelier cell anatomy and function reveal a variably distributed but common signal*. Tech. rep., Apr. 2020. URL: <https://www.biorxiv.org/content/10.1101/2020.03.31.018952v1>. 21, 22
- [SND*21] SHERIDAN A., NGUYEN T., DEB D., LEE W.-C. A., SAALFELD S., TURAGA S., MANOR U., FUNKE J.: *Local Shape Descriptors for Neuron Segmentation*. preprint, Neuroscience, Jan. 2021. URL: <http://biorxiv.org/lookup/doi/10.1101/2021.01.18.427039>. 8
- [SPB*15] SERGEJEVA M., PAPP E. A., BAKKER R., GAUDNEK M. A., OKAMURA-OHO Y., BOLINE J., BJAALIE J. G., HESS A.: Anatomical landmarks for registration of experimental image data to volumetric rodent brain atlas templates. *Journal of Neuroscience Methods* 240 (Jan. 2015), 161–169. URL: <https://www.sciencedirect.com/science/article/pii/S0165027014003975>, doi: 10.1016/j.jneumeth.2014.11.005. 7
- [SSKH11] SOMMER C., STRAEHLE C., KÖTHE U., HAMPRECHT F. A.: Ilastik: Interactive learning and segmentation toolkit. In *IEEE International Symposium on Biomedical Imaging: From Nano to Macro* (2011), pp. 230–233. doi: 10.1109/ISBI.2011.5872394. 9
- [SSR*05] SONG S., SJÖSTRÖM P. J., REIGL M., NELSON S., CHKLOVSKII D. B.: Highly Nonrandom Features of Synaptic Connectivity in Local Cortical Circuits. *PLoS Biology* 3, 3 (Mar. 2005), e68. URL: <https://dx.plos.org/10.1371/journal.pbio.0030068>, doi: 10.1371/journal.pbio.0030068. 10
- [STK05] SPORN O., TONONI G., KÖTTER R.: The Human Connectome: A Structural Description of the Human Brain. *PLOS Computational Biology* 1, 4 (Sept. 2005). URL: <https://journals.plos.org/ploscompbiol/article?id=10.1371/journal.pcbi.0010042>. 3
- [SXJ*20] SCHEFFER L. K., XU C. S., JANUSZEWSKI M., LU Z., TAKEMURA S.-Y., HAYWORTH K. J., HUANG G. B., SHINOMIYA K., MAITLIN-SHEPARD J., BERG S., CLEMENTS J., HUBBARD P. M., KATZ W. T., UMAYAM L., ZHAO T., ACKERMAN D., BLAKELY T., BOGOVIC J., DOLAFI T., KAINMUELLER D., KAWASE T., KHAIRY K. A., LEAVITT L., LI P. H., LINDSEY L., NEUBARTH N., OLBRIS D. J., OTSUNA H., TRAUTMAN E. T., ITO M., BATES A. S., GOLDAMMER J., WOLFF T., SVIRSKAS R., SCHLEGEL P., NEACE E., KNECHT C. J., ALVARADO C. X., BAILEY D. A., BALLINGER S., BORYCZ J. A., CANINO B. S., CHEATHAM N., COOK M., DREHER M., DUCLOS O., EUBANKS B., FAIRBANKS K., FINLEY S., FORK-NALL N., FRANCIS A., HOPKINS G. P., JOYCE E. M., KIM S., KIRK N. A., KOVALYAK J., LAUCHE S. A., LOHFF A., MALDONADO C., MANLEY E. A., MCINNIS S., MOONEY C., NDAMA M., OGUNDEYI O., OKEOMA N., ORDISH C., PADILLA N., PATRICK C. M., PATERSON T., PHILLIPS E. E., PHILLIPS E. M., RAMPALLY N., RIBEIRO C., ROBERTSON M. K., RYMER J. T., RYAN S. M., SAMMONS M., SCOTT A. K., SCOTT A. L., SHINOMIYA A., SMITH C., SMITH K., SMITH N. L., SOBESKI M. A., SULEIMAN A., SWIFT J., TAKEMURA S., TALEBI I., TARNOGORSKA D., TENSHERE E., TOKHI T., WALSH J. J., YANG T., HORNE J. A., LI F., PAREKH R., RIVLIN P. K., JAYARAMAN V., COSTA M., JEFFERIS G. S., ITO K., SAALFELD S., GEORGE R., MEINERTZHAGEN I. A., RUBIN G. M., HESS H. F., JAIN V., PLAZA S. M.: A connectome and analysis of the adult Drosophila central brain. *eLife* 9 (Sept. 2020). URL: <https://elifesciences.org/articles/57443>, doi: 10.7554/eLife.57443. 10, 14, 16
- [TAOZ12] TAGLIASACCHI A., ALHASHIMI I., OLSON M., ZHANG H.: Mean Curvature Skeletons. *Computer Graphics Forum* 31, 5 (2012), 1735–1744. URL: <https://onlinelibrary.wiley.com/doi/abs/10.1111/j.1467-8659.2012.03178.x>, doi: 10.1111/j.1467-8659.2012.03178.x. 11
- [TCG*22] TROIDL J., CALI C., GRÖLLER E., PFISTER H., HADWIGER

- M., BEYER J.: Barrio: Customizable Spatial Neighborhood Analysis and Comparison for Nanoscale Brain Structures. *Computer Graphics Forum (Proceedings Eurographics/IEEE Symposium on Visualization, Eurovis 2022)* 41, 3 (2022), to appear. 19
- [TKG*10] TASDIZEN T., KOSHEVOY P., GRIMM B. C., ANDERSON J. R., JONES B. W., WATT C. B., WHITAKER R. T., MARC R. E.: Automatic mosaicking and volume assembly for high-throughput serial-section transmission electron microscopy. *Journal of Neuroscience Methods* 193, 1 (Oct. 2010), 132–144. URL: <https://www.sciencedirect.com/science/article/pii/S0165027010004413>, doi:10.1016/j.jneumeth.2010.08.001. 6
- [TKH*12] TAPIA J. C., KASTHURI N., HAYWORTH K. J., SCHALEK R., LICHTMAN J. W., SMITH S. J., BUCHANAN J.: High-contrast en bloc staining of neuronal tissue for field emission scanning electron microscopy. *Nature Protocols* 7, 2 (Feb. 2012), 193–206. URL: <https://www.nature.com/articles/nprot.2011.439>, doi:10.1038/nprot.2011.439. 4
- [TBL*11] TSAI C.-L., LISTER J., BJORNSSON C., SMITH K., SHAIN W., BARNES C., ROYSAM B.: Robust, globally consistent and fully automatic multi-image registration and montage synthesis for 3-D multi-channel images. *Journal of Microscopy* 243, 2 (Aug. 2011), 154–171. URL: <https://onlinelibrary.wiley.com/doi/10.1111/j.1365-2818.2011.03489.x>, doi:10.1111/j.1365-2818.2011.03489.x. 6
- [TLRSH17] TINATI R., LUCZAK-ROESCH M., SIMPERL E., HALL W.: An investigation of player motivations in Eyewire, a gamified citizen science project. *Computers in Human Behavior* 73 (2017), 527–540. URL: <https://doi.org/10.1016/j.chb.2016.12.074>. 12
- [TRFE*16] TOHARIA P., ROBLES O. D., FERNAUD-ESPINOZA I., MAKAROVA J., GALINDO S. E., RODRIGUEZ A., PASTOR L., HERERAS O., DEFELIPE J., BENAVIDES-PICCIONE R.: PyramidalExplorer: A New Interactive Tool to Explore Morpho-Functional Relations of Human Pyramidal Neurons. *Frontiers in Neuroanatomy* 9 (2016), 159. URL: <https://www.frontiersin.org/article/10.3389/fnana.2015.00159>, doi:10.3389/fnana.2015.00159. 15, 18, 19
- [UBK*19] URAKUBO H., BULLMANN T., KUBOTA Y., OBA S., ISHII S.: UNI-EM: An environment for deep neural network-based automated segmentation of neuronal electron microscopic images. *Scientific reports* 9, 1 (2019), 1–9. URL: <https://doi.org/10.1038/s41598-019-55431-0>. 8
- [UHM*21] UDVARY D., HARTH P., MACKE J. H., HEGE H.-C., KOCK C. P. J. D., SAKMANN B., OBERLAENDER M.: *The Impact of Neuron Morphology on Cortical Network Architecture*. Tech. rep., Sept. 2021. URL: <https://www.biorxiv.org/content/10.1101/2020.11.13.381087v4>. 10
- [UKF*18] USHER W., KLACANSKY P., FEDERER F., BREMER P.-T., KNOLL A., YARCH J., ANGELUCCI A., PASCUCCI V.: A Virtual Reality Visualization Tool for Neuron Tracing. *IEEE Transactions on Visualization and Computer Graphics* 24, 1 (Jan. 2018), 994–1003. doi:10.1109/TVCG.2017.2744079. 9
- [Uni] UNIVERSITY G. M.: NeuroMorpho.org, last accessed: 2/1/2022. URL: <http://neuromorpho.org/>. 20, 22
- [UP20] USHER W., PASCUCCI V.: Interactive Visualization of Terascale Data in the Browser: Fact or Fiction? In *2020 IEEE 10th Symposium on Large Data Analysis and Visualization (LDav)* (Oct. 2020), pp. 27–36. URL: <https://ieeexplore.ieee.org/document/9308044/>, doi:10.1109/LDav51489.2020.00010. 15
- [Val70] VALVERDE F.: The Golgi Method. A Tool for Comparative Structural Analyses. In *Contemporary Research Methods in Neuroanatomy*, Nauta W. J. H., Ebbesson S. O. E., (Eds.). 1970, pp. 12–31. URL: https://doi.org/10.1007/978-3-642-85986-1_2, doi:10.1007/978-3-642-85986-1_2. 4
- [VMH*16] VOGELSTEIN J. T., MENSCH B., HÄUSSER M., SPRUSTON N., EVANS A. C., KORDING K., AMUNTS K., EBELL C., MULLER J., TELEFONT M., OTHERS: To the cloud! A grassroots proposal to accelerate brain science discovery. *Neuron* 92, 3 (2016), 622–627. URL: <https://doi.org/10.1016/j.neuron.2016.10.033>. 14
- [VMK*16] VIERGEVER M. A., MAINTZ J. A., KLEIN S., MURPHY K., STARING M., PLUIM J. P.: A survey of medical image registration—under review, 2016. URL: <https://doi.org/10.1016/j.media.2016.06.030>. 2
- [VMM*22] VELICKY P., MIGUEL E., MICHALSKA J. M., WEI D., LIN Z., WATSON J. F., TROIDL J., BEYER J., BEN-SIMON Y., SOMMER C., JAHR W., CENAMERI A., BROICHHAGEN J., GRANT S. G. N., JONAS P., NOVARINO G., PFISTER H., BICKEL B., DANZL J. G.: *Saturated reconstruction of living brain tissue*. preprint, Neuroscience, Mar. 2022. URL: <http://biorxiv.org/lookup/doi/10.1101/2022.03.16.484431>, doi:10.1101/2022.03.16.484431. 22
- [VPF*18] VOGELSTEIN J. T., PERLMAN E., FALK B., BADEN A., RONCAL W. G., CHANDRASHEKHAR V., COLLMAN F., SESHAMANI S., PATSOLIC J. L., LILLANEY K., OTHERS: A community-developed open-source computational ecosystem for big neuro data. *Nature methods* 15, 11 (2018), 846–847. URL: <https://doi.org/10.1038/s41592-018-0181-1>. 14
- [VRMP09] VAZQUEZ-REINA A., MILLER E., PFISTER H.: Multiphase geometric couplings for the segmentation of neural processes. In *2009 IEEE Conference on Computer Vision and Pattern Recognition* (June 2009), IEEE, pp. 2020–2027. URL: <https://ieeexplore.ieee.org/document/5206524/>, doi:10.1109/CVPR.2009.5206524. 9
- [VRVP13] VOGELSTEIN J. T., RONCAL W. G., VOGELSTEIN R. J., PRIEBE C. E.: Graph Classification Using Signal-Subgraphs: Applications in Statistical Connectomics. *IEEE Transactions on Pattern Analysis and Machine Intelligence* 35, 7 (July 2013), 1539–1551. URL: <http://ieeexplore.ieee.org/document/6341752/>, doi:10.1109/TPAMI.2012.235. 10
- [WBF*19] WINNUBST J., BAS E., FERREIRA T. A., WU Z., ECONOMO M. N., EDSON P., ARTHUR B. J., BRUNS C., ROKICKI K., SCHAUER D., OLBRIS D. J., MURPHY S. D., ACKERMAN D. G., ARSHADI C., BALDWIN P., BLAKE R., ELSAYED A., HASAN M., RAMIREZ D., DOS SANTOS B., WELDON M., ZAFAR A., DUDMAN J. T., GERFEN C. R., HANTMAN A. W., KORFF W., STERNSON S. M., SPRUSTON N., SVOBODA K., CHANDRASHEKAR J.: Reconstruction of 1,000 Projection Neurons Reveals New Cell Types and Organization of Long-Range Connectivity in the Mouse Brain. *Cell* 179, 1 (Sept. 2019), 268–281.e13. URL: <https://linkinghub.elsevier.com/retrieve/pii/S0092867419308426>, doi:10.1016/j.cell.2019.07.042. 18
- [WBH*10] WON-KI JEONG, BEYER J., HADWIGER M., BLUE R., LAW C., VAZQUEZ-REINA A., REID R. C., LICHTMAN J., PFISTER H.: Ssecret and NeuroTrace: Interactive Visualization and Analysis Tools for Large-Scale Neuroscience Data Sets. *IEEE Computer Graphics and Applications* 30, 3 (May 2010), 58–70. URL: <http://ieeexplore.ieee.org/document/5455822/>, doi:10.1109/MCG.2010.56. 9
- [WBH14] WEAVER C., BRUNS C., HELVENSTEIJN M.: Sharkviewer 1.1, Aug. 2014. URL: <https://zenodo.org/record/11290>, doi:10.5281/ZENODO.11290. 15, 16, 23
- [WCV*14] WEILER N. C., COLLMAN F., VOGELSTEIN J. T., BURNS R., SMITH S. J.: Synaptic molecular imaging in spared and deprived columns of mouse barrel cortex with array tomography. *Scientific Data* 1, 1 (Dec. 2014). URL: <http://www.nature.com/articles/sdata201446>, doi:10.1038/sdata.2014.46. 20, 22
- [Wil] WILSON M.: Introduction to Widefield Microscopy. URL: <https://www.leica-microsystems.com/science-lab/introduction-to-widefield-microscopy/>. 4
- [WLFB*20] WEI D., LIN Z., FRANCO-BARRANCO D., WENDT N., LIU X., YIN W., HUANG X., GUPTA A., JANG W.-D., WANG X.,

- ARGANDA-CARRERAS I., LICHTMAN J. W., PFISTER H.: MitoEM Dataset: Large-Scale 3D Mitochondria Instance Segmentation from EM Images. In *Medical Image Computing and Computer Assisted Intervention – MICCAI 2020*, Martel A. L., Abolmaesum P., Stoyanov D., Mateus D., Zuluaga M. A., Zhou S. K., Racocceanu D., Joskowicz L., (Eds.), vol. 12265. Springer International Publishing, Cham, 2020, pp. 66–76. Series Title: Lecture Notes in Computer Science. URL: https://link.springer.com/10.1007/978-3-030-59722-1_7, doi:10.1007/978-3-030-59722-1_7. 21, 22
- [WLL*21] WEI D., LEE K., LI H., LU R., BAE J. A., LIU Z., ZHANG L., DOS SANTOS M., LIN Z., URAM T., WANG X., ARGANDA-CARRERAS I., MATEJEK B., KASTHURI N., LICHTMAN J., PFISTER H.: AxonEM Dataset: 3D Axon Instance Segmentation of Brain Cortical Regions. In *Medical Image Computing and Computer Assisted Intervention – MICCAI 2021*, de Bruijne M., Cattin P. C., Cotin S., Paday N., Speidel S., Zheng Y., Essert C., (Eds.), vol. 12901. Springer International Publishing, Cham, 2021, pp. 175–185. Series Title: Lecture Notes in Computer Science. URL: https://link.springer.com/10.1007/978-3-030-87193-2_17, doi:10.1007/978-3-030-87193-2_17. 21, 22
- [WNTR11] WANG Y., NARAYANASWAMY A., TSAI C.-L., ROYSAM B.: A Broadly Applicable 3-D Neuron Tracing Method Based on Open-Curve Snake. *Neuroinformatics* 9, 2 (Sept. 2011), 193–217. URL: <https://doi.org/10.1007/s12021-011-9110-5>, doi:10.1007/s12021-011-9110-5. 8
- [WOCH12] WAN Y., OTSUNA H., CHIEN C.-B., HANSEN C.: FluoRender: An Application of 2D Image Space Methods for 3D and 4D Confocal Microscopy Data Visualization in Neurobiology Research. *IEEE Pacific Visualisation Symposium* (2012), 201–208. URL: <https://www.ncbi.nlm.nih.gov/pmc/articles/PMC3622106/>. 14
- [WOH*17] WAN Y., OTSUNA H., HOLMAN H. A., BAGLEY B., ITO M., LEWIS A. K., COLASANTO M., KARDON G., ITO K., HANSEN C.: FluoRender: joint freehand segmentation and visualization for many-channel fluorescence data analysis. *BMC Bioinformatics* 18, 1 (May 2017), 280. URL: <https://doi.org/10.1186/s12859-017-1694-9>, doi:10.1186/s12859-017-1694-9. 14, 15, 23
- [WSLS21] WU J., SILVERSMITH W. M., LEE K., SEUNG H. S.: Chunkflow: hybrid cloud processing of large 3D images by convolutional nets. *Nature Methods* 18, 4 (Apr. 2021), 328–330. URL: <http://www.nature.com/articles/s41592-021-01088-5>, doi:10.1038/s41592-021-01088-5. 8
- [WTY*15] WERTZ A., TRENHOLM S., YONEHARA K., HILLIER D., RAICS Z., LEINWEBER M., SZALAY G., GHANEM A., KELLER G., RÓZSA B., CONZELMANN K.-K., ROSKA B.: Single-cell-initiated monosynaptic tracing reveals layer-specific cortical network modules. *Science* 349, 6243 (July 2015), 70–74. URL: <https://www.science.org/doi/10.1126/science.aab1687>, doi:10.1126/science.aab1687. 5
- [WZB19] WASSIE A. T., ZHAO Y., BOYDEN E. S.: Expansion microscopy: principles and uses in biological research. *Nature methods* 16, 1 (2019), 33–41. Publisher: Nature Publishing Group. 5
- [XJL*20] XU C. S., JANUSZEWSKI M., LU Z., TAKEMURA S.-Y., HAYWORTH K. J., HUANG G., SHINOMIYA K., MAITIN-SHEPARD J., ACKERMAN D., BERG S., BLAKELY T., BOGOVIC J., CLEMENTS J., DOLAFI T., HUBBARD P., KAINMUELLER D., KATZ W., KAWASE T., KHAIRY K. A., LEAVITT L., LI P. H., LINDSEY L., NEUBARTH N., OLBRIS D. J., OTSUNA H., TROUTMAN E. T., UMAYAM L., ZHAO T., ITO M., GOLDAMMER J., WOLFF T., SVIRSKAS R., SCHLEGEL P., NEACE E. R., KNECHT C. J., ALVARADO C. X., BAILEY D. A., BALLINGER S., BORYCZ J. A., CANINO B. S., CHEATHAM N., COOK M., DREHER M., DUCLOS O., EUBANKS B., FAIRBANKS K., FINLEY S., FORKNALL N., FRANCIS A., HOPKINS G. P., JOYCE E. M., KIM S., KIRK N. A., KOVALYAK J., LAUCHIE S. A., LOHFF A., MALDONADO C., MANLEY E. A., MCILIN S., MOONEY C., NDAMA M., OGUNDEYI O., OKEOMA N., ORDISH C., PADILLA N., PATRICK C., PATERSON T., PHILLIPS E. E., PHILLIPS E. M., RAMPALLY N.,
- RIBEIRO C., ROBERTSON M. K., RYMER J. T., RYAN S. M., SAMMONS M., SCOTT A. K., SCOTT A. L., SHINOMIYA A., SMITH C., SMITH K., SMITH N. L., SOBESKI M. A., SULEIMAN A., SWIFT J., TAKEMURA S., TALEBI I., TARNOGORSKA D., TENSHAW E., TOKHI T., WALSH J. J., YANG T., HORNE J. A., LI F., PAREKH R., RIVLIN P. K., JAYARAMAN V., ITO K., SAALFELD S., GEORGE R., MEINERTZHAGEN I., RUBIN G. M., HESS H. F., SCHEFFER L. K., JAIN V., PLAZA S. M.: *A Connectome of the Adult Drosophila Central Brain*. Tech. rep., Jan. 2020. Type: article. URL: <https://www.biorxiv.org/content/10.1101/2020.01.21.911859v1>. 8, 18, 21, 22
- [XP13] XIAO H., PENG H.: APP2: automatic tracing of 3D neuron morphology based on hierarchical pruning of a gray-weighted image distance-tree. *Bioinformatics* 29, 11 (June 2013), 1448–1454. URL: <https://academic.oup.com/bioinformatics/article-lookup/doi/10.1093/bioinformatics/btt170>, doi:10.1093/bioinformatics/btt170. 8
- [YBB*20] YIN W., BRITTAINE D., BORSETH J., SCOTT M. E., WILLIAMS D., PERKINS J., OWN C. S., MURFITT M., TORRES R. M., KAPNER D., MAHALINGAM G., BLECKERT A., CASTELLI D., REID D., LEE W.-C. A., GRAHAM B. J., TAKENO M., BUMBARGER D. J., FARRELL C., REID R. C., DA COSTA N. M.: A petascale automated imaging pipeline for mapping neuronal circuits with high-throughput transmission electron microscopy. *Nature Communications* 11, 1 (Dec. 2020), 4949. URL: <https://www.nature.com/articles/s41467-020-18659-3>, doi:10.1038/s41467-020-18659-3. 1, 13
- [YFZ*20] YU S., FENG Y., ZHANG D., BEDRU H. D., XU B., XIA F.: Motif discovery in networks: A survey. *Computer Science Review* 37 (2020), 100267. URL: <https://www.sciencedirect.com/science/article/pii/S1574013719302850>, doi:https://doi.org/10.1016/j.cosrev.2020.100267. 2, 10
- [YHL*19] YANG J., HAO M., LIU X., WAN Z., ZHONG N., PENG H.: FMST: an Automatic Neuron Tracing Method Based on Fast Marching and Minimum Spanning Tree. *Neuroinformatics* 17, 2 (Apr. 2019), 185–196. URL: <https://doi.org/10.1007/s12021-018-9392-y>, doi:10.1007/s12021-018-9392-y. 8
- [YHT*17] YOO I., HILDEBRAND D. G. C., TOBIN W. F., LEE W.-C. A., JEONG W.-K.: ssEMnet: Serial-Section Electron Microscopy Image Registration Using a Spatial Transformer Network with Learned Features. In *Deep Learning in Medical Image Analysis and Multimodal Learning for Clinical Decision Support* (Cham, 2017), Cardoso M. J., Arbel T., Carneiro G., Syeda-Mahmood T., Tavares J. M. R., Moradi M., Bradley A., Greenspan H., Papa J. P., Madabhushi A., Nascimento J. C., Cardoso J. S., Belagiannis V., Lu Z., (Eds.), Springer International Publishing, pp. 249–257. doi:10.1007/978-3-319-67558-9_29. 8
- [YN13] YIGITSOY M., NAVAB N.: Structure Propagation for Image Registration. *IEEE Transactions on Medical Imaging* 32, 9 (Sept. 2013), 1657–1670. doi:10.1109/TMI.2013.2263151. 6, 7
- [YP11] YU Y., PENG H.: Automated high speed stitching of large 3D microscopic images. In *2011 IEEE International Symposium on Biomedical Imaging: From Nano to Macro* (Mar. 2011), pp. 238–241. ISSN: 1945-8452. doi:10.1109/ISBI.2011.5872396. 6
- [YSST07] YANG G., STEWART C. V., SOFKA M., TSAI C.-L.: Registration of challenging image pairs: initialization, estimation, and decision. *IEEE transactions on pattern analysis and machine intelligence* 29, 11 (Nov. 2007), 1973–1989. doi:10.1109/TPAMI.2007.1116. 6
- [ZKPL18] ZHOU Z., KUO H.-C., PENG H., LONG F.: DeepNeuron: an open deep learning toolbox for neuron tracing. *Brain Informatics* 5, 2 (June 2018), 3. URL: <https://doi.org/10.1186/s40708-018-0081-2>, doi:10.1186/s40708-018-0081-2. 8
- [ZLP*18] ZHENG Z., LAURITZEN J. S., PERLMAN E., ROBINSON C. G., NICHOLS M., MILKIE D., TORRENS O., PRICE J., FISHER C. B., SHARIFI N., CALLE-SCHULER S. A., KMECOVA L., ALI I. J.,

- KARSH B., TRAUTMAN E. T., BOGOVIC J. A., HANSLOVSKY P., JEF-FERIS G. S. X. E., KAZHDAN M., KHAIRY K., SAALFELD S., FET-TER R. D., BOCK D. D.: A Complete Electron Microscopy Volume of the Brain of Adult *Drosophila melanogaster*. *Cell* 174, 3 (2018), 730–743.e22. URL: <https://www.sciencedirect.com/science/article/pii/S0092867418307876>, doi:<https://doi.org/10.1016/j.cell.2018.06.019>. 21, 22
- [ZOYP18] ZHAO T., OLBRIS D. J., YU Y., PLAZA S. M.: NeuTu: Software for Collaborative, Large-Scale, Segmentation-Based Connectome Reconstruction. *Frontiers in Neural Circuits* 12 (2018), 101. URL: <https://www.frontiersin.org/article/10.3389/fncir.2018.00101>. 9, 12, 23
- [ZTLS17] ZUNG J., TARTAVULL I., LEE K., SEUNG H. S.: An Error Detection and Correction Framework for Connectomics. In *Advances in Neural Information Processing Systems* (2017), vol. 30. URL: <https://proceedings.neurips.cc/paper/2017/hash/4500e4037738e13c0c18db508e18d483-Abstract.html>. 12
- [ZWJ17] ZENG T., WU B., JI S.: DeepEM3D: approaching human-level performance on 3D anisotropic EM image segmentation. *Bioinformatics* 33, 16 (2017), 2555–2562. URL: <https://doi.org/10.1093/bioinformatics/btx188>. 8
- [J*09] ČAPEK M., BRŮŽA P., JANÁČEK J., KAREN P., KUBÍNOVÁ L., VAGNEROVÁ R.: Volume reconstruction of large tissue specimens from serial physical sections using confocal microscopy and correction of cutting deformations by elastic registration. *Microscopy Research and Technique* 72, 2 (2009), 110–119. URL: <https://onlinelibrary.wiley.com/doi/abs/10.1002/jemt.20652>. 7